POLYTECHNIC UNIVERSITY OF TURIN

Master of Science Program in Environmental and Land Engineering

Department of Environmental and Land Engineering

Assessing the Potential of GNSS-Derived Precipitable Water Vapor for Rainfall Prediction and Climate Variability Analysis

Master Thesis

Supervisors:

Prof. Paolo Dabove

Dr. Milad Bagheri

Candidate:

Mehraneh Zamanian

(s325569)

July 2026

To My Father, who taught me the value of perseverance and his passion for engineering inspired my own path.

To My Mother, the source of my strength, hope, and determination, whose love has carried me through every challenge.

To My Sister, my first friend, my dearest companion, and my unwavering supporter.

To My Spouse, the love of my life, who walked beside me through every uncertainty, never stopped believing in me, and made the longest journeys feel possible.

I would also like to express my sincere gratitude to Professor Paolo Dabove for giving me the opportunity to undertake this research, whose knowledge, experience, and vision illuminated my path throughout this work.

My heartfelt thanks go to Dr. Milad Bagheri for his constant guidance, patience, and encouragement, whose kindness and commitment created a supportive and welcoming environment that made this work both enjoyable and rewarding.

This thesis is the reflection of a journey shaped by the support, love, and belief of all these remarkable people and it belongs to each of them.

Finaly, to My Homeland; Iran. No matter where life may lead me, my roots will always remain in that ancient land. With enduring hope for freedom and a brighter tomorrow filled with peace and prosperity for its people, who so deeply deserve it.

Abstract

Atmospheric water vapor plays a significant role in weather systems, precipitation processes, and the hydrological cycle. Hence, accurate monitoring of its spatial and temporal variability is necessary. This study evaluates the potential of Global Navigation Satellite System (GNSS)-derived Precipitable Water Vapor (PWV) for atmospheric moisture monitoring and its capability as a complementary indicator for short-term rainfall forecasting across different climatic and topographic conditions. The methodology integrates GNSS observations, ERA5 atmospheric reanalysis data, and ground-based precipitation measurements for an annual period, January-December 2025. Raw GNSS data from three stations, including urban (FALA, Italy), coastal (NICE, France), and mountainous (SAVE, Switzerland), were post-processed through the Canadian Spatial Reference System Precise Point Positioning (CSRS-PPP) service to estimate Zenith Wet Delay (ZWD). These stations utilize low-cost GNSS receivers from the Centipede Real Time Kinematic (RTK) network, across different environments. Thereafter, ZWD values were converted into PWV applying a physical conversion formula and Weighted Mean Temperature (T_m), derived from ERA5 reanalysis data. The resulting PWV time series were compared with ERA5 Total Column Water Vapor (TCWV) based on statistical metrics, including Mean Bias Error (MBE), Root Mean Square Error (RMSE), and the coefficient of determination (R^2).

The results demonstrated acceptable agreement between GNSS-derived PWV and ERA5 TCWV across all stations, where R^2 varied between 0.93 and 0.96. The urban station indicated the highest overall agreement, while the coastal and mountainous stations reflected the effect of land–sea interactions, rapid moisture variability, and complex topography on PWV representation. Despite these challenges, GNSS-derived PWV consistently captured atmospheric moisture dynamics under different environmental conditions. Furthermore, four distinct precipitation scenarios have been considered in this study, including dry conditions, a day before a storm, extreme rainfall events, and sustained low-intensity precipitation. The analysis indicated different PWV trends due to different climates and topographies. In several cases, considerable increases in PWV were observed prior to rainfall initiation, highlighting the capability of GNSS observation to detect atmospheric water vapor accumulation before precipitation. These findings demonstrate the value of GNSS-derived PWV as a high-temporal-resolution indicator of atmospheric water vapor variability and its potential contribution to short-term rainfall forecasting.

Overall, this study confirms that low-cost GNSS meteorology represents a reliable and economically feasible approach for continuous PWV monitoring, proving its potential to significantly enhance network density and reduce costs compared to permanent GNSS stations. Moreover, the results also highlight the potential of this approach to be used as a complementary indicator in addition to existing traditional meteorological observations methods and numerical weather prediction tools, supporting future applications in rainfall forecasting and climate research.

Keywords: Global Navigation Satellite System (GNSS), Zenith Wet Delay (ZWD), Precipitable Water Vapor (PWV), Low-cost Centipede Real Time Kinematic (RTK), Precise Point Positioning (PPP), ERA5 Reanalysis, Atmospheric Water Vapor Monitoring, Short-Term Rainfall Forecasting.

Table of Contents

List of Figures

List of Tables

1. Introduction

Water vapor plays a crucial role in the atmosphere that acts over a wide range of temporal and spatial scales, from global to local climate. Water vapor is the most variable component of the atmosphere. The distribution of water vapor is strongly correlated with the distribution of clouds and rainfall. Because of the large latent heat associated with water phase change, the distribution of water vapor plays a critical role in the vertical stability of the atmosphere and in the structure and evolution of storm [1].

Water vapor is also a key element of the hydrological cycle. Although the residence time of water in the atmosphere is relatively short, approximately ten days, the continuous cycling of water vapor is highly effective in transferring energy from the Earth’s surface to the atmosphere. At the global scale, precipitation and evaporation are approximately balanced; however, at regional scales, the horizontal transport of water vapor by winds becomes essential for explaining the spatial distribution of precipitation [2].

In the climate system, atmospheric water vapor plays a major role in climate as a dominant feedback variable and a key greenhouse gas. As the climate warms, the amount of moisture hold in the atmosphere, is expected to rise much faster than the total precipitation amount, which is limited by how fast water can evaporate from the Earth's surface. This means the atmosphere holds the moisture much longer, resulting in fewer but more intense rainstorms. Consequently, character of precipitation will alter through the following ways. To balance this heightened precipitation intensity there will be a reduction in the duration or a in frequency of rain events, or a transition from snowfall to rainfall [3].

According to the chapter 8 of the IPCC[1]’s sixth assessment report (2021), although global temperatures drive a 1–3% increase in overall precipitation and evaporation per 1°C, the atmosphere's capacity to hold water vapor grows about 7% per 1°C. As a result, more moisture enters into weather systems, making wet seasons and heavy storms much more intense, and

[1] *Intergovernmental Panel on Climate Change*

increases the risk of severe flooding. In summary, the climate change due to greenhouse gases rise the atmospheric water vapor leading to a sharp increase in extreme events [4].

For these reasons, understanding and monitoring atmospheric water vapor is essential for meteorology, hydrology, and climate research. Since water vapor behavior is closely connected to rainfall formation and flood occurrence, accurate observation of its temporal and spatial variability will develop an important complementary tool for extreme rainfall forecasting.

1.1. Importance of Atmospheric Moisture Monitoring

Atmospheric water vapor has a complex life cycle, including vertical and horizontal transport, mixing, condensation, precipitation, and evaporation. According to its high temporal variation, which is more than 50% within a few hours, and its complex spatial distribution, the understanding of water vapor is essential for climate research and numerical weather prediction. Because it is relative to atmospheric dynamics. However, while being a critical atmospheric parameter, it is very challenging to monitor, simultaneously [5].

Traditionally, since the 1950s, the standard technique for measuring atmospheric water vapor has been the radiosonde. While these weather balloons provide invaluable observations, they have inherent limitations, such as limited temporal and spatial resolution. To address these limitations, various remote sensing techniques have emerged, such as ground-based microwave radiometers and satellite-based instruments. There is no best single technique universally due to various systematic errors [5].

The need for improved atmospheric moisture observations motivated the development of alternative monitoring techniques capable of providing continuous measurements with higher temporal resolution. Tralli and Lichten (1990) first introduced the use of Global Positioning System (GPS) signals for atmospheric analysis, recognizing that signals transmitted from satellites experience propagation delays while crossing the atmosphere [6]. Since this delay, is nearly proportional to the precipitable water, Bevis et al. (1994) presented a new method for mapping the observed delay in order to estimate precipitable water [7]. This approach provided an opportunity for meteorological applications while benefiting from continuous observations and high temporal resolution. The remotely sensing of water vapor was proposed in a time when even GPS, the first Global Navigation System (GNSS) constellation, was not still completed [8].

Over the past three decades, GNSS meteorology has proven to be a reliable method for capturing atmospheric water vapor, low-cost, weather independent, highly accurate and precise, and with high temporal resolution [8].

1.2. GNSS Meteorology and PWV Estimation

The atmosphere delays the GNSS signals traveling between satellites and ground receivers. This delay is commonly expressed as the Zenith Total Delay (ZTD). Because water vapor is the main atmospheric component, this delay is mainly due to the presence of water vapor, which is called Zenith Wet Delay (ZWD) and scientists can measure it accurately [7], [8]. A major breakthrough in GNSS meteorology was achieved when Bevis et al. (1994) established a practical method for converting ZWD into Precipitable Water Vapor (PWV) [7].

Recent reviews indicate that GNSS-derived PWV are suitable for several applications including numerical weather prediction, climate monitoring, atmospheric model validation, severe weather analysis, and water vapor trend studies. GNSS networks are becoming denser, leading to be largely used in order to determine the high spatio-temporal variability and long-term trends of atmospheric water vapor [8]. However, expanding these traditional GNSS stations to achieve the higher network density requires a high equipment and maintenance costs. To overcome these financial barriers, low-cost GNSS network, such as the Centipede-Real-Time Kinematic (RTK) network, have emerged as a feasible and cost-effective alternative for high density atmospheric monitoring [9].

Analyzing data from large GPS networks simultaneously creates a heavy computational burden that grows rapidly with the number of receivers. Precise Point Positioning (PPP) solves this problem by fixing satellite orbits and clock corrections to determined values, allowing data from each receiver to be processed one at a time. This method dramatically reduces computing costs, making it possible to process thousands of sites every day on an economical computer.

Despite its low cost, PPP provides results of an acceptable quality. Furthermore, processing one receiver at a time makes it easy to diagnose specific hardware or environmental errors at individual sites while keeping the results independent from distortions caused by incorrect constant constraints on any sites [10].

1.3. Research Gap, Objectives, and Questions

Recent studies have demonstrated the significant potential of GNSS-derived PWV for atmospheric monitoring and precipitation prediction, as different prediction models have been proposed based on GNSS-derived PWV. Several papers reported that PWV typically increases before occurrence of rainfall and decreases after the cessation of rainfall. Hence, it can serve as a useful indicator for short-term precipitation forecasting [11], [12], [13], [14].

Additionally, several studies have compared the GNSS-derived PWV products with atmospheric reanalysis datasets such as ERA5[2] and MERRA-2[3]. These papers generally reported an acceptable agreement between GNSS observations and reanalysis products [15], [16], [17]. Most of these studies focused on a single large geographical region and emphasized statistical validation of the mentioned datasets, rather than analyzing the behavior of atmospheric moisture during specific rainfall events and comparing it across climate conditions.

Other studies have shown that the spatial and temporal characteristics of PWV are strongly influenced by geographical conditions. Spatially, average PWV values vary notably, as the tropical and subtropical monsoon climate experience the highest moisture content, followed by the midlatitude monsoon climate, the humid continental climate, and finally the plateau climate, which maintains the lowest average moisture content. Temporally, these patterns are characterized by seasonal fluctuations, defined by a condensation in summer and a sharp reduction in winter across all regions [18]. According to other investigations, in addition to

[2] *fifth generation of the European Center for Medium-Range Weather Forecasts (ECMWF) Reanalysis*

[3] *Modern-Era Retrospective Analysis for Research and Applications, Version 2*

climatic conditions, topography and proximity to the sea play important roles in controlling atmospheric moisture variability and distribution, as well [19], [20].

Limited attention has been given to the simultaneous investigation of GNSS-derived PWV behavior under different rainfall conditions while also assessing its reliability with reanalysis-based PWV across different geographical environments. This study, particularly, compares atmospheric water vapor variations in urban, coastal, and mountainous environments, located in Italy, France, and Switzerland, under various rainfall scenarios. Furthermore, GNSS-derived PWV observations are compared with ERA5 Total Column Water Vapor (TCWV) products to capture their agreement under varying atmospheric conditions.

In conclusion, the main objective of this study is to figure out the behavior of GNSS-derived PWV under different precipitation conditions and geographical environments, as well as compare its reliability with ERA5-derived TCWV, which finally leads to evaluating the capability of GNSS-derived PWV in rainfall prediction.

The following research questions guide this study:

- How does GNSS-derived PWV vary under different rainfall scenarios?
- Are there observable differences in PWV behavior between urban, coastal, and mountainous environments?
- To what extent do GNSS-derived PWV and ERA5 TCWV products agree under different atmospheric conditions?
- Is GNSS-derived PWV capable to be utilize as a complementary indicator for rainfall prediction?

1.4. Thesis Structure

This thesis is organized into five main chapters:

Chapter 1 introduces the scientific background of atmospheric water vapor and its importance within the climate system. It reviews the significance of atmospheric moisture monitoring, presents the fundamentals of GNSS meteorology and PWV estimation, identifies the existing research gap, and defines the objectives and research questions of the study.

Chapter 2 reviews the relevant literature concerning GNSS-based atmospheric water vapor monitoring, PWV measurement techniques, precipitation-related applications of GNSS-derived PWV, and comparisons between GNSS observations and atmospheric reanalysis products. Previous studies addressing atmospheric moisture variability across different geographical and climatic environments are also discussed.

Chapter 3 describes the methodology adopted in this study. The chapter presents the GNSS station network, the processing method used for PWV measurement, the integration of ERA5 reanalysis data, the definition of rainfall scenarios, and the statistical methods employed for comparing GNSS-derived PWV with ERA5 TCWV products.

Chapter 4 presents the results and discussion. The temporal behavior of PWV is analyzed for different rainfall scenarios and geographical environments, including urban, coastal, and mountainous stations. Comparisons between GNSS-derived PWV and ERA5 TCWV are presented, followed by an interpretation of the observed atmospheric moisture patterns and their relationship with precipitation events.

Chapter 5 summarizes the main findings of the study, discusses the limitations of the adopted methodology and available datasets, and provides recommendations for future research concerning GNSS-based atmospheric moisture monitoring and precipitation-related applications.

The appendices include supplementary figures, statistical tables, and the codes developed for GNSS data processing, PWV computation, ERA5 data handling, and comparative analyses performed throughout the study.

2. Theorical Background and Literature Review

Atmospheric water vapor is a fundamental component of the Earth's climate system and plays a key role in the global water cycle. Water continuously circulates between the ocean, land, atmosphere, and cryosphere through processes, including evaporation, transpiration, condensation, and precipitation. Although the atmosphere contains only a very tiny fraction of the Earth's total water, atmospheric water vapor strongly influences weather processes, cloud formation, precipitation development, and Earth's energy balance [4]. Figure 1 represents the water distribution and water cycle as well.

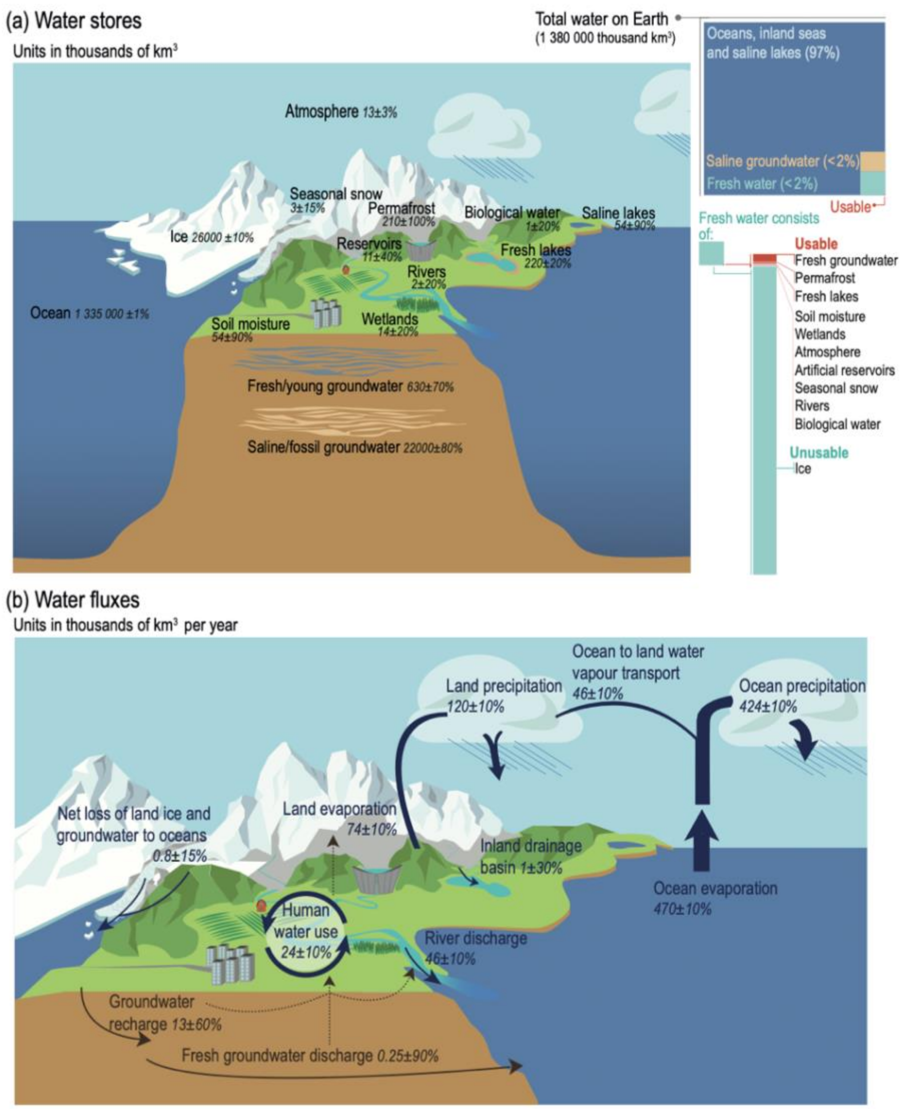

Figure 1. Water distribution and water cycle (chapter 8 of the IPCC's sixth assessment report (2021))

Because atmospheric moisture can change significantly within a few hours and varies considerably across different regions, its accurate observation is essential for meteorological applications, weather prediction, and climate monitoring. The importance of this matter goes beyond weather forecasting. Changes in atmospheric moisture influence precipitation intensity, drought occurrence, and flooding events. According to the chapter 8 of the IPCC's sixth assessment report (2021), a warmer atmosphere can hold more moisture, leading to increased moisture transport and precipitation intensity in many regions. Consequently, monitoring atmospheric water vapor has become increasingly important for understanding both short-term weather phenomena and long-term climate change [4].

The increasing need for continuous and accurate monitoring of atmospheric water vapor leads to the development of new observation techniques. Traditional observing systems such as radiosondes provide valuable measurements of atmospheric humidity; however, their temporal and spatial coverage is often limited. The emergence of GNSS meteorology has provided an alternative approach for monitoring atmospheric water vapor with high spatiotemporal resolution. Hence, GNSS have become an important approach for meteorological and climate-related applications [5].

The foundation of GNSS meteorology is based on the interaction between GNSS signals and the atmosphere. As GNSS signals propagate through the atmosphere, they experience delays caused by atmospheric components, particularly water vapor, named zenith wet delay, which is derived from GNSS observations and can be converted into an estimate of precipitable water vapor [7]. This development created the basis for the practical use of GNSS in atmospheric water vapor monitoring and opened new opportunities for weather forecasting and climate research.

Rocken et al. (1995) expressed PWV as the height of liquid water that would result if all water vapor contained in the atmospheric column were condensed and precipitated [21]. Therefore, PWV provides a physically meaningful measure of the total atmospheric moisture available above a specific location.

2.1. Water Vapor Observation Techniques

2.1.1. Radiosonde Observations

Radiosondes are instruments intended to be carried by a balloon through the atmosphere, equipped with devices to measure meteorological variables, such as pressure, temperature, and humidity, and provided with a radio transmitter for sending this information to the observing station [22]. Since 1950s radiosondes have been the standard technique for atmospheric water vapor measurements. An advantage of radiosonde is the ability to provide vertical information on atmospheric humidity. However, radiosondes have several limitations. Its launch is typically performed only once or twice per day. In addition, its stations are relatively sparsely distributed, with typical spatial coverage of the network of 250 km or more in Europe. Another disadvantage of radiosondes is in making comparisons with other tools, because their horizontal paths are uncontrolled and drift with wind, and their rise takes one or two hours, which makes it ineffective for instantaneous observation. Consequently, radiosonde observations may not adequately capture the temporal and spatial variability of atmospheric water vapor [5].

2.1.2. Satellite-Based Instruments

Satellite remote sensing is important tool for monitoring atmospheric water vapor. Satellite observations provide larger spatial coverage and allow the continuous monitoring of atmospheric moisture over both land and ocean regions, but their accuracy may be influenced by cloud cover, surface characteristics, and sensor limitations [5], [23].

2.1.3. Ground-Based Microwave Radiometers

Ground-based radiometric measurements of atmospheric thermal emission have been useful in several applications, including meteorological observations and forecasting. Because radiometers can be operated in a long-term unattended mode with careful design, they are able to provide continuous measurements with high temporal resolution. These microwave radiometers estimate atmospheric water vapor by measuring the natural microwave radiation emitted by atmospheric components. However, generally they do not provide meaningful atmospheric water vapor observations during rainy conditions [5], [24].

2.1.4. GNSS-Based Monitoring

GNSS has emerged as an important evolution in atmospheric water vapor observation. As mentioned before GNSS can estimate tropospheric zenith wet delay and subsequently atmospheric water vapor information. GNSS meteorology has several advantages compared to traditional systems. They are continuous and can provide atmospheric information with high spatiotemporal resolution, and with relatively low operational costs. Furthermore, its measurements can be obtained under almost all the weather conditions. The increasing density of GNSS networks has enabled atmospheric moisture monitoring over large regions. GNSS-derived tropospheric products are now used in numerical weather prediction, climate studies, and atmospheric water vapor trend analysis routinely [5], [7]. Due to these characteristics, GNSS has become an increasingly valuable tool that complements traditional observing systems.

2.2. Fundamentals of GNSS Meteorology

2.2.1. GNSS Signal Propagation Through the Atmosphere

GNSS signals experience delays when passing through the atmosphere before reaching ground-based antenna, due to the presence of free electrons in the ionosphere and air density in the non-ionized part of the atmosphere, known as the troposphere [9]. During propagation, the signals are affected by atmospheric components. According to Davis et al. (1985), this atmospheric delay is associated with the refractive index along the signal path and depends on the vertical profile of the atmosphere and the elevation angle of the radio source [25].

Estimating atmospheric delays by GNSS outputs has enabled the use of GNSS networks as remote sensing systems for atmospheric monitoring. Bevis et al. (1992) highlighted that GNSS observations can provide continuous information on atmospheric water vapor through the estimation of tropospheric delays, creating new opportunities for climate research [1].

Despite the fact that the utilization of GNSS for atmospheric water vapor estimation dates back several decades, the spatial density of high-precision GNSS networks is still inefficient in modern meteorology. Traditional GNSS stations offer high-quality data, but their large-scale implementation is costly because of hardware, installation, and maintenance costs (ranging from $10000 to $25000). Consequently, current operational GNSS network resolutions are not completely sufficient for the scale of a few kilometers that regional climate and numerical weather models are increasingly adopting. Shifting to low-cost GNSS solves this matter without sacrificing data precision. According to Dabove and Bagheri (2024), the low-cost networks, such as the Centipede-RTK network can estimate ZTD, that are almost identical to those computed from geodetic frameworks like the EUREF Permanent Network (EPN), with mean differences within acceptable thresholds (less than 3.5 cm). Furthermore, when processed using PPP software, which is fully explained in section 2.3, these low-cost outputs are still very similar to the official EUREF ZTD products. Considering this confirmation, this thesis employs the low-cost RTK/GNSS framework as a dense and low-cost network [9]. Figure 2 represent the Centipede-RTK GNSS network map[4] over Europe.

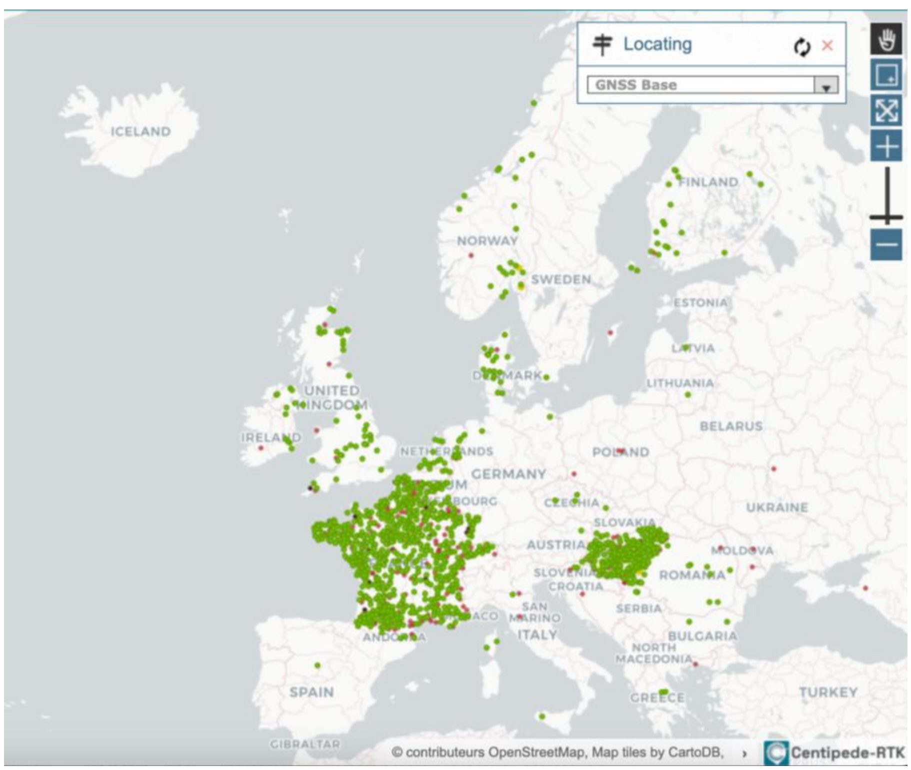

Figure 2. Centipede-RTK GNSS network map over Europe (https://map.centipede-rtk.org/index.php/view/map/)

[4] *https://map.centipede-rtk.org/index.php/view/map/*

2.2.2.ZTD, ZHD, and ZWD

As mentioned earlier, GNSS signals pass through the atmosphere and experience a delay relative to propagation in a vacuum. This delay is caused by the refractive properties of the atmosphere [25]. The GNSS processing for obtaining the position of the receiver needs to consider this delay, which is called Slant Tropospheric Delay (STD). This is usually given in terms of the ZTD, since it is not satellite-dependent, therefore in order to convert STD to ZTD, a mapping function is needed [8]. According to Guerova et al. (2016) this delay is the total signal delay in the zenith direction, which comes from directly overhead and typically averages about 2.4 meters at sea level [5]. Bevis et al. (1992) demonstrated that this delay contains valuable information about atmospheric water vapor and can therefore be used for meteorological applications [1].

Once ZTD is determined through mapping function, meteorological data, typically surface atmospheric pressure, are used to compute the non-dipolar component of this ZTD, known as the zenith hydrostatic delay (ZHD). By subtracting ZHD from ZTD, only the dipolar component remains known as the Zenith Wet Delay (ZWD). Because water vapor is the only major atmospheric component with a permanent dipolar moment, this remaining ZWD component is mainly due to the presence of water vapor [8]. This separation of hydrostatic and non-hydrostatic components was proposed by Davis et al. (1985), who used separate mapping functions for the wet and dry components of the delay [25].

Thus, total tropospheric delay consists of two physically distinct components. The first component is associated with dry atmospheric gases. It is nearly constant and makes the largest contribution to the total delay. The second component is caused by atmospheric water vapor and shows mainly spatial and temporal variability. Consequently, ZTD can be expressed as Formula 1. This decomposition forms the foundation of GNSS meteorology because only the wet component is directly linked to atmospheric moisture [5], [9].

$$ZTD = ZHD + ZWD \tag{1}$$

Since GNSS stations provide observations continuously, with high temporal resolution, atmospheric moisture can be monitored almost continuously. By utilizing a wide spatial range of satellite-to-receiver vectors across distinct elevations and azimuths, GNSS networks can estimate precipitable water vapor at approximately 10-minute intervals [1]. This continuous geometric sampling provides a high temporal resolution and provides a direct connection between geometric measurements and meteorological purposes as well, leading to the improvement of atmosphere monitoring [8].

2.2.3. Conversion of ZWD to PWV

One of the most significant developments in GNSS meteorology was the establishment of a quantitative relationship between ZWD and PWV by Bevis et al. (1994), expressed as Formula 2 [7].

$$PWV = Q \times ZWD \tag{2}$$

where Q is a dimensionless conversion factor that depends primarily on the Weighted Mean Atmospheric Temperature (T_m), which is defined by Davis et al. (1985) as expressed in Formula 3. However, Bevis et al. (1992) introduced an alternative empirical relationship to estimate T_m only based on the observed surface temperature (T_s), [1], [25] which is fully explained in section 2.5.2.

$$T_m = \frac{\int \left({P_v}/{T} \right) dz}{\int \left({P_v}/{T^2} \right) dz} \tag{3}$$

where P_v is water vapor pressure (hPa) and T is temperature (°K).

According to Bevis et al. (1994), the conversion factor is computed using Formula 4.

$$Q = \frac{10^6}{\rho_w R_v (\frac{k_3}{T_m} + k_2')} \tag{4}$$

where ρ_w= 1000 kg/m^3, representing the density of liquid water, R_v= 461.5 J/kg. K, representing the specific gas constant for water vapor, k_2'= 22.1 K/hPa, and k_3= 373900

K^2/hPa, representing the physical refractivity constants [7]. It should be denoted that the physical refractivity constants need unit conversion into K/Pa and K^2/Pa, respectively.

In general, PWV value represents the integral of the concentration of water vapor along the vertical path. According to Vaquero-Martínez and Antón (2021), PWV is the height of liquid water that results from condensing all the atmospheric water vapor in that column. This can be visually represented as the height at which water vapor condenses into liquid water in a vessel with a unit cross-section. Due to its physical meaning and continuous availability from GNSS observations, PWV has become one of the most widely used parameters in GNSS meteorology for weather forecasting, and climate monitoring [8].

2.3. GNSS Approaches for Tropospheric Delay Estimation

2.3.1. Positioning Techniques

There are two principal approaches for GNSS positioning techniques, including differential positioning such as Real-Time Kinematic (RTK), and stand-alone positioning such as Precise Point Positioning (PPP), which was utilized in this study. Differential Positioning is a high accurate technique (centimeter-level) that uses a nearby reference station to remove common satellite and receiver errors, which make it unsuitable for atmospheric monitoring. Unlike differential approach, where common atmospheric errors are removed through differencing between multiple receivers, PPP operates as an absolute technique using a single receiver. Instead of removing environmental effects, estimates ZTD in addition to positioning coordinates, making it an ideal tool for GNSS meteorology. It should be denoted that, ZTD is estimated using estimators such as the Extended Kalman Filter (EKF) or the Least Squares technique. Moreover, PPP relies on precise satellite orbit and clock products to estimate receiver-specific parameters. To be clear, GNSS receivers record two different types of data, including pseudorange (code) and carrier phase. Pseudorange data gives meter-level initial positioning, while carrier phase observations provide millimeter-level precision but requires resolving integer ambiguities [26], [27].

Zumberge et al. (1997) proposed PPP as an efficient strategy to analyze large volumes of GNSS data from large receiver networks with a significantly reduced computational complexity. This method involves a two-step process; first, the precise satellite orbits and clock corrections are determined from a global network, and then by holding these parameters fixed, the receiver-specific parameters are obtained. Thus, a positioning accuracy similar to that of full network solutions is provided [10]. Through this station-by-station procedure parameters such as receiver coordinates, receiver clock offsets, and atmospheric delays with centimeter-level precision are obtained. It should be denoted that as PPP does not remove common errors, accurate modeling of systematic effects influencing the satellite-to-receiver range is essential for obtaining reliable tropospheric products [26]. As a result, PPP can be applied in GNSS meteorology.

2.3.2. CSRS-PPP Service

Canadian Spatial Reference System Precise Point Positioning (CSRS-PPP)[5] service, developed by Natural Resources Canada (NRCan), is an online PPP processing service that was employed is this thesis. It utilizes a dynamic filter to estimate the station position in static or kinematic mode, the station-clock states, the local tropospheric zenith delays and the carrier-phase ambiguities. The approach used in CSRS-PPP for ZTD estimation is to smooth the estimates by a backward substitution with the satellite ambiguity parameters held fixed for all epochs [27].

This service generates several output files describing positioning, clock, and atmospheric parameters. Among these products, the tropospheric output file (TRO) provides estimates of ZHD and ZWD for each processed epoch. Additional information regarding ambiguity resolution, positioning mode, and quality indicators is also included in the processing reports.

2.4. GNSS-Derived PWV and Precipitation Prediction

GNSS-derived atmospheric products have become increasingly important in meteorological applications. According to Guerova et al. (2016), GNSS observations are

[5] *https://webapp.csrs-scrs.nrcan-rncan.gc.ca/*

currently used in Numerical Weather Prediction (NWP) systems as well as nowcasting. They emphasized that the UK Met Office and Météo France were the first to start large-scale operational use of GNSS data in Europe in 2005. Today both institutions report a positive impact from the use of GNSS data in both regional and global NWP models. Several other institutions now use GNSS delay data operationally, and it is expected that many more will follow in the near future. Thus, assimilation of GNSS-derived atmospheric information into weather prediction models has improved forecasting performance, particularly during extreme weather conditions [5].

PWV derived from GNSS has been studied as a heavy rainfall indicator. In northern Italy (Lombardy and Piedmont) widespread rain fronts leave a clear atmospheric pattern over regional GNSS stations, as shown by Barindelli et al. (2018). They figured out PWV values peak when the heavy precipitation core is near the station and then sharply decrease by 5–10 mm within about an hour as the storm is over. This research is the confirmation that time variations in GNSS-derived water vapor were related to the evolution of the rainfall events. While these temporal variations clearly reflect the large-scale rainfall evolution, the smaller-scale event was not detected by the regional GNSS network, but strong fluctuations in water vapor were detected by a low-cost station located near the area of interest [28].

Serrano-Vincenti et al. (2022) showed the relationship between the PWV and rainfall, with the aim of predicting the occurrence of an intense rainfall event in different climatic zones in South America, including coast, high land valley, high mountain, and Amazon. The most correlated was the coast, where all rainfall events were indicated by peaks in PWV with 95% confidence. The comparison between these results and previous investigations in other coastal areas such as Portugal, Italy, and China confirms the importance of the PWV variations for the occurrence of intense rain events but with different lags. In contrast, in high land valley, this correlation reduces to 53% to 77% confidence, showing the importance of the topography in the occurrence of intense rainfall events [29].

According to previous studies, it was found that PWV is correlated with rainfall and can be used to detect intense rainfall. However, Benevides et al. (2019) investigated a significant number of false positives, meaning that the evolution of PWV does not contain enough information to predict future rain. For this reason, they have combined GNSS-derived PWV with surface pressure, surface temperature, and relative humidity obtained continuously from a ground-based meteorological station. A neural network model was used to process five years of GNSS data from one station in Lisbon, Portugal, and meteorological data to forecast the hourly precipitation. The proposed methodology improves the detection of intense rainfall events and reduces the number of false positives. This method achieved an almost 100% rate for rain vs. no rain detection, with close to no false alarms [30].

In another recent study, the two main challenges of weather forecasting using NWP models were mentioned. First the updates on weather conditions, including alerts for precipitation, are delivered every 6 hours. Second, these updates may not represent the real weather conditions near the area of interest. On the other hand, increasing the spatial and temporal coverage by meteorological radars is a very costly solution. Although many studies have evidenced the reliability of GNSS-derived PWV with lower cost, Giannadaki et al. (2025) declared that there is still a great difficulty in determining a rigid relationship between rainfall and PWV that could be incorporated into a nowcasting model. Their analysis of 81 heavy precipitation events over Cyprus Island showed an increase in PWV before most heavy rain events, with the time lag of PWV peaks from the heavy rain ranging from one to six hours in most events. However, the correlation coefficient between maximum PWV peaks and the related maximum precipitation peaks varied among different geographical environments, which shows R=0.85 over the mountainous region and R=0.5 both in coastal and all Cyprus regions [31].

Overall, the reviewed studies indicate that GNSS-derived PWV provides valuable information on atmospheric moisture variability and often shows significant increases before heavy precipitation events. At the same time, the literature consistently shows that the timing and magnitude of PWV changes vary according to local meteorological conditions, topography, and regional climate characteristics. These findings motivated the development of GNSS-derived PWV as an indicator of precipitation occurrence.

2.5. ERA5 Reanalysis TCWV vs. GNSS-PWV

2.5.1. ERA5 Reanalysis Dataset

ERA5 is the fifth-generation atmospheric reanalysis produced by the European Centre for Medium-Range Weather Forecasts (ECMWF) within the Copernicus Climate Change Service. It provides a comprehensive and continuous record of the global atmosphere, land surface, and ocean waves over from1950 onwards, making it highly valuable for climate studies, weather analysis, and atmospheric research. In terms of resolution, ERA5 offers a grid spacing of approximately 31 km and provides data at hourly intervals. These characteristics make ERA5 particularly suitable for applications that require high special (both horizontally and vertically) and temporal resolution and information about atmospheric variability, such as GNSS-based PWV studies [32].

2.5.2. Weighted Mean Temperature Retrieval

In this study, ERA5 was used to provide Weighted Mean Atmospheric Temperature (T_m). Bevis et al. (1992) introduced a simple empirical relationship to estimate T_m only based on the observed surface temperature (°K), as expressed in Formula 5 with an error of less than 2% [1].

$$T_m \approx 70.2 + 0.72 \,.T_s \tag{5}$$

Several studies have used ERA5 atmospheric variables such as hourly geopotential (z) and temperature ($t2m$) to support the calculation of T_m. The $t2m$ variable is used as the surface air temperature input. However, it needs a primary adjustment to be representative for the actual GNSS station elevation through Formula 6. Geopotential is used for this adjustment to derive the ERA5 model height as expressed in Formula 7. They are two important steps especially over complex terrain, to reduce the effect of height differences between reanalysis grid points and ground-based GNSS stations [15], [17], [33].

$$T_s = t2m + \Gamma\,(h_{gnss} - h_{ERA5}) \tag{6}$$

$$h_{ERA5} = \frac{z}{g} \tag{7}$$

where $t2m$ is the ERA5 2-meter air temperature (°K), h_{gnss} is the GNSS station elevation (m), h_{ERA5} is the ERA5 model height (m), Γ is the lapse rate equl to -0.0065 °K/m, and g is gravitational coefficient equal to 9.80665 m/s^2.

2.5.3. ERA5 TCWV for Comparison with GNSS-Derived PWV

Reanalysis products provide continuous atmospheric fields with broad spatial and temporal coverage. However, they are produced through numerical models and data assimilation, and because of that their reliability needs to be evaluated in different regions. GNSS-derived PWV is not assimilated into many reanalysis products and provides high accuracy and high temporal resolution atmospheric water vapor observations. Therefore, they can be used as independent validation data [15], [17].

In recent years several researchers have declared that the assessments across the Tibetan Plateau, China, and the United States demonstrate a high correlation between GNSS-derived PWV and ERA5 reanalysis products. The spatial distributions, mean values, and seasonal variations of the PWV time series derived from GNSS observations are in good agreement with those extracted from the ERA5 reanalysis products. Quantitatively, the evaluation of ERA5-derived PWV against GNSS data shows a high correlation in China, with an overall Root Mean Square Error (RMSE) of 1.8 mm in the United States, 1.99 mm in China, and 1.77 mm over the Tibetan Plateau. These biases and RMS errors depend on regional and seasonal conditions [15], [16], [17].

As a result, these reviewed studies motivated the selection of TCWV as an independent reanalysis-based atmospheric water vapor product for comparison with GNSS-derived PWV. This comparison allows to assess the agreement between ground-based GNSS retrievals, and gridded ERA5 TCWV estimates, across urban, coastal, and mountainous environments.

2.6. Environmental Influences on PWV Variability

PWV has a considerable spatial and temporal variability and plays a major role in atmospheric energy transfer in the atmosphere, as well as cloud formation, precipitation, and radiative forcing. Due to this high variability, PWV has become one of the most widely investigated atmospheric parameters in GNSS meteorology, climate monitoring, and weather prediction. Continuous GNSS observations have enhanced the capability to investigate this variability under different climatic conditions [34]. Temperature is one of the primary factors affecting PWV. Since the moisture-holding capacity of air increases with temperature, warmer atmospheric conditions generally correspond to higher PWV values. In addition, altitude, atmospheric pressure, latitude, and seasonal variability significantly influence the spatial distribution of PWV. Increasing elevation generally reduces the total atmospheric water vapor contained within the atmospheric column because atmospheric pressure decreases with altitude. Using a long term GNSS observations from 248 stations in different climatic regions over China, Yang et al. (2024) demonstrated that PWV shows positive correlations with temperature and negative correlations with elevation and latitude, indicating that climatic conditions and topographic characteristics jointly determine regional PWV variability [18].

Obviously, increasing elevation generally reduces the total atmospheric water vapor contained within the atmospheric column because atmospheric pressure decreases with altitude. This, the influence of mountainous condition on GNSS-derived PWV is significant for rainfall monitoring applications. Mawandha et al. (2019) evaluated GNSS-derived PWV in a mountainous region in Mt. Merapi, located in Indonesia, which has a wet climate with complex terrain conditions. The authors reported that; first, PWV increased before rainfall events, second, complex topography introduces additional variability into PWV observations, which emphasized the importance of considering terrain characteristics. To be more specific, rainfalls in the mountainous region are mostly influenced by the confusion caused by the hydrodynamic environments, such as wind direction, air temperature collision, and many others. This situation denotes the rainfall in the mountainous region, is mainly categorized as short term and high intensity rainfalls [19].

The environmental influence on PWV is not limited to elevation. Geographic location also controls the availability and transport of atmospheric moisture. Coastal zones are one of the most interesting locations for PWV monitoring as they experience notably different oceanic and topographic influences compared inland and mountainous areas. In coastal areas, PWV gradually decreases from the coastal regions toward the arid land, as they are directly affected by water vapor evaporated from warm ocean surfaces, which acts as a critical moisture source. However, the exact impact varies significantly depending on the seasonal variability. Zhao et al. (2025) utilized PWV data from 15 GNSS stations to investigate the spatiotemporal distribution of atmospheric water vapor across Australia. The spatial pattern demonstrates a decreasing trend from south to north. They also reported that Eastern coastal areas are influenced by southeastern trade winds, which carry water vapor from the Pacific Ocean. Meanwhile, the western coastal areas receive water vapor transported from the Indian Ocean. Overall, the authors indicate that although topographic elevation influences the distribution of water vapor, its effect is not as significant as the differences in climate conditions between coastal and inland areas [20].

Additionally, Gouveia et al. (2026) emphasized the usefulness of GNSS-derived PWV as a real time atmospheric indicator for monitoring extreme events in urban areas. The objective of their study was to understand the extreme event that occurred as a disaster in the southern region of Brazil, specifically in the state of Rio Grande do Sul, in April and May 2024. The region was under the influence of El Niño, a phenomenon that typically increases precipitation and storm frequency in southern Brazil. In one of the stations, the highest PWV value reached 60 mm, known as PWV-GNSS jump. At that same hour, the pluviometer measured 3 mm of precipitation. In the following hour, PWV sharply dropped to 10 mm, while precipitation increased significantly to 26 mm, representing a nine-times increase, approximately. These results demonstrate that GNSS-derived PWV is a valuable tool for detecting short-term hydrometeorological risks. They also declared that the link between PWV and rainfall supports its integration into real-time flood early warning systems in Southern Brazil. Water vapor measurements are inherently challenging to model, and these difficulties are even more during extreme weather events. Nevertheless, GNSS-derived PWV ensures continuous data availability, that can be applied in nowcasting, with the ability to detect significant variations in PWV up to 60 minutes or less before the occurrence of flood events [35].

Collectively, the studies reviewed in this section demonstrate that PWV variability is influenced by a set of combined parameters such as climatic conditions, topography, geographical condition, temperature, elevation, atmospheric circulation, and proximity to large water bodies. All these factors contribute to the spatial and temporal variation of atmospheric moisture. Consequently, differences in PWV observed at GNSS stations cannot be interpreted only in terms of precipitation processes, but should also be considered within the environmental condition.

3. Materials and Methods

This section represents the methodology and outcomes of processing GNSS observations, integrated with Copernicus ERA5 atmospheric reanalysis models and in-situ meteorological station records. The objective is to compute and evaluate the spatial and temporal dynamics of PWV for all available days of the year 2025. Figure 3 illustrates a clear overview of this study's methodology.

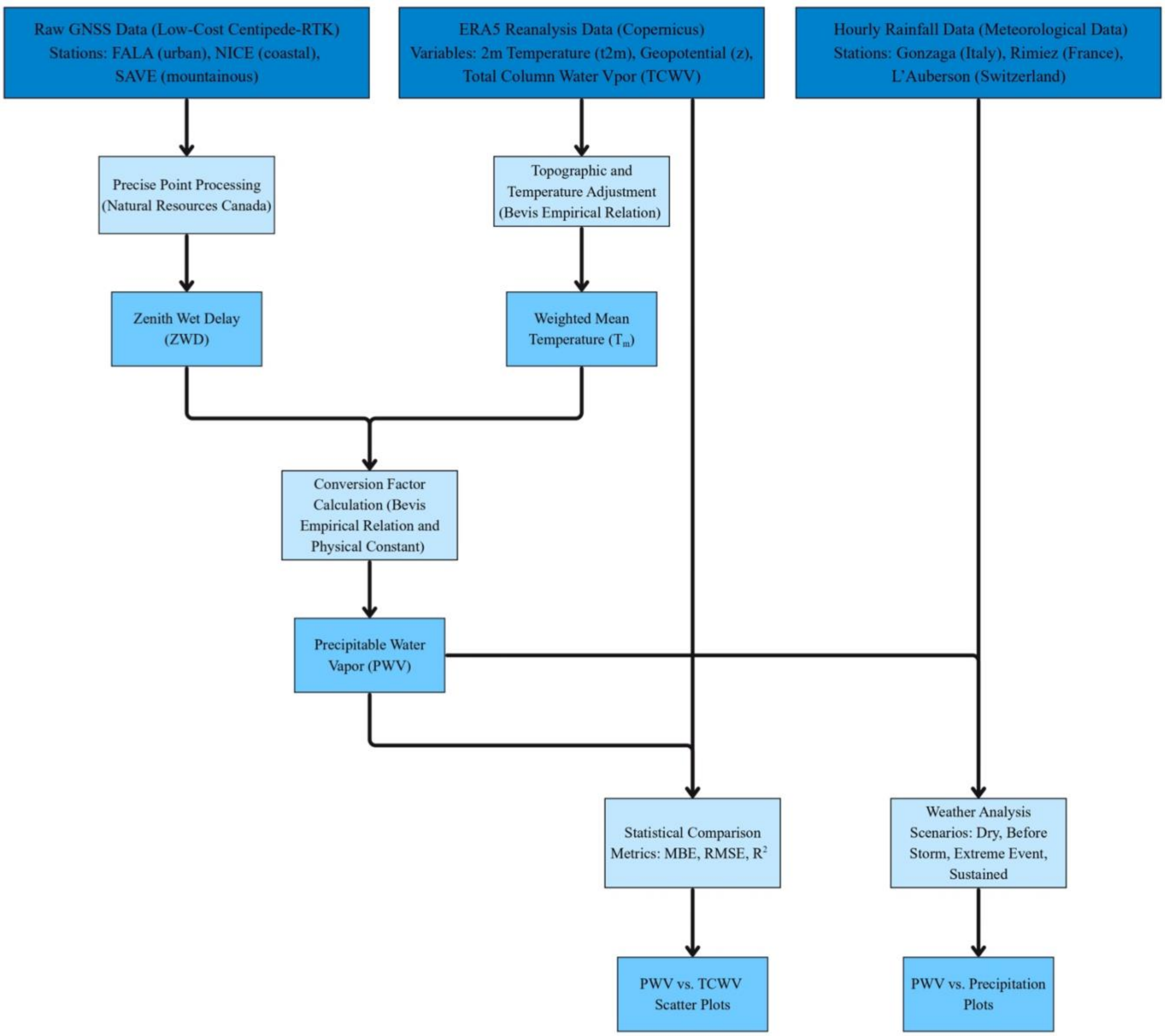

Figure 3. Methodological Flowchart

3.1. GNSS Stations Network

Raw GNSS observations were obtained from the low-cost Centipede-RTK network for three distinct stations characterized by varied altitudes and climatic environments. To retrieve high-accuracy tropospheric parameters, the raw observation files were processed utilizing the PPP approach of the CSRS-PPP, that provided the ZWD series calculated every 30 seconds. The specific details about the stations are listed in Table 1 and Figure 4. In fact, the primary atmospheric variables used in this research were extracted from the CSRS-PPP tropospheric output files. According to its description, the TRO file contains estimates of dry zenith path delay (TRODRY), wet zenith path delay (TROWET), and their associated uncertainties for every processed epoch. These parameters correspond respectively to ZHD and ZWD discussed in Section 2.3. Because the wet component is directly related to atmospheric water vapor, the TROWET values are the fundamental input for PWV retrieval.

Table 1. geometric and environmental characteristics of each GNSS station

No.	Name	Rinex Code	Location	Climate	Latitude (°N)	Longitude (°E)	Height (m)
1	FALA	B46400ITA	Italy	Urban	44.92277356	10.75420074	67.319
2	NICE	A69800FRA	France	Coastal	43.72549612	7.2999717	427.311
3	SAVE	B39600CHZ	Switzerland	Mountainous	46.91032007	6.49854465	1028.369

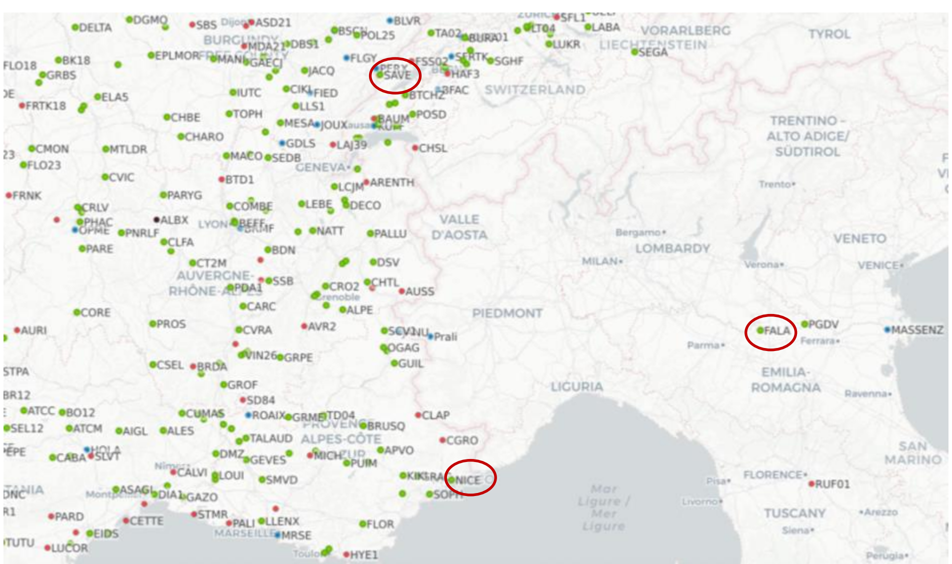

Figure 4. Location of GNSS Stations (https://map.centipede-rtk.org/index.php/view/map/)

3.2. Reanalysis Data Integration

To convert ZWD into absolute PWV quantities, auxiliary physical parameters -specifically 2-meter temperature (t2m) and geopotential- were retrieved for the entire duration of 2025 from the Copernicus Climate Data Store[6] (CDS).

As mentioned before in section 2.5.2, since the GNSS station height (h_{gnss}) often differs from the ERA5 model grid height (h_{ERA5}), $t2m$ was brought down or up to the actual station height (surface temperature) with a lapse-rate correction using the following formula (Formula 6).

$$T_s = t2m + \Gamma\ (h_{gnss} - h_{ERA5})$$

Where Γ = −0.0065 K/m, and $h_{ERA5} = {}^{z}/_{g}$ m.

Then Weighted Mean Temperature (T_m) was estimated using the Bevis empirical relation shown in the following formula (Formula 5).

$$T_m \approx 70.2 + 0.72\ .T_s$$

Because these reanalysis atmospheric inputs provide an hourly sampling while the GNSS-derived ZWD operates on a 30-second interval, a linear interpolation was applied on T_m to align the time-series.

As mentioned before in section 2.2.3, the core conversion from ZWD to PWV is passing thorough the following formula (Formula 2).

$$PWV = Q \times ZWD$$

[6] *https://cds.climate.copernicus.eu/*

Where the dimensionless conversion factor (Q) is formulated as a function of T_m, which is empirically linked to the surface skin temperature ($t2m$) shown in the following formula (Formula 4).

$$Q = \frac{10^6}{\rho_w R_v (\frac{k_3}{T_m} + k_2')}$$

Where ρ_w= 1000 kg/m^3, representing the density of liquid water, R_v= 461.5 J/kg. K, representing the specific gas constant for water vapor, k_2'= 22.1 K/hPa, and k_3= 373900 K^2/hPa, representing the physical refractivity constants. It should be denoted that the physical refractivity constants need unit conversion into K/Pa and K^2/Pa, respectively.

3.3. Precipitation Scenario Selection

The actual hourly precipitation observations in 2025 were obtained from the official nearest meteorological stations in Italy[7], France[8], and Switzerland[9], which are named Gonzaga, Rimiez, and L'Auberson, respectively to ensure spatial representativeness for each GNSS site. Table 2 and Figure 5 represent the specific details of the stations. Also, Figures 6, 7, and 8 represent the rainfall plots of each station in 2025.

Table 2. characteristics of each meteorological station

No.	Name	Nearest GNSS station	Location	Climate	Latitude (°N)	Longitude (°E)	Height (m)
1	Gonzaga	FALA	Italy	Urban	44.960372	10.758281	22
2	Rimiez	NICE	France	Coastal	43.738667	7.279167	238
3	L'Auberson	SAVE	Switzerland	Mountainous	46.823450	6.440692	1096

[7] *https://www.arpalombardia.it/*
[8] *https://www.data.gouv.fr/*
[9] *https://opendata.swiss/*

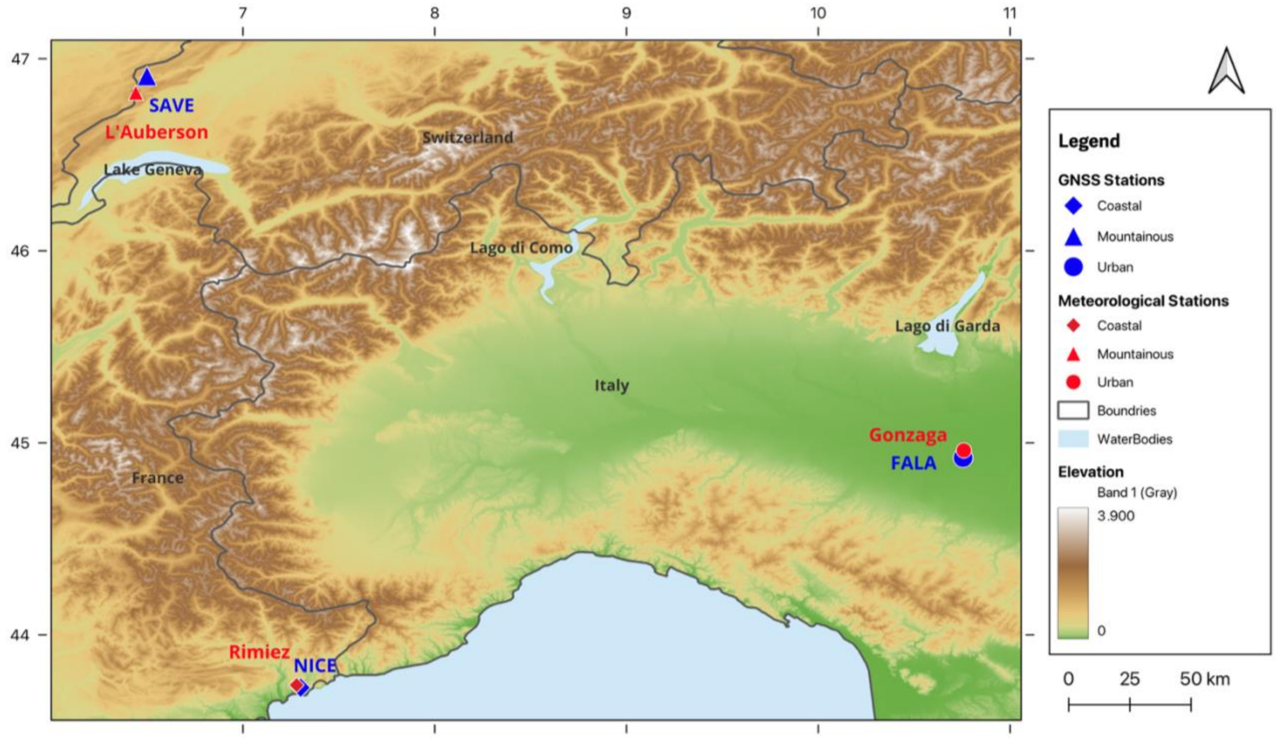

Figure 5. Location of the selected GNSS and meteorological stations over the digital elevation model (DEM)

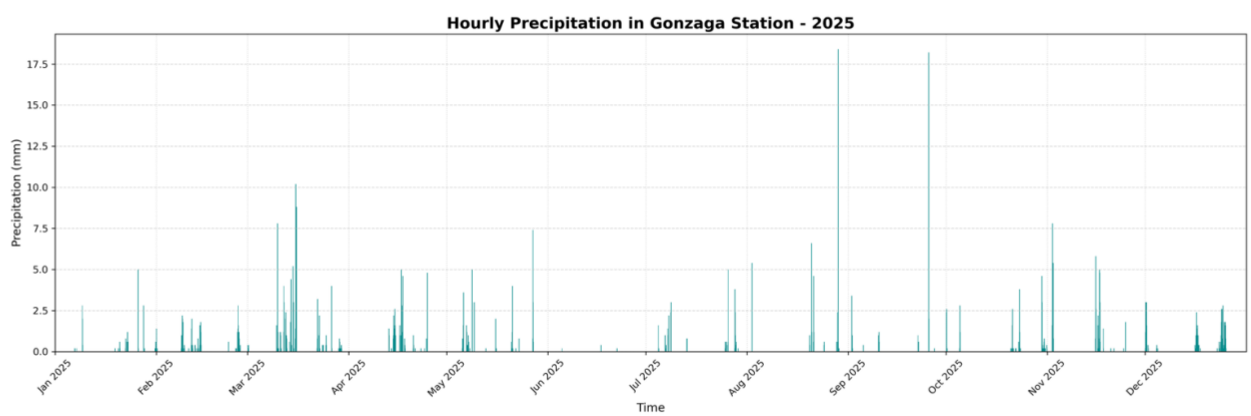

Figure 6. Annual Hourly Precipitation in Gonzaga Station (Italy)

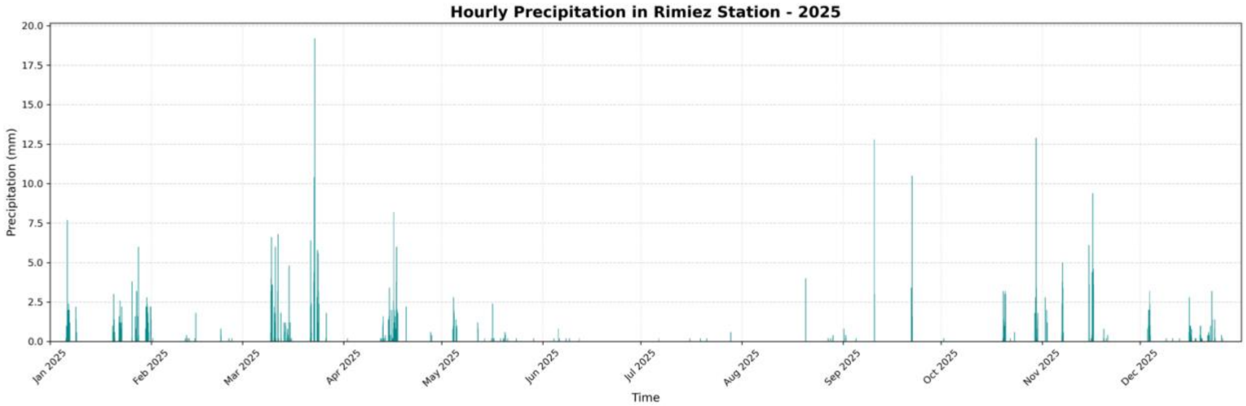

Figure 7. Annual Hourly Precipitation in Rimiez Station (France)

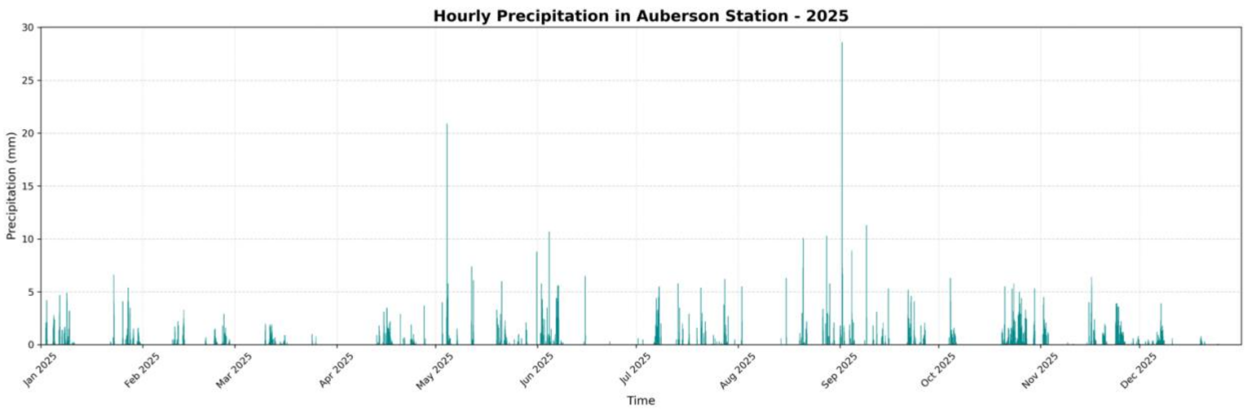

Figure 8. Annual Hourly Precipitation in L'Auberson Station (Switzerland)

In order to represent the coherent results (shown in section 4), four distinct meteorological scenarios were strategically adopted to evaluate the most crucial weather conditions. This selection allows for a focused assessment of how low-cost GNSS technology monitors rapid water vapor variations under different environmental conditions:

- Scenario 1 (Completely Dry Day)
- Scenario 2 (A Day Before a Storm)
- Scenario 3 (Peak Hourly Extreme Event)
- Scenario 4 (Sustained and Low-Intensity)

The dry day is marked by a constantly low level of PWV and zero rain. It sets a baseline for how the local atmosphere behaves when it is completely dry and stable. Before the storm a sharp and rapid rise in PWV, but without any immediate rain on the ground shows how high-resolution GNSS-PWV data can successfully predict storms before they actually start. During the extreme event the PWV series demonstrates a sharp peak a few hours before the storm, followed by a quick drop after the rainfall. The last scenario shows a steady, high, continuous, and with little oscillations of PWV, lacking the sudden drops.

3.4. Statistical Comparison with TCWV Data

The retrieved PWV series was compared with independent TCWV gridded fields, obtained from CDS. The statistical metrics, such as Mean Bias Error (MBE), Root Mean Square Error (RMSE), and Coefficient of Determination (R^2), were computed for each individual day levels and across the whole days with available data, using formulas 8, 9, and 10.

$$MBE = \frac{1}{n}\sum_{i=1}^{n}(\hat{y}_i - y_i) \tag{8}$$

Where, MBE or Bias represents the average systematic error (overestimation or underestimation) between the datasets, $\hat{y}_i$ is PWV value derived from the ground-based GNSS observations, and y_i is the corresponding TCWV value extracted from the ERA5 reanalysis model.

A positive Bias indicates that the GNSS-PWV model, on average, overestimates the total atmospheric water vapor compared to the ERA5 reference data. Conversely, a negative Bias indicates an underestimation by the GNSS model. A value close to zero represents a well-calibrated system with minimum bias.

$$RMSE = \sqrt{\frac{1}{n}\sum_{i=1}^{n}(y_i - \hat{y}_i)^2} \tag{9}$$

Where, RMSE represents the average magnitude of absolute error between the datasets.

Unlike Bias, RMSE does not show the direction of the error but measures its overall size. Lower RMSE values indicate that GNSS data is highly precise and stays very close to the ERA5 reference data.

$$R^2 = 1 - \frac{\sum_{i=1}^{n}(y_i - \hat{y}_i)^2}{\sum_{i=1}^{n}(y_i - \bar{y}_i)^2} \tag{10}$$

Where, R^2 represents the proportion of variance in the reference dataset that is predictable from the GNSS observations, and $\bar{y}_i$ is the computed mean of the reference ERA5 dataset (TCWV).

R^2 tracks how well the GNSS model follows the natural temporal dynamics and trends of atmospheric moisture. An R^2 of 1 indicates that 100% of the true variations in atmospheric moisture are successfully caught and explained by your model.

4. Results and Discussion

In this section the results of the GNSS-derived PWV potential assessment are presented and interpreted. These outcomes were compared to actual ground-based precipitation measurement, obtained from the nearest meteorological station to desired GNSS station. In addition, they were compared to TCWV obtained from ERA5 reanalysis data as well, in order to evaluate their capability as a complementary indicator for rainfall prediction through distinct climates and elevations, specifically in four main rainfall scenarios. It should be denoted that the obtained data from Centipede-RTK were not uninterrupted throughout the entire year of 2025. These unavoidable gaps in data availability affected the overall results and some scenarios were evaluated using only one or two stations where data coverage was sufficient. The considered station through each scenario and the exact number of available observation days for each station during the continuous annual processing is shown in Table 3. However, to make it brief, the statistical parameters and the rainfall plots for each single day are provided in the Appendix.

Table 3. Data Availability

Scenarios	FALA (Urban Station)	NICE (Coastal Station)	SAVE (Mountainous Station)
Scenario 1 (Completely Dry Day)	✓	✓	✓
Scenario 2 (A Day Before a Storm)	✓	✗	✗
Scenario 3 (Peak Hourly Extreme Event)	✓	✗	✓
Scenario 4 (Sustained and Low Intensity)	✓	✓	✓
Number of Available Days	138	74	213

4.1. Scenario 1: Completely Dry Day

4.1.1. Urban Station (FALA)

As shown in Figure 9, the total atmospheric moisture is extremely low, that its maximum amount is 13 mm. According to a completely dry day baseline, precipitation remains at zero, showing how the processing matches with clear, stable, and low humidity urban conditions. As demonstrated in Figure 10, the day is characterized by a low error.

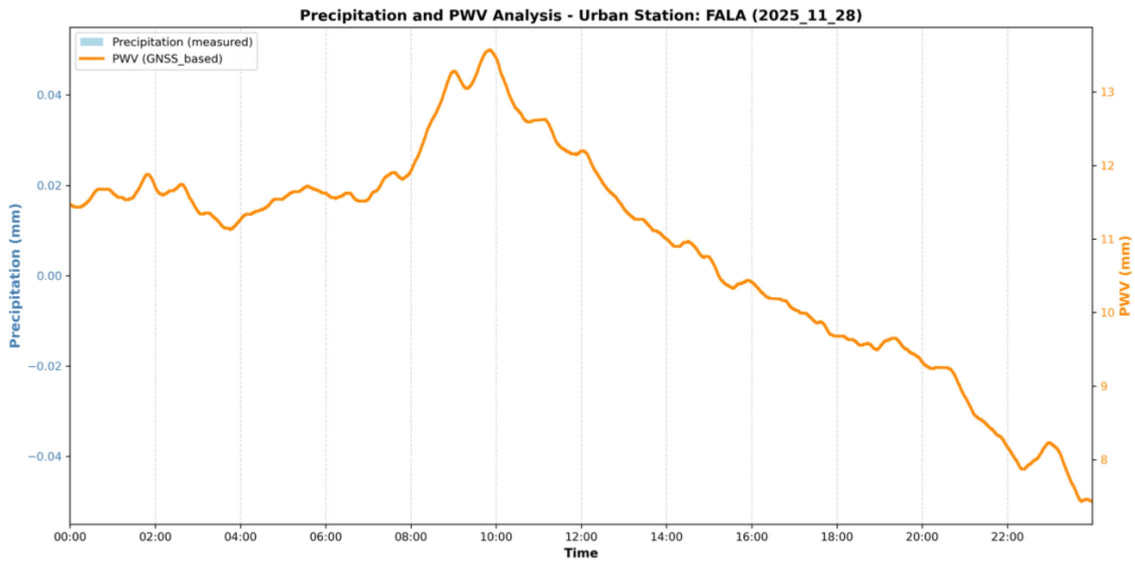

Figure 9. Precipitation vs. PWV on November 28th in an Italian Station

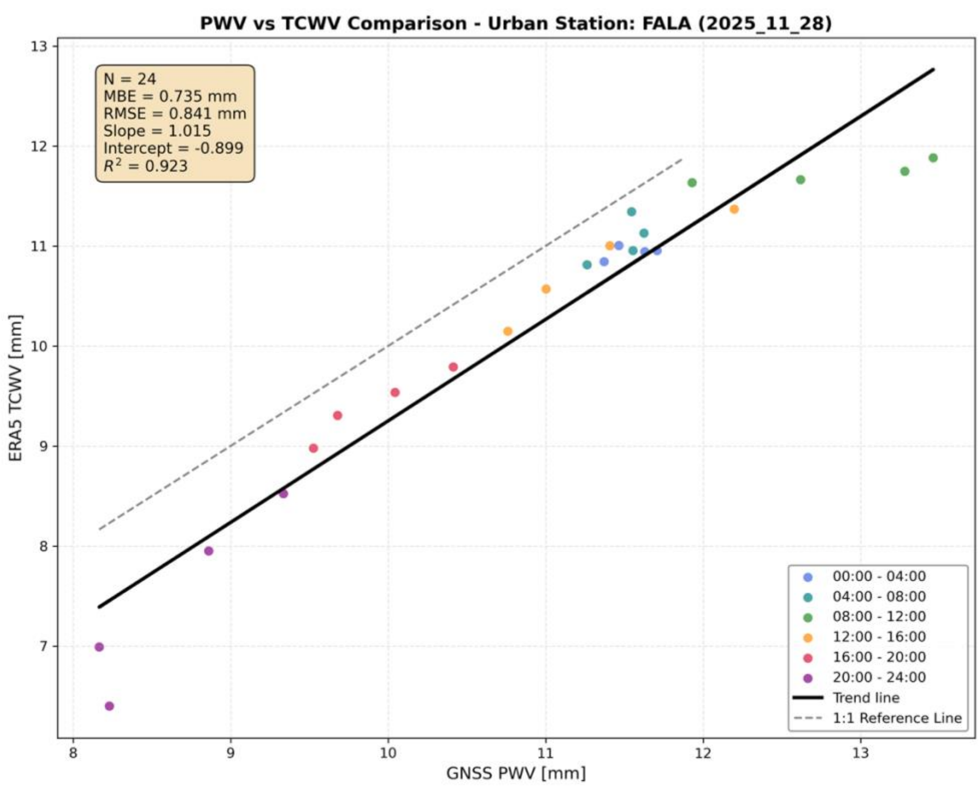

Figure 10. PWV vs. TCWV on November 28th in an Italian Station

4.1.2. Coastal Station (NICE)

The time-series in Figure 11 shows an example of a stable and rain free coastal day. Obviously, measured precipitation remains at zero for the entire day. The moisture starts at a minimum of 5 mm at midnight and gradually rises to a daytime peak of 13.5 mm by late evening. This pattern reflects the daily sea breeze cycle that carries moisture from sea toward the station. As shown in Figure 12 the GNSS-PWV processing matches the reanalysis data beautifully on a clear day. The comparison shows a high correlation and a small error.

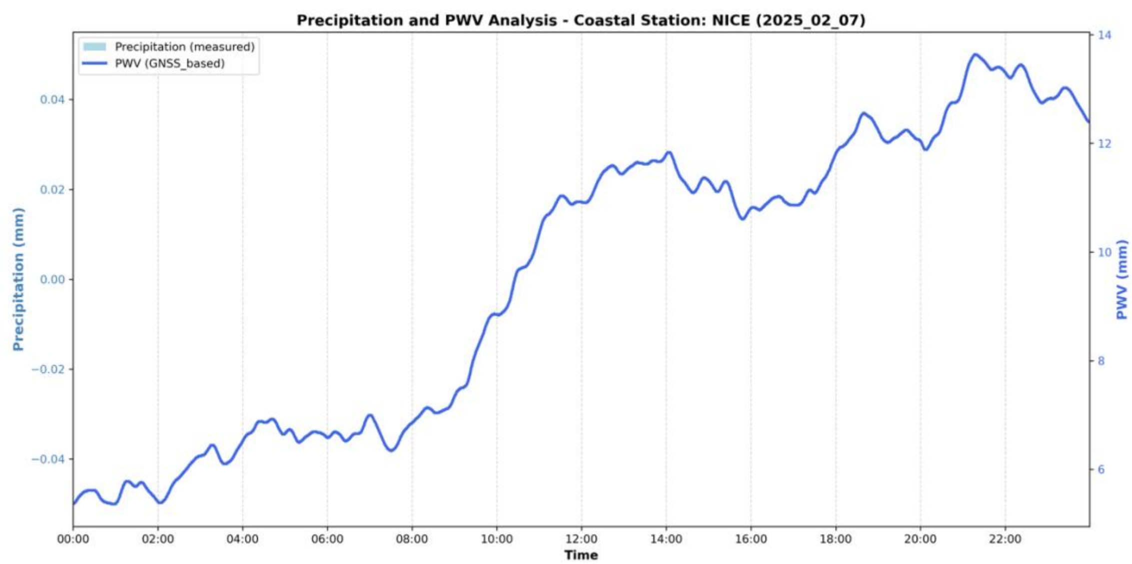

Figure 11. Precipitation vs. PWV on February 7th in a French Station

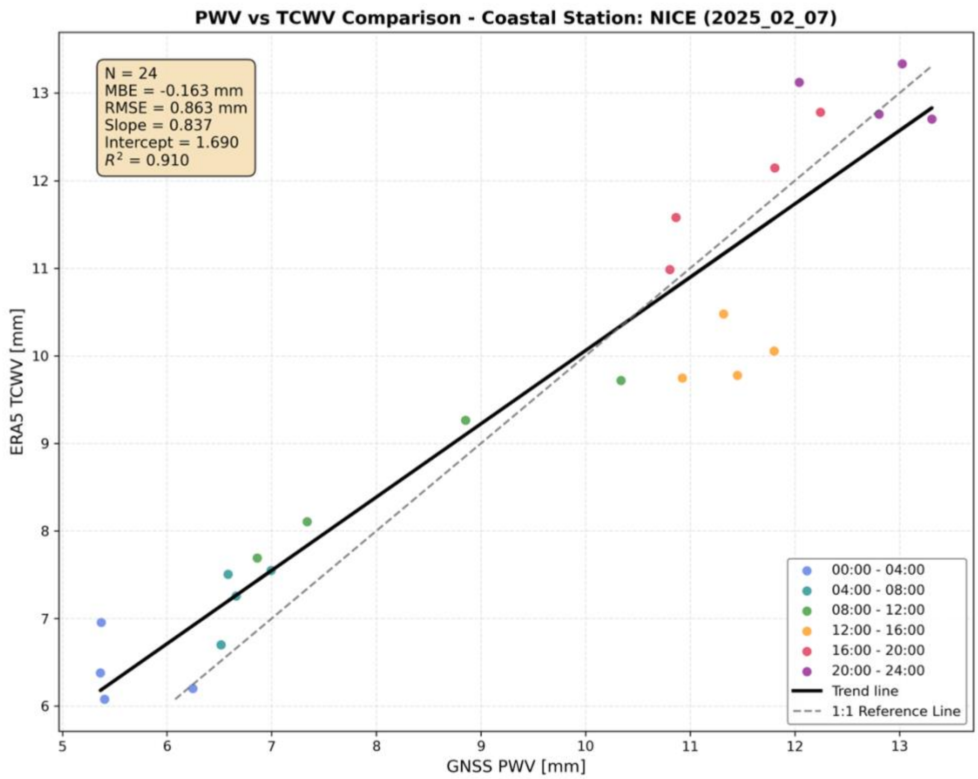

Figure 12. PWV vs. TCWV on February 7th in a French Station

4.1.3. Mountainous Station (SAVE)

The time-series in Figure 13 confirms the stable and rain free mountain environment. Due to the high altitude and cool temperature, the total water vapor is exceptionally low, starting at 9.5 mm at midnight and falling to a 4 mm the end of the day. As shown in Figure 14, the model tracks the weather variations well during low humidity conditions. The negative bias shows that the GNSS model tends to read lower moisture values than ERA5, which is a known pattern in high-altitude stations, due to topographic mismatch.

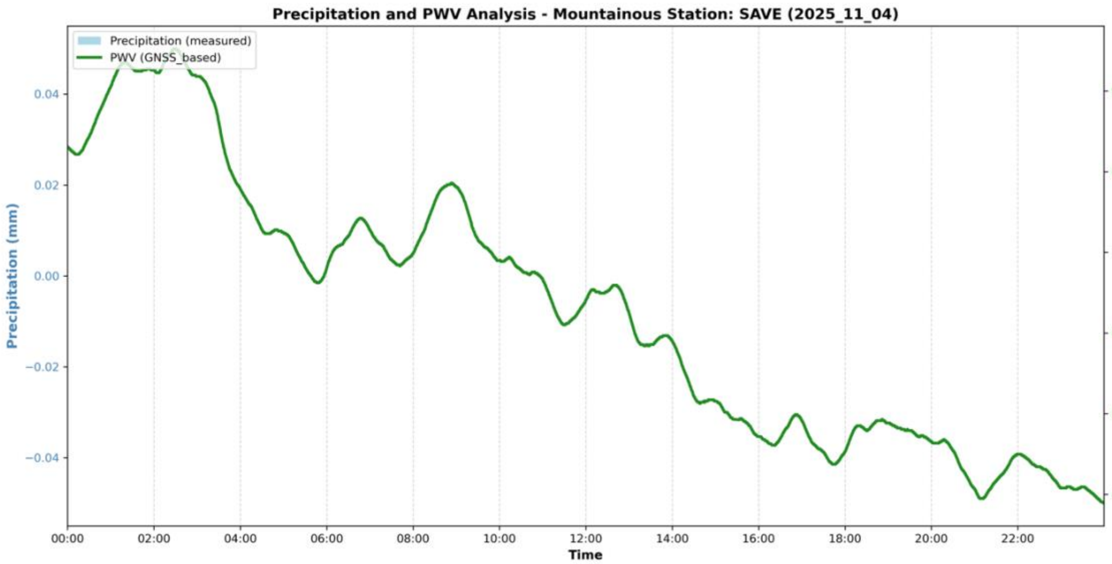

Figure 13. Precipitation vs. PWV on November 4th in a Swiss Station

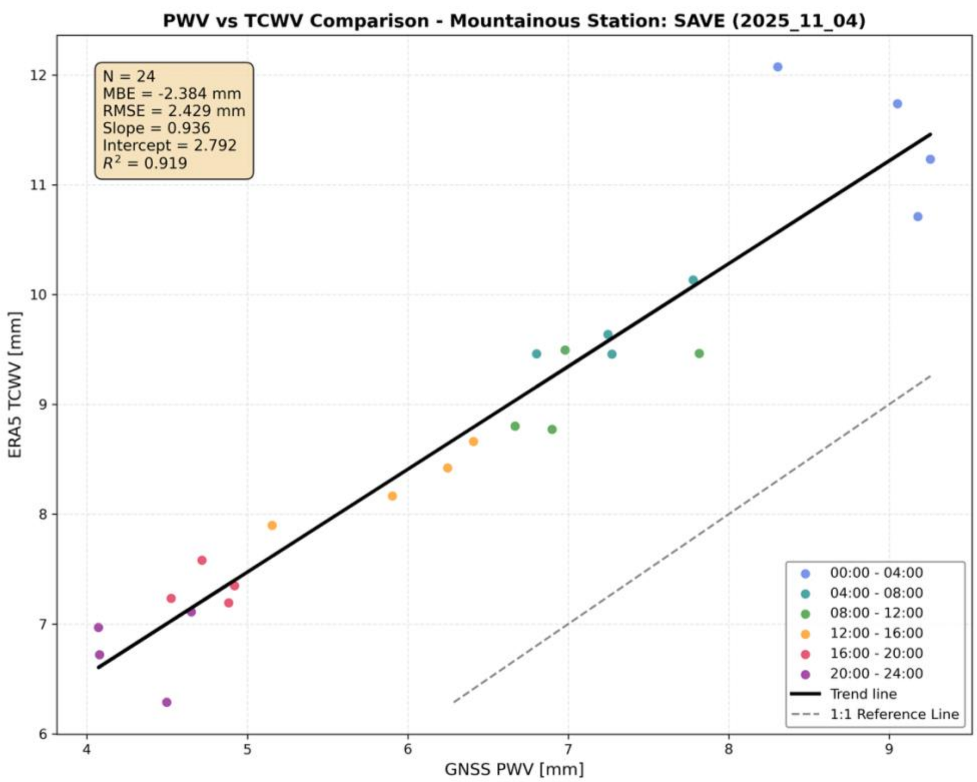

Figure 14. PWV vs. TCWV on November 4th in a Swiss Station

4.2. Scenario 2: A Day Before a Storm

4.2.1. Urban Station (FALA)

The prediction capability of the GNSS-PWV is seen in Figure 15. Throughout the day, measured precipitation is zero. However, the PWV curve shows an increasing moisture to reach the peak of 47 mm. This can act as an indicator of the upcoming weather event. Moreover, Figure 16 demonstrates a comparable correlation and error.

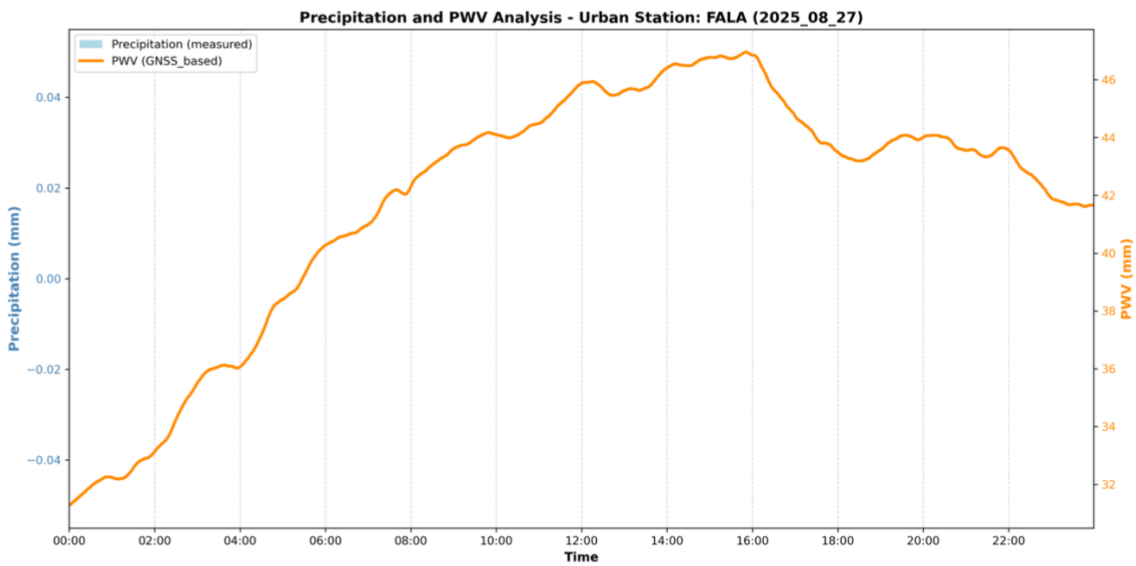

Figure 15. Precipitation vs. PWV on August 27th in an Italian Station

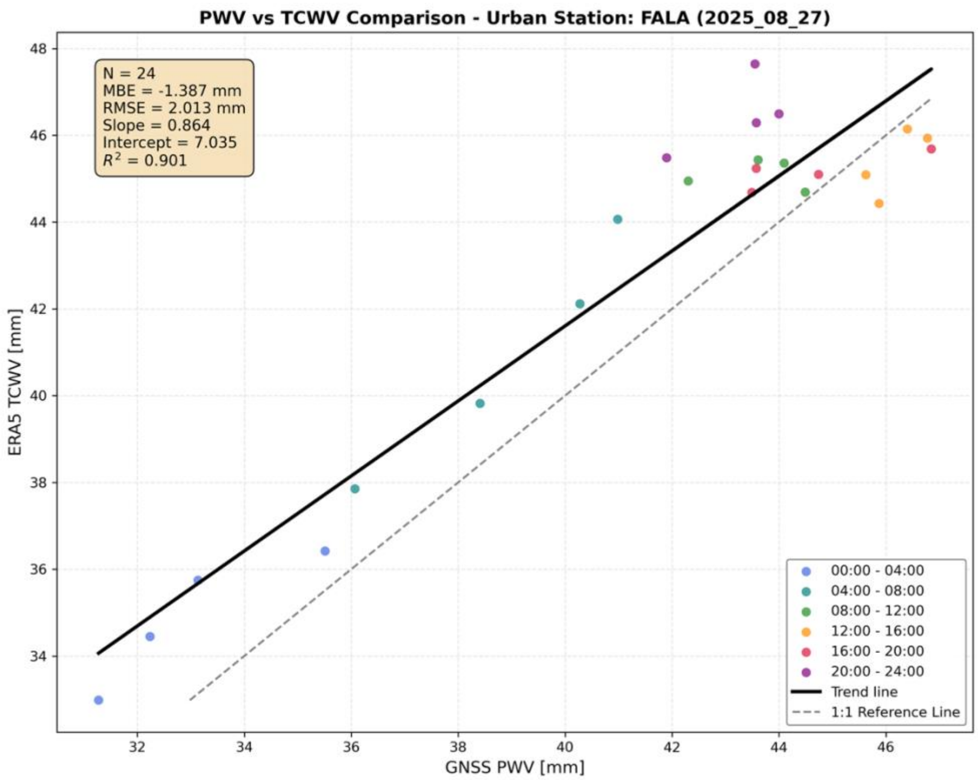

Figure 16. PWV vs. TCWV on August 27th in an Italian Station

4.3. Scenario 3: Peak Hourly Extreme Event

4.3.1. Urban Station (FALA)

Figure 17 highlights an extreme storm. The water vapor level maintains high all day. Right as the PWV reached to its daily peak, which is 48 mm in the evening, it causes a heavy rainfall measuring over 18 mm. Immediately following this summer rainfall, the PWV curve drops quickly as the heavy rain completely empties the moisture in the air. As shown in Figure 18, the storm causes a significant reduction in correlation and growth in error. This is typical issue, where a global model (ERA5) fails to align with rapid and local atmospheric events, while they can be captured in real time by ground-based GNSS.

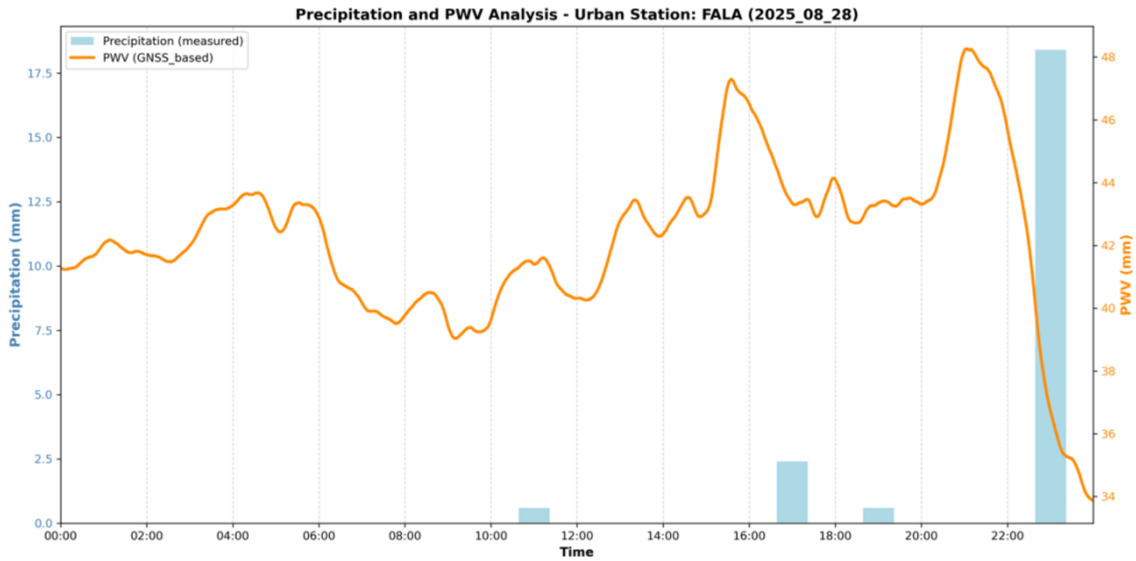

Figure 17. Precipitation vs. PWV on August 28th in an Italian Station

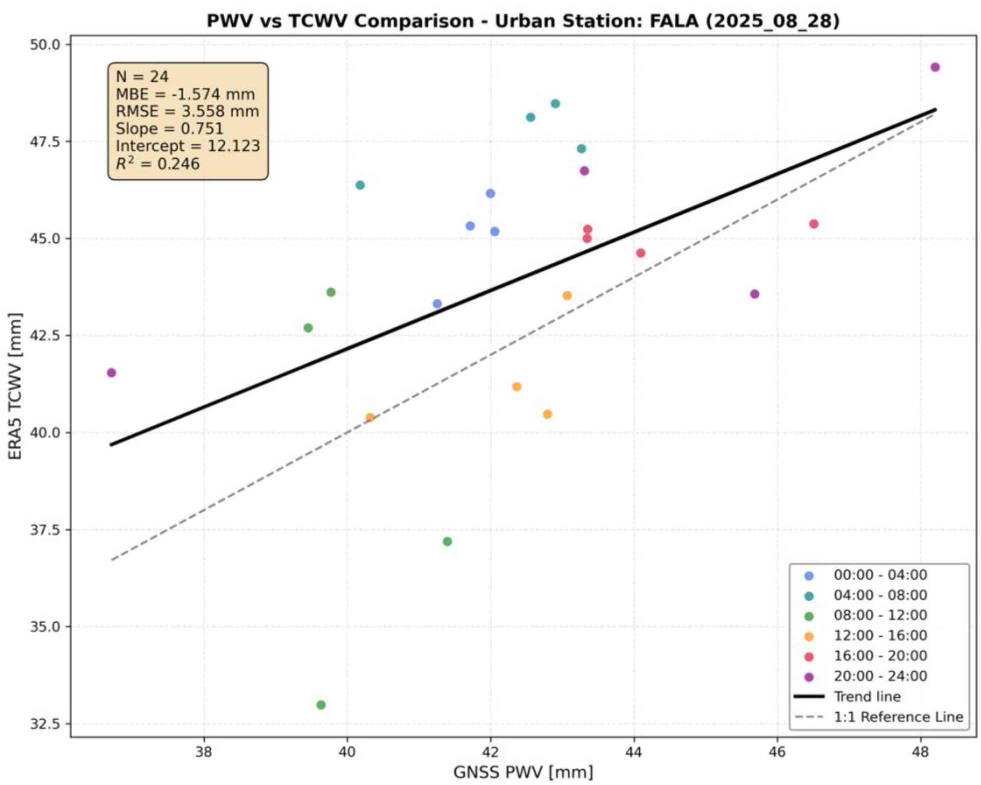

Figure 18. PWV vs. TCWV on August 28th in an Italian Station

4.3.2. Mountainous Station (SAVE)

Figure 19 beautifully tracks a storm in the mountains. At the midnight, small rain showers occur while the PWV remains at high level of 27 mm. Then in the morning drops down to 16 mm, and then moisture rapidly recovers. It peaks at 23 mm around 15:00, causing a massive precipitation of over 28 mm of rain in a single hour. Right after this heavy rainfall, the PWV drops sharply to 15 mm as the storm empties the air. The scatter plot in Figure 20 shows a strong correlation. However, the storm causes a high error and shift. This happens because global gridded models struggle to capture sudden, massive moisture specially over mountain slopes.

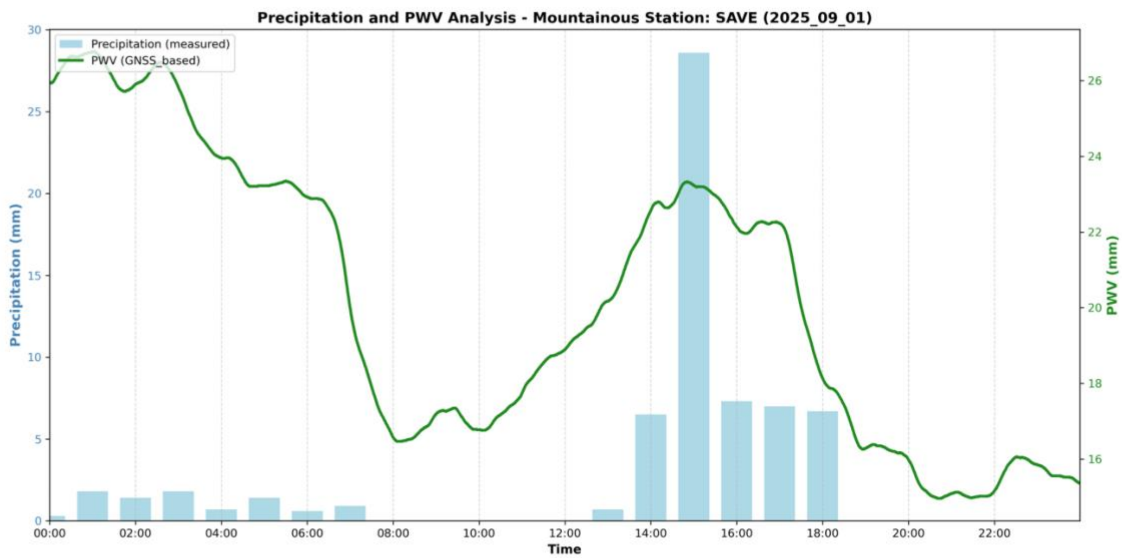

Figure 19. Precipitation vs. PWV on September 1st in a Swiss Station

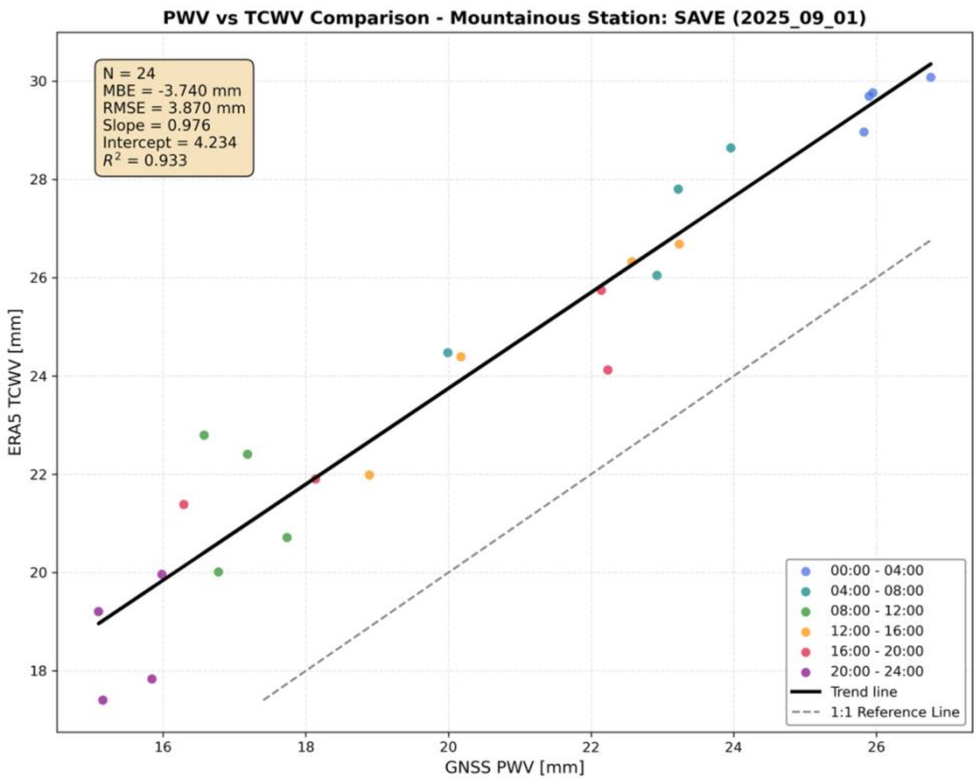

Figure 20. PWV vs. TCWV on September 1st in a Swiss Station

4.4. Scenario 4: Sustained and Low-Intensity

4.4.1. Urban Station (FALA)

The time-series in Figure 21 indicates a consistently wet day. Unlike the single peak seen in Scenario 3, this scenario features a steady, multi hour sequence of low intensity rain. Because the rain is light, the air does not become instantly empty of water vapor. Instead, the PWV remains high and only after the continuous rain completely stops, reduces slightly. According to Figure 22, the model achieves a strong correlation and a minimal bias.

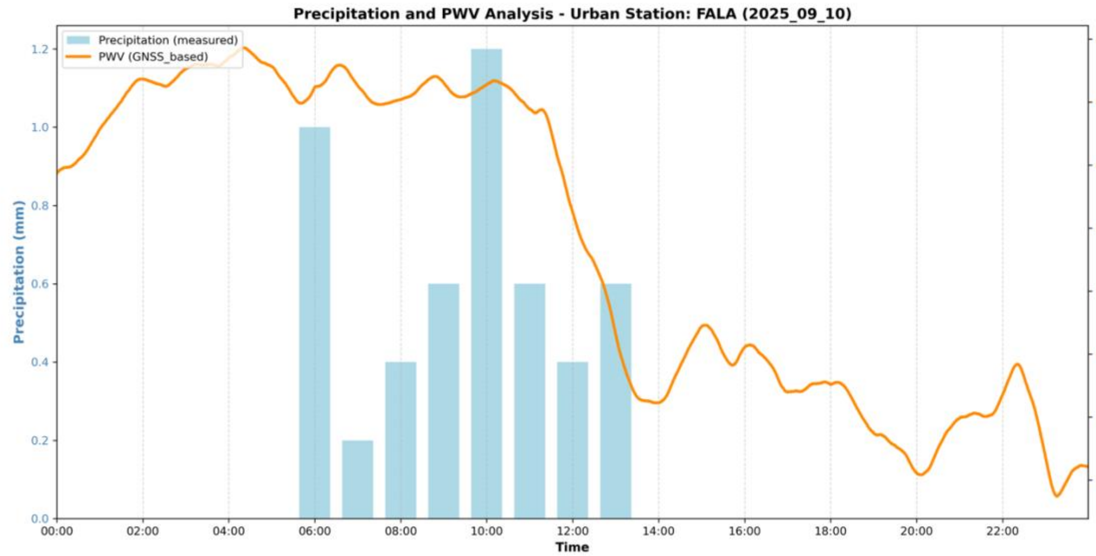

Figure 21. Precipitation vs. PWV on September 10th in an Italian Station

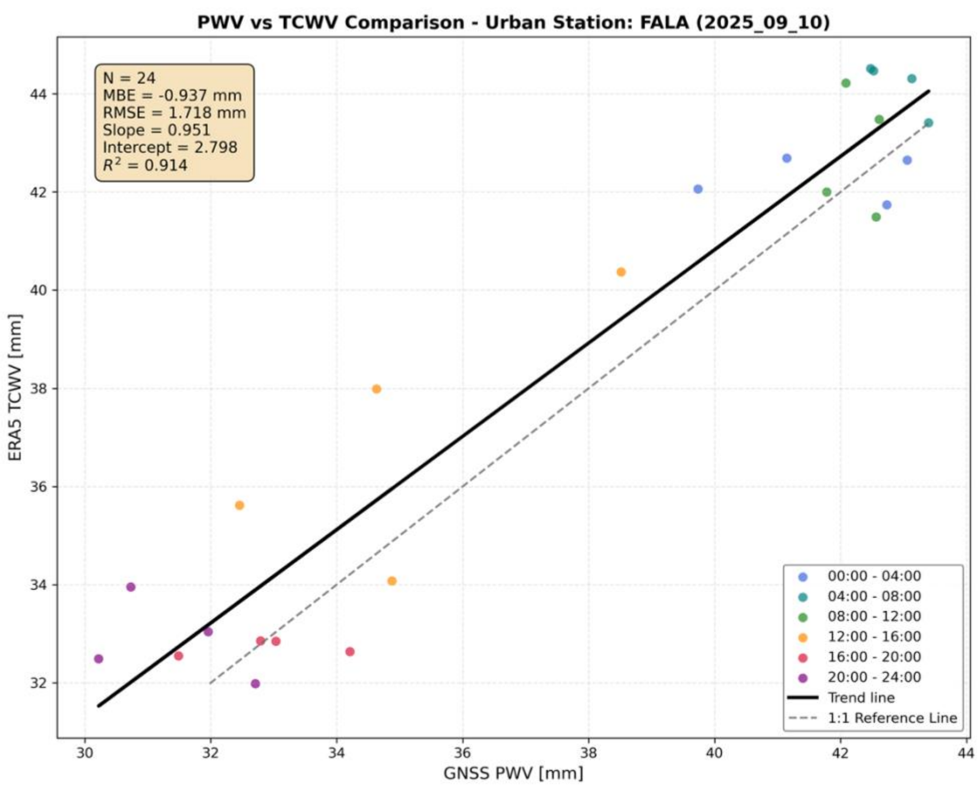

Figure 22. PWV vs. TCWV on September 10th in an Italian Station

4.4.2. Coastal Station (NICE)

Figure 23 shows a long term and low intensity precipitation event. This day features a scattered rainfall. Because the precipitation is sustained and the air is constantly supplied by the sea, it does not immediately drop. Instead, the water vapor drops slightly after the rainfall but recovers rapidly. The scatter plot in Figure 24 demonstrates a reliable agreement between the datasets during rainy weather, achieving a good correlation and a low error. The data points are more scattered compared to the dry day, which is a typical error for coastal areas, where rapid changes in ocean air make it difficult for gridded reanalysis models to capture local hourly changes.

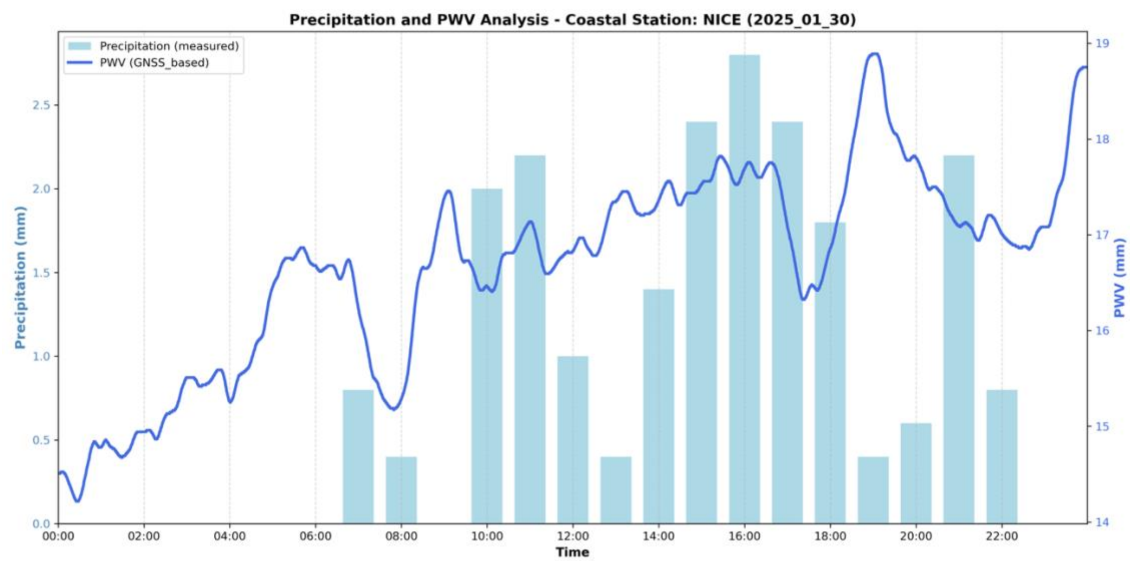

Figure 23. Precipitation vs. PWV on January 30th in a French Station

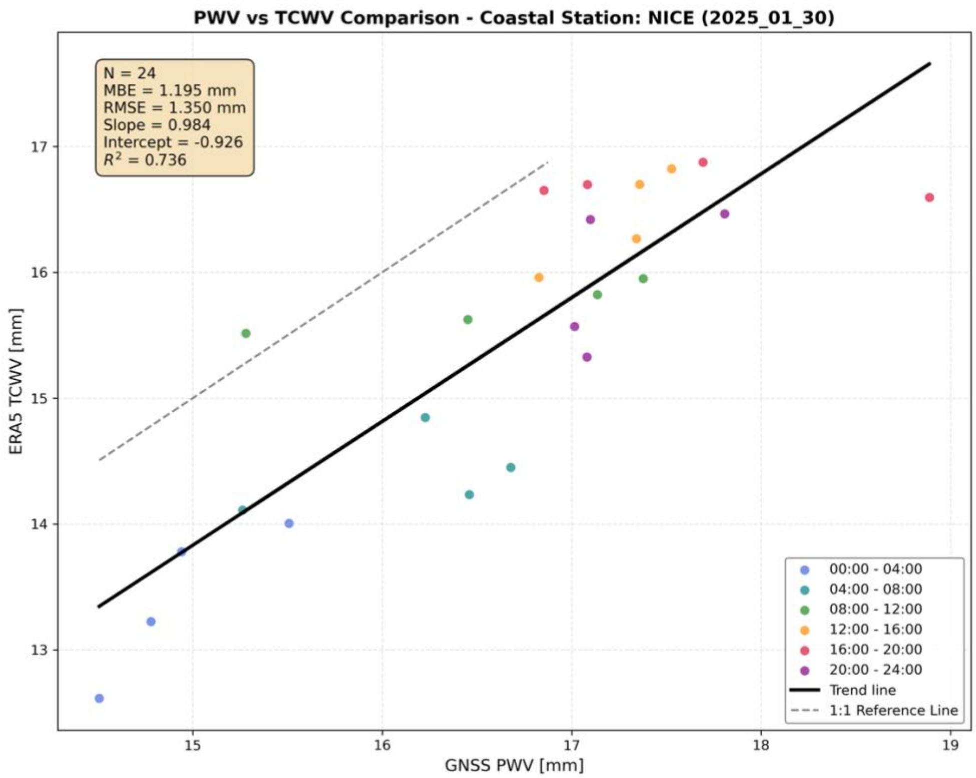

Figure 24. PWV vs. TCWV on January 30th in a French Station

4.4.3. Mountainous Station (SAVE)

The time-series in Figure 25 illustrates a rainy day, where a moderate rainfall is seen continuously. Because the rain is steady, the PWV remains locked at a high level for the first 9 hours. Once the first rain stops after 13:00, the PWV falls sharply and then picking up slightly during the evening showers before decreasing again. According to Figure 26, the model behaves satisfactory during long rain events, reaching a high correlation. Moreover, the error drops, proving that the datasets match when weather patterns are steady.

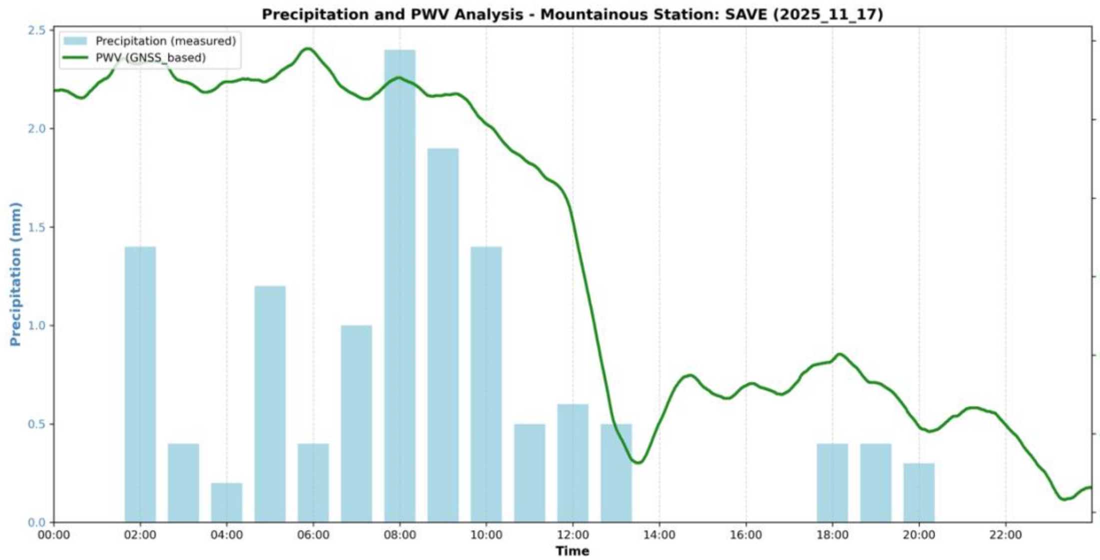

Figure 25. Precipitation vs. PWV on November 17th in a Swiss Station

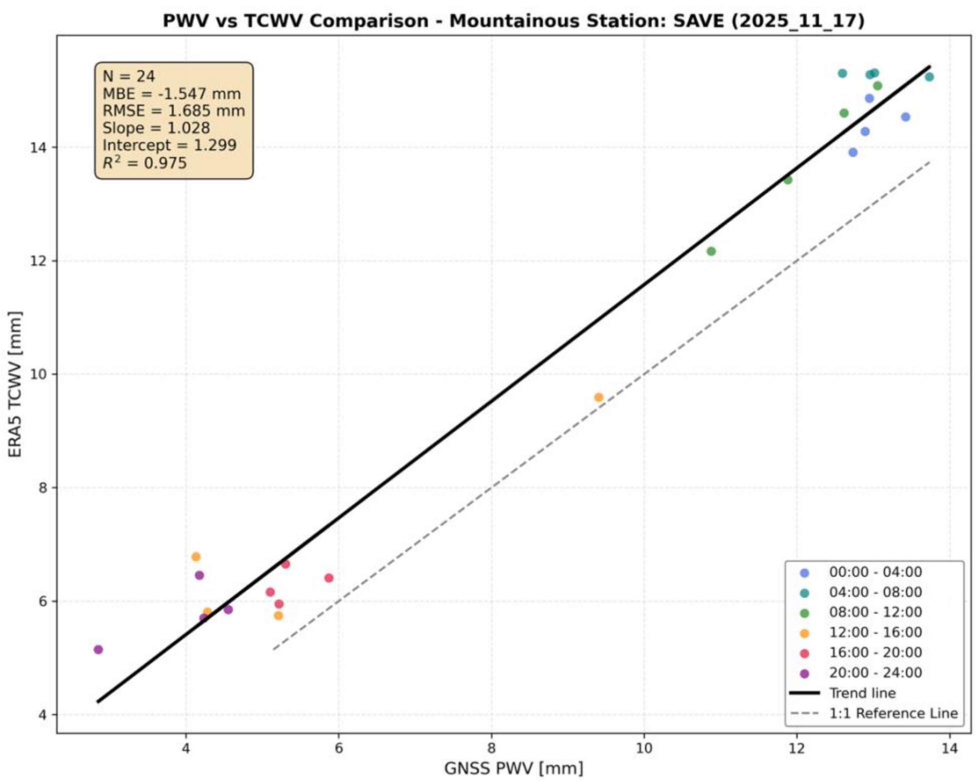

Figure 26. PWV vs. TCWV on November 17th in a Swiss Station

4.5. All Available Days

The statistical evaluation of the GNSS-derived PWV against the Copernicus ERA5 TCWV was also performed across all available days in three distinct environmental topologies: urban (FALA), coastal (NICE), and mountainous (SAVE). The comprehensive scatter plots and linear regression metrics for each station are presented in Figures 27, 28, and 29, respectively. In addition, Table 4 indicate the comprehensive statistical metrices for all the stations in all available days.

4.5.1. Urban Station (FALA)

The highest R^2 value among all stations indicates that the GNSS processing accurately tracks atmospheric moisture. The RMSE magnitude represents high precision, with data points well clustered around the reference line. A negative value of MBE demonstrates a small underestimation by the GNSS relative to ERA5. Regression slope is very close to the ideal unity (1:1), showing strong alignment.

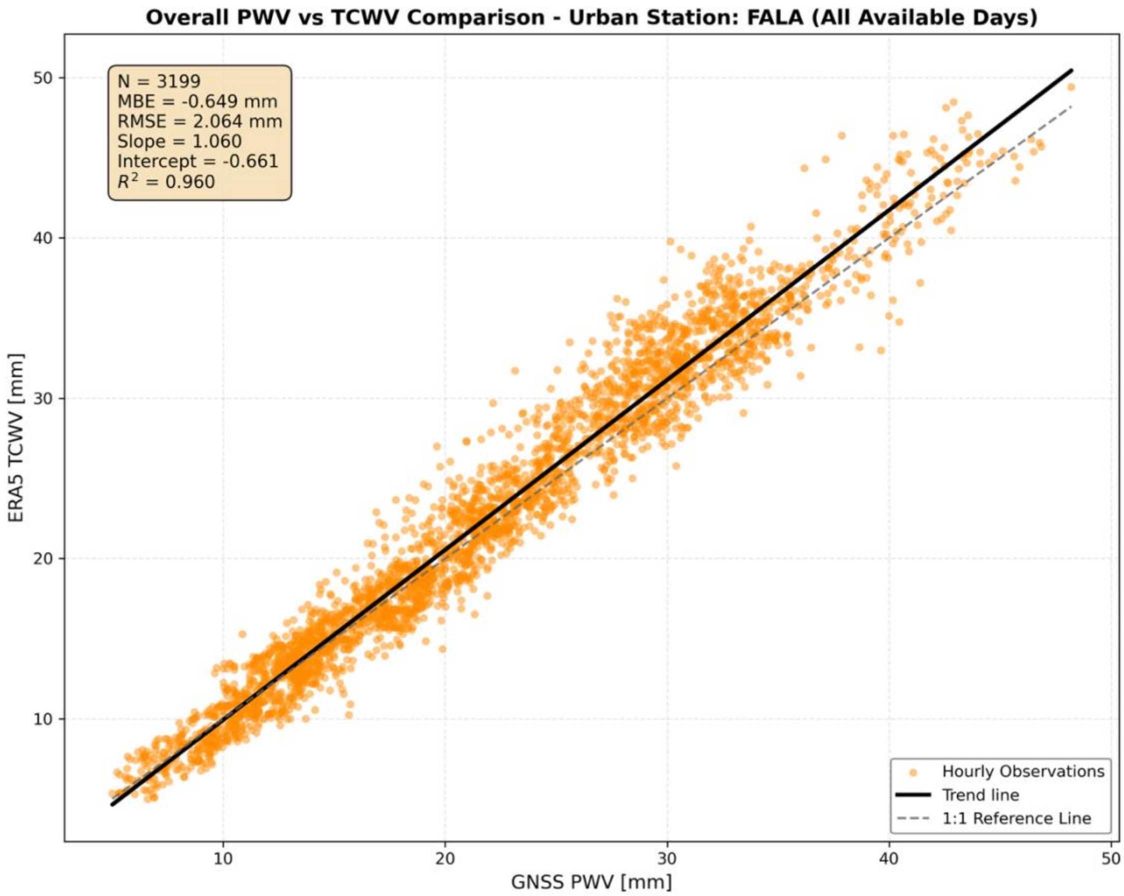

Figure 27. PWV vs. TCWV in an Italian Station

4.5.2. Coastal Station (NICE)

This station shows the lowest RMSE, proving that the distance between the model and ERA5 is small. Also, MBE remains negligible, meaning the overall GNSS-PWV dataset is closely aligned with the reanalysis data, showing minimal systematic bias. While R^2 remains very high, the lower slope shows that the model overestimates very wet days and underestimates very dry days. This might be a justifiable issue near the sea, where land sea breezes change the air. The lower number of data points might be due to the reflection of satellite signals from the sea surface before reaching the GNSS antenna. These reflections lead to noisy data that get filtered out by CSRS-PPP.

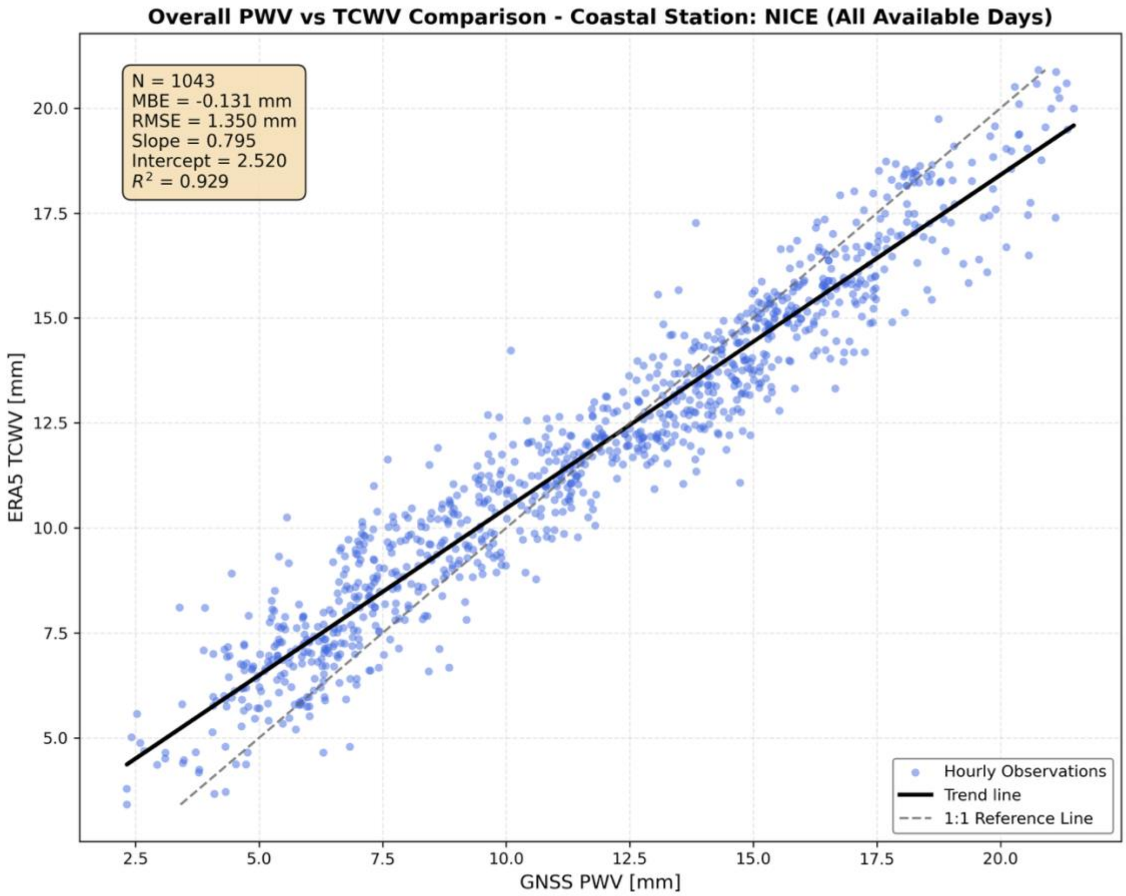

Figure 28. PWV vs. TCWV in a French Station

4.5.3. Mountainous Station (SAVE)

High-altitude environments introduce intense topographic complexities. First of all, the largest dataset, provides a high statistical confidence. However, this station has the highest MBE. This high negative bias shows that the GNSS model underestimates the moisture compared to ERA5. It is acceptable, because the ERA5 model is based on a gridded spatial resolution that flattens the terrain. Consequently, the model neglects the sudden humidity fluctuations that naturally occur along mountain peaks and deep valleys.

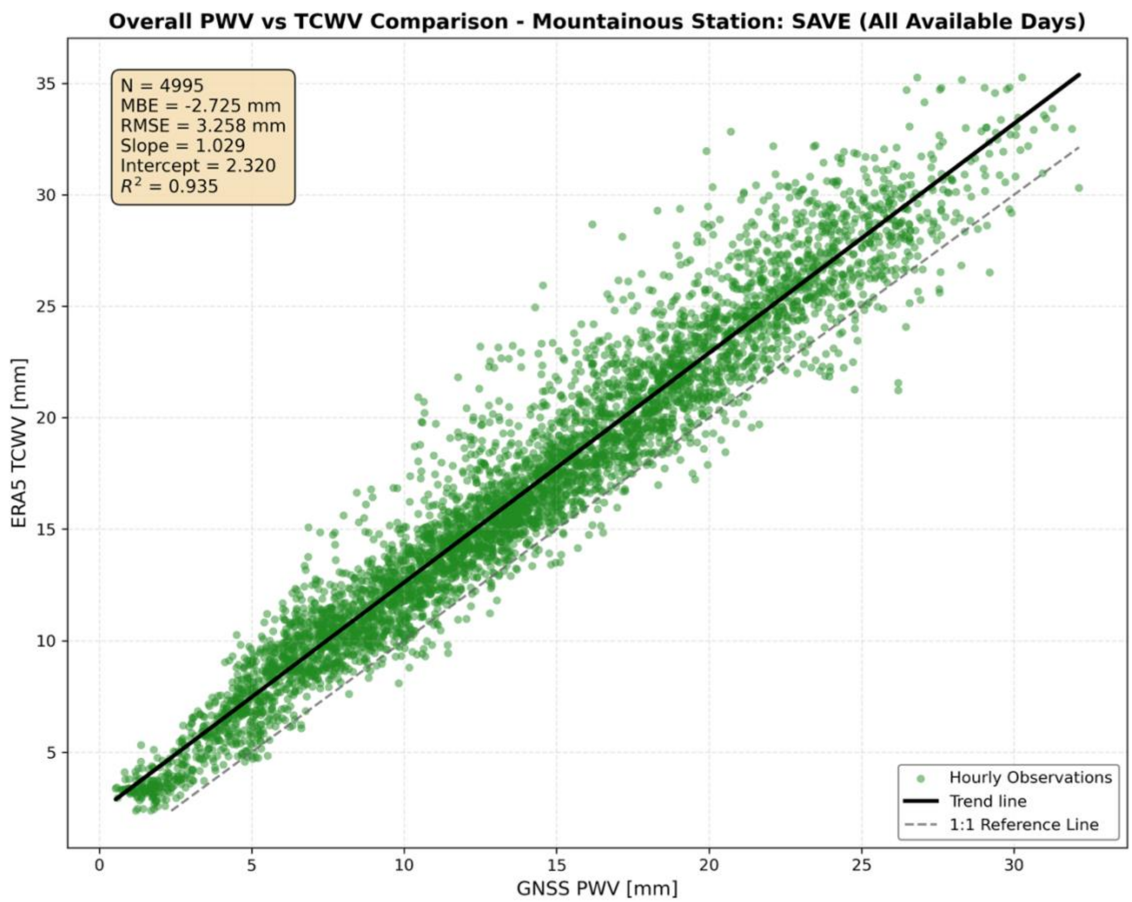

Figure 29. PWV vs. TCWV in a Swiss Station

Table 4. Statistical Metrics of All Stations and All Available Days

Station	Elevation (m)	N	MBE (mm)	RMSE (mm)	Slope	Intercept (mm)	R^2 (mm)
FALA	67.32	3199	-0.65	2.06	1.06	-0.66	0.96
NICE	427.31	1043	-0.13	1.35	0.80	2.52	0.93
SAVE	1028.37	4995	-2.73	3.26	1.03	2.32	0.94

4.5.4. Comparative Environmental Discussion

A comprehensive look at the three outputs indicates that topography and climate heavily influence validation metrics. In flat zone (FALA), the absence of altitude fluctuations allows the gridded ERA5 model and the point-based GNSS receiver to see almost the exact same water vapor, which was the highest. In coastal zone (NICE), the precision is good, but the land sea condition causes a change in the bias according to wet and dry hours. In mountainous zone

(SAVE), the limitations of reanalysis models in sub-grid complex terrain, causes the higher RMSE and Bias, even though the GNSS outputs have a promising tracking capability.

Furthermore, the behavior of PWV matches the seasonal patterns of atmospheric moisture. During warmer periods (such as August and September), higher temperatures lead to more water vapor in the air, creating larger and more frequent PWV oscillations. Conversely, during colder periods (such as November and January), the low moisture content naturally leads to a more stable and with minimal fluctuations.

The statistical comparison confirms that the developed GNSS-PWV processing is reliable, robust, and scientific, proving that the GNSS tracking of atmospheric water vapor can be confidently utilized for real time meteorological applications and storm forecasting.

In conclusion, while the processing achieves strong accuracy in flat urban settings, the two other climate represents their own pattern. In coastal zones, the main obstacle is data gaps caused by marine signal noise and GNSS disconnections. In contrast, the mountainous zone proves that global models such as ERA5 need support from local and high-resolution GNSS networks to capture moisture changes over complex mountain altitudes. Table 5 provides a compact comparison of hourly rainfall maximum value, PWV maximum value and its variations during the day under peak hourly extreme and sustained low-intensity rainfall conditions. It should be mentioned that lead time is the time difference between the occurrence of maximum PWV and the occurrence of maximum hourly rainfall. The negative lead time observed for the NICE on January 30th, indicates that the maximum hourly rainfall occurred before the maximum PWV. This suggests that, for this continuous and low-intensity event, PWV did not act as a clear indicator to rainfall intensity, but rather continued to increase after the rainfall peak.

Table 5. Summary of PWV variations and rainfall characteristics

Station	Weather Scenario	Date	Max. PWV (mm)	ΔPWV (mm)	Lead Time (min.)	Max. Hourly Rainfall (mm)
FALA	Peak Hourly Extreme event	2025.8.28	48.26	14.39	118	18.4
	Sustained and low intensity	2025.9.10	43.73	14.24	340	1.2
NICE	Sustained and low intensity	2025.1.30	18.89	4.67	-186	2.8
SAVE	Peak Hourly Extreme event	2025.9.1	26.76	11.80	120	28.6
	Sustained and low intensity	2025.11.17	13.80	11.48	130	2.4

5. Conclusion

In this study the potential of GNSS-derived Precipitable Water Vapor (PWV) for atmospheric moisture monitoring and its capability as a complementary indicator for short-term rainfall forecasting in different climates and elevations was evaluated. The processing was developed by integrating GNSS observations, ERA5 reanalysis data, and actual precipitation measurements. Zenith Wet Delay (ZWD) timeseries were estimated through Precise Point Positioning (PPP) processing and converted into PWV timeseries using physical conversion models, which led to continuous monitoring of atmospheric water vapor at high temporal resolution, resulting in its variability assessment associated with precipitation occurrence.

The methodology was implemented on three GNSS stations representing urban (FALA), coastal (NICE), and mountainous (SAVE) environments. The comparison results demonstrated an acceptable correlation between GNSS-derived PWV and ERA5 Total Column Water Vapor (TCWV). The obtained statistical metrics indicated a good agreement between GNSS-derived PWV and ERA5 estimates, confirming the capability of GNSS observations to calculate atmospheric water vapor in distinct climates and elevations.

The comparative analysis highlighted the influence of topography and local climate conditions on the model's performance. The urban station achieved the highest overall agreement with ERA5, while the coastal station showed deviations attributed to two primary reasons. First, representativeness of reanalysis data in land–sea interactions and rapid moisture changes. Second, the potential filtering of multipath-affected observations within the CSRS-PPP processing, due to sea-surface reflections. The mountainous station showed larger biases and errors, mainly due to the limitations of reanalysis data in representing complex terrain and high topographic gradient. Nevertheless, GNSS-derived PWV is strongly able to monitor atmospheric moisture variability even in high elevations and rapid change conditions.

The rainfall event analysis demonstrated the capability of GNSS-derived PWV in meteorological analysis. Different PWV patterns were observed for four days, including dry, pre-storm, extreme rainfall events, and sustained low intensity. In several cases, significant increases in PWV were detected before rainfall initiated, indicating that atmospheric moisture accumulation can be identified before precipitation. During extreme storms, PWV reached high levels, and afterwards rapidly decreased just after rainfall initiation. However, sustained precipitation events displayed continuously high PWV values. These observations confirm that GNSS-derived PWV can provide valuable information regarding atmospheric moisture variations. Thus, the incorporation of GNSS-derived PWV into traditional weather prediction systems may enhance its capabilities, as it may be adopted as an effective complementary indicator for short-term rainfall forecasting, particularly in coastal and mountainous regions.

Overall, the mentioned methodology produced consistent results across diverse environmental conditions. The results demonstrate that GNSS-derived PWV represents a cost-effective and high-temporal-resolution atmospheric parameter capable of supporting meteorological monitoring and providing complementary information for precipitation forecasting purposes.

5.1. Limitations

First, the analysis was performed using only three GNSS stations representing specific urban, coastal, and mountainous climates. Although these stations were selected to consider different climates and topographies, a larger number of GNSS stations would provide a more comprehensive analysis of spatial variability.

Second, the comparison was performed against ERA5 TCWV data. While ERA5 is scientifically validated reanalysis data, simultaneously it is a model-based dataset rather than a direct observation. Consequently, part of the observed difference may rise from uncertainties within the reanalysis data itself.

Third, the current analysis focused specifically on the year 2025 and therefore does not fully consider long-term climate variability. The temporal coverage is sufficient for investigating short-term atmospheric moisture variations but limited for evaluating long-term decadal climate trends.

Fourth, the ZWD was converted to PWV using the weighted mean temperature (T_m) from Bevis (1992) relationship, which was originally calibrated using North American radiosonde observations. Although it is widely used, it may introduce a small systematic bias for estimation of PWV in European mid-latitudes, particularly at the mountainous SAVE station. Other models that estimate T_m, such as GPT3[10] or ERA5 would have been an alternative.

Fifth, data coverage varied considerably among the investigated stations, meaning that the stations lacked full temporal coverage for the entire year. These gaps in data availability affects statistical robustness of the results, particularly for NICE station, where data availability was more limited due to coastal modeling and signal multipath.

Sixth, rainfall generation is influenced by many other atmospheric factors beyond PWV. Temperature, pressure, humidity, and wind play significant roles in rainfall generation. Therefore, PWV should be considered as an important complementary parameter for rainfall prediction rather than an independent predictor.

5.2. Future Work

A natural next step of this study is extending to multiyear datasets. Thus, long-term variability of PWV can be investigated. Such studies could contribute to a better understanding of the climate-driven changes in the regional hydrological cycle.

Another obvious step is extending the coverage and incorporating additional stations across different regions, which would enhance the spatial diversity and allow for large-scale analysis of PWV.

Future studies may also integrate GNSS-derived PWV with additional meteorological variables, including temperature, relative humidity, atmospheric pressure, and wind velocity. Merging these parameters may increase forecasting reliability.

[10] *Global Pressure and Temperature*

Another important next step is the independent validation of GNSS-derived PWV against different reference datasets, such as radiosonde measurements or EUREF GNSS stations. This validation would help evaluate PWV accuracy and also uncertainties related to the processing and the conversion models.

Finally, integrating machine learning and artificial intelligence techniques with high-resolution GNSS-derived PWV allows the development of predictive models in order to figure out the complex relationships between PWV and precipitation.

Such developments would further strengthen the role of GNSS meteorology as a valuable tool for environmental monitoring, hydrological applications, and climate research.

References

[1] M. Bevis, S. Businger, T. A. Herring, C. Rocken, R. A. Anthes, and R. H. Ware, “GPS meteorology: Remote sensing of atmospheric water vapor using the global positioning system,” J. Geophys. Res. Atmospheres, vol. 97, no. D14, pp. 15787–15801, Oct. 1992, do

[2] J. M. Wallace and P. V. Hobbs, Atmospheric science: an introductory survey, 2nd ed. in International geophysics series, no. volume 92. Amsterdam Paris: Academic press, 2006.

[3] K. E. Trenberth, J. Fasullo, and L. Smith, “Trends and variability in column-integrated atmospheric water vapor,” Clim. Dyn., vol. 24, no. 7–8, pp. 741–758, Jun. 2005, doi: 10.1007/s00382-005-0017-4.

[4] Intergovernmental Panel On Climate Change (IPCC), Climate Change 2021 – The Physical Science Basis: Working Group I Contribution to the Sixth Assessment Report of the Intergovernmental Panel on Climate Change, 1st ed. Cambridge University Press, 2023. doi

[5] G. Guerova et al., “Review of the state of the art and future prospects of the ground-based GNSS meteorology in Europe,” Atmospheric Meas. Tech., vol. 9, no. 11, pp. 5385–5406, Nov. 2016, doi: 10.5194/amt-9-5385-2016.

[6] D. M. Tralli and S. M. Lichten, “Stochastic estimation of tropospheric path delays in global positioning system geodetic measurements,” vol. 64, 1990, doi: https://doi.org/10.1007/BF02520642.

[7] M. Bevis et al., “GPS Meteorology: Mapping Zenith Wet Delays onto Precipitable Water,” J. Appl. Meteorol., vol. 33, no. 3, pp. 379–386, 1994.

[8] J. Vaquero-Martínez and M. Antón, “Review on the Role of GNSS Meteorology in Monitoring Water Vapor for Atmospheric Physics,” Remote Sens., vol. 13, no. 12, p. 2287, Jun. 2021, doi: 10.3390/rs13122287.

[9] P. Dabove and M. Bagheri, “Enhancing Atmospheric Monitoring Capabilities: A Comparison of Low- and High-Cost GNSS Networks for Tropospheric Estimations,” Remote Sens., vol. 16, no. 12, p. 2223, Jun. 2024, doi: 10.3390/rs16122223.

[10] J. F. Zumberge, M. B. Heflin, D. C. Jefferson, M. M. Watkins, and F. H. Webb, “Precise point positioning for the efficient and robust analysis of GPS data from large networks,” J. Geophys. Res. Solid Earth, vol. 102, no. B3, pp. 5005–5017, Mar. 1997, doi:

[11] Y. Liu, Q. Zhao, Z. Li, Y. Yao, and X. Li, “GNSS-derived PWV and meteorological data for short-term rainfall forecast based on support vector machine,” Adv. Space Res., vol. 70, no. 4, pp. 992–1003, Aug. 2022, doi: 10.1016/j.asr.2022.05.057.

[12] Q. Zhao, Y. Liu, X. Ma, W. Yao, Y. Yao, and X. Li, “An Improved Rainfall Forecasting Model Based on GNSS Observations,” IEEE Trans. Geosci. Remote Sens., vol. 58, no. 7, pp. 4891–4900, Jul. 2020, doi: 10.1109/TGRS.2020.2968124.

[13] Y. Yao, L. Shan, and Q. Zhao, “Establishing a method of short-term rainfall forecasting based on GNSS-derived PWV and its application,” Sci. Rep., vol. 7, no. 1, p. 12465, Sep. 2017, doi: 10.1038/s41598-017-12593-z.

[14] H. Li et al., “Development of an Improved Model for Prediction of Short-Term Heavy Precipitation Based on GNSS-Derived PWV,” Remote Sens., vol. 12, no. 24, p. 4101, Dec. 2020, doi: 10.3390/rs12244101.
[15] L. Huang et al., “High-precision GNSS PWV retrieval using dense GNSS sites and in-situ meteorological observations for the evaluation of MERRA-2 and ERA5 reanalysis products over China,” Atmospheric Res., vol. 276, p. 106247, Oct. 2022, doi: 10.1016/j.atm
[16] P. Gao and J. Cui, “Comparisons of precipitable water vapor and zenith total delay derived from GNSS measurements, radiosondes, and ERA5 reanalysis data in the contiguous United States,” J. Atmospheric Sol.-Terr. Phys., vol. 280, p. 106741, Mar. 2026, doi
[17] L. Huang et al., “Evaluation of Hourly PWV Products Derived From ERA5 and MERRA-2 Over the Tibetan Plateau Using Ground-Based GNSS Observations by Two Enhanced Models,” Earth Space Sci., vol. 8, no. 5, p. e2020EA001516, May 2021, doi: 10.1029/2020EA001516
[18] F. Yang et al., “Spatiotemporal distribution and impact factors of GNSS-PWV in China based on climate region,” Adv. Space Res., vol. 73, no. 8, pp. 4187–4201, Apr. 2024, doi: 10.1016/j.asr.2024.01.022.
[19] H. G. Mawandha, M. Kishimoto, Sulistiyani, and S. Oishi, “GNSS-based PWV Application for Short Term Rainfall Prediction in Mountainous Region,” IOP Conf. Ser. Earth Environ. Sci., vol. 355, no. 1, p. 012070, Nov. 2019, doi: 10.1088/1755-1315/355/1/012070.
[20] P. Zhao, F. Ke, H. Wu, and M. Wei, “Spatiotemporal distribution of GNSS-derived PWV in Australia from 2010 to 2019,” Geod. Geodyn., vol. 16, no. 4, pp. 454–464, Jul. 2025, doi: 10.1016/j.geog.2024.12.006.
[21] C. Rocken et al., “GPS/STORM—GPS Sensing of Atmospheric Water Vapor for Meteorology,” J. Atmospheric Ocean. Technol., vol. 12, no. 3, pp. 468–478, 1995.
[22] Guide to Meteorological Instruments and Methods of Observation. Geneva: World Meteorological Organization, 2023.
[23] M. Schröder, M. Lockhoff, J. M. Forsythe, H. Q. Cronk, T. H. Vonder Haar, and R. Bennartz, “The GEWEX Water Vapor Assessment: Results from Intercomparison, Trend, and Homogeneity Analysis of Total Column Water Vapor,” J. Appl. Meteorol. Climatol., vol. 55
[24] M. A. Janssen, Ed., Atmospheric remote sensing by microwave radiometry. in Wiley series in remote sensing. New York, NY: Wiley, 1993.
[25] J. L. Davis, T. A. Herring, I. I. Shapiro, A. E. E. Rogers, and G. Elgered, “Geodesy by radio interferometry: Effects of atmospheric modeling errors on estimates of baseline length,” Radio Sci., vol. 20, no. 6, pp. 1593–1607, Nov. 1985, doi: 10.1029/RS020
[26] J. Kouba and P. Heroux, “Precise Point Positioning using IGS orbit and clock products,” GPS Solut., vol. 5, 2001.
[27] J. Mendez Astudillo, L. Lau, Y.-T. Tang, and T. Moore, “Analysing the Zenith Tropospheric Delay Estimates in On-line Precise Point Positioning (PPP) Services and PPP Software Packages,” Sensors, vol. 18, no. 2, p. 580, Feb. 2018, doi: 10.3390/s18020580.

[28] S. Barindelli, E. Realini, G. Venuti, A. Fermi, and A. Gatti, “Detection of water vapor time variations associated with heavy rain in northern Italy by geodetic and low-cost GNSS receivers,” Earth Planets Space, vol. 70, no. 1, p. 28, Dec. 2018, doi: 10.1
[29] S. Serrano-Vincenti et al., “Harmonic Analysis of the Relationship between GNSS Precipitable Water Vapor and Heavy Rainfall over the Northwest Equatorial Coast, Andes, and Amazon Regions,” Atmosphere, vol. 13, no. 11, p. 1809, Oct. 2022, doi: 10.3390/atmo
[30] P. Benevides, J. Catalao, and G. Nico, “Neural Network Approach to Forecast Hourly Intense Rainfall Using GNSS Precipitable Water Vapor and Meteorological Sensors,” Remote Sens., vol. 11, no. 8, p. 966, Apr. 2019, doi: 10.3390/rs11080966.
[31] D. Giannadaki, C. Oikonomou, and H. Haralambous, “Correlation of precipitable water vapor and heavy rainfall over Cyprus using GNSS sensors network,” Front. Signal Process., vol. 5, p. 1622256, Sep. 2025, doi: 10.3389/frsip.2025.1622256.
[32] H. Hersbach et al., “The ERA5 global reanalysis,” Q. J. R. Meteorol. Soc., vol. 146, no. 730, pp. 1999–2049, Jul. 2020, doi: 10.1002/qj.3803.
[33] Z. Sun, B. Zhang, and Y. Yao, “An ERA5-Based Model for Estimating Tropospheric Delay and Weighted Mean Temperature Over China With Improved Spatiotemporal Resolutions,” Earth Space Sci., vol. 6, no. 10, pp. 1926–1941, Oct. 2019, doi: 10.1029/2019EA000701.
[34] A. Maciejewska, “Use of Tropospheric Delay in GNSS-Based Climate Monitoring—A Review,” Remote Sens., vol. 17, no. 9, p. 1501, Apr. 2025, doi: 10.3390/rs17091501.
[35] T. A. F. Gouveia et al., “Analysis of atmospheric variations using GNSS signal as atmospheric sensor (PWV-GNSS) in the extreme rainfall events in Rio Grande do Sul (Brazil) in 2024,” Nat. Hazards, vol. 122, no. 5, p. 212, Mar. 2026, doi: 10.1007/s11069-02

Appendix: Statistical Indices and Daily Plots[11]

1. FALA

No.	Date	N	MBE (mm)	RMSE (mm)	R^2
1	2025-08-05	13	-4.25	4.67	0.57
2	2025-08-06	24	0.49	1.56	0.91
3	2025-08-07	24	-2.71	2.79	0.80
4	2025-08-08	24	-3.17	3.48	0.07
5	2025-08-09	24	-3.99	4.28	0.38
6	2025-08-10	24	-3.64	4.06	0.58
7	2025-08-11	24	-3.37	4.02	0.40
8	2025-08-12	24	-2.84	3.78	0.00
9	2025-08-13	24	-4.46	5.05	0.37
10	2025-08-14	24	-2.49	3.26	0.06
11	2025-08-15	24	-0.57	1.55	0.27
12	2025-08-16	24	-0.81	1.42	0.18
13	2025-08-17	24	-1.28	2.21	0.55
14	2025-08-18	24	-2.01	2.72	0.69
15	2025-08-19	24	-2.97	3.58	0.68
16	2025-08-20	24	-2.62	3.72	0.07
17	2025-08-21	24	-0.53	1.80	0.60
18	2025-08-22	24	0.46	2.13	0.71
19	2025-08-23	24	-0.49	1.58	0.49
20	2025-08-24	24	-1.34	2.36	0.32
21	2025-08-25	24	-1.86	2.04	0.20
22	2025-08-26	24	-2.10	2.54	0.03
23	2025-08-27	24	-1.39	2.01	0.90
24	2025-08-28	24	-1.57	3.56	0.25
25	2025-08-29	24	-3.30	3.75	0.91
26	2025-08-30	24	-0.90	1.96	0.67
27	2025-09-01	24	-0.64	1.54	0.84
28	2025-09-02	24	-0.81	3.19	0.63
29	2025-09-03	24	-3.47	3.75	0.17
30	2025-09-04	24	-3.72	3.85	0.77
31	2025-09-05	24	-3.49	4.32	0.64
32	2025-09-06	24	-2.35	2.55	0.58
33	2025-09-07	24	-2.34	2.65	0.35
34	2025-09-08	24	-1.34	2.50	0.95
35	2025-09-09	24	-1.62	2.69	0.04
36	2025-09-10	24	-0.94	1.72	0.91
37	2025-09-11	22	-0.27	2.25	0.41
38	2025-09-12	22	-1.11	1.92	0.38
39	2025-09-13	13	-1.77	2.56	0.27
40	2025-09-15	10	-2.38	2.48	0.79
41	2025-09-17	3	-0.63	1.96	0.92
42	2025-09-18	14	-0.42	1.78	0.60
43	2025-09-19	24	-0.80	1.19	0.32

[11] *Notice that in some specific days, despite low RMSE and MBE, the low R^2, is a mathematical bias due to low atmospheric variance (stable or flat PWV trends), not data inaccuracy.*

44	2025-09-20	24	-1.80	2.29	0.93
45	2025-09-21	24	-3.68	4.01	0.73
46	2025-09-22	24	-1.27	2.81	0.74
47	2025-09-23	24	-1.60	2.74	0.41
48	2025-09-24	24	-3.00	3.63	0.65
49	2025-09-25	24	-0.11	1.11	0.73
50	2025-09-26	24	-1.65	2.05	0.67
51	2025-09-27	24	-2.27	2.97	0.14
52	2025-09-28	24	0.35	0.63	0.86
53	2025-09-30	24	-1.85	2.42	0.82
54	2025-10-01	10	-0.36	1.13	0.83
55	2025-10-02	12	0.46	0.54	0.53
56	2025-10-03	24	-0.50	1.17	0.81
57	2025-10-04	24	-0.78	1.79	0.86
58	2025-10-05	24	-0.11	2.22	0.90
59	2025-10-06	24	-0.98	1.29	0.73
60	2025-10-07	24	-0.37	0.55	0.92
61	2025-10-08	24	0.63	1.02	0.35
62	2025-10-09	24	-1.15	2.01	0.30
63	2025-10-10	24	-0.90	1.29	0.29
64	2025-10-11	24	-1.97	2.01	0.54
65	2025-10-12	24	0.33	0.94	0.19
66	2025-10-13	24	-0.75	0.87	0.15
67	2025-10-15	24	-0.94	1.45	0.75
68	2025-10-16	23	-1.24	1.94	0.13
69	2025-10-17	24	-0.90	1.36	0.34
70	2025-10-18	24	-0.39	0.80	0.75
71	2025-10-19	24	-1.25	1.38	0.83
72	2025-10-20	24	0.30	1.02	0.95
73	2025-10-21	24	0.08	0.97	0.66
74	2025-10-22	24	0.30	0.87	0.65
75	2025-10-23	24	-0.62	1.63	0.98
76	2025-10-25	24	-0.66	1.27	0.83
77	2025-10-28	24	-1.37	1.49	0.91
78	2025-10-30	24	0.87	1.27	0.70
79	2025-10-31	24	0.46	0.68	0.97
80	2025-11-01	24	-1.03	1.32	0.88
81	2025-11-02	24	-0.60	1.61	0.90
82	2025-11-03	24	-2.25	2.38	0.41
83	2025-11-04	24	-0.67	1.07	0.67
84	2025-11-05	24	-0.72	1.00	0.94
85	2025-11-06	24	-1.10	1.18	0.87
86	2025-11-07	24	-0.37	0.76	0.44
87	2025-11-08	24	0.61	0.77	0.24
88	2025-11-09	24	-0.44	0.77	0.66
89	2025-11-10	24	-0.98	1.12	0.84
90	2025-11-11	24	-1.04	1.23	0.71
91	2025-11-12	22	-0.71	1.00	0.66
92	2025-11-13	23	-0.41	0.86	0.30
93	2025-11-14	23	-0.20	0.71	0.91
94	2025-11-15	24	0.75	1.62	0.36

95	2025-11-16	24	-0.68	1.49	0.75
96	2025-11-17	24	-0.98	2.00	0.64
97	2025-11-18	24	2.41	2.94	0.89
98	2025-11-19	24	0.90	1.09	0.93
99	2025-11-20	16	0.53	1.63	0.12
100	2025-11-21	23	1.13	1.40	0.27
101	2025-11-22	24	1.61	1.77	0.30
102	2025-11-23	24	1.04	1.10	0.98
103	2025-11-24	24	2.13	2.19	0.82
104	2025-11-25	24	0.65	0.88	0.95
105	2025-11-26	24	1.62	1.68	0.66
106	2025-11-27	24	0.93	1.16	0.75
107	2025-11-28	24	0.73	0.84	0.92
108	2025-11-29	24	1.20	1.29	0.87
109	2025-11-30	23	0.07	0.64	0.98
110	2025-12-01	24	1.39	1.48	0.70
111	2025-12-02	24	0.99	1.01	0.84
112	2025-12-03	24	0.58	0.76	0.49
113	2025-12-04	24	0.72	1.01	0.03
114	2025-12-05	24	1.25	1.32	0.96
115	2025-12-06	24	0.24	0.81	0.54
116	2025-12-07	24	0.19	0.75	0.97
117	2025-12-08	24	-0.13	0.66	0.87
118	2025-12-09	24	-1.02	1.21	0.32
119	2025-12-10	24	-0.67	1.50	0.05
120	2025-12-11	24	-0.06	1.20	0.51
121	2025-12-12	24	-0.52	0.78	0.90
122	2025-12-13	24	-0.29	0.50	0.89
123	2025-12-14	24	-0.58	0.66	0.68
124	2025-12-15	23	-0.89	1.15	0.95
125	2025-12-16	24	1.65	1.76	0.80
126	2025-12-17	24	0.38	0.68	0.90
127	2025-12-20	24	0.10	0.42	0.95
128	2025-12-21	24	0.51	0.98	0.51
129	2025-12-22	24	1.50	1.62	0.79
130	2025-12-23	24	1.07	1.34	0.31
131	2025-12-24	24	1.88	1.98	0.96
132	2025-12-25	24	2.37	2.42	0.58
133	2025-12-26	24	1.84	1.90	0.87
134	2025-12-27	24	0.82	0.97	0.83
135	2025-12-28	24	-0.09	0.45	0.90
136	2025-12-29	24	-0.51	0.76	0.45
137	2025-12-30	24	0.51	1.01	0.81
138	2025-12-31	24	1.69	1.72	0.67

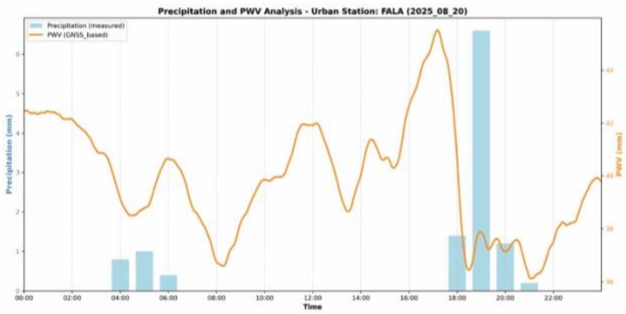
Precipitation and PWV Analysis - Urban Station: FALA (2025_08_20)
Precipitation (measured)
PWV (GNSS_based)
Precipitation (mm)
PWV (mm)
Time

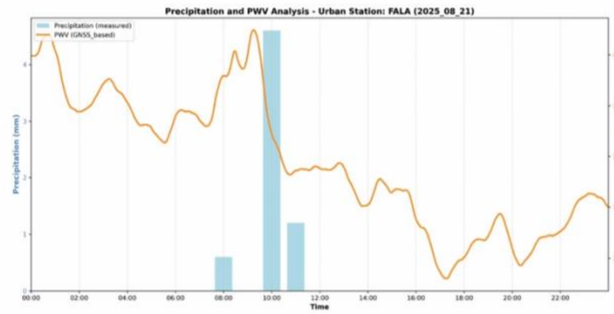
Precipitation and PWV Analysis - Urban Station: FALA (2025_08_21)
Precipitation (measured)
PWV (GNSS_based)
Precipitation (mm)
PWV (mm)
Time

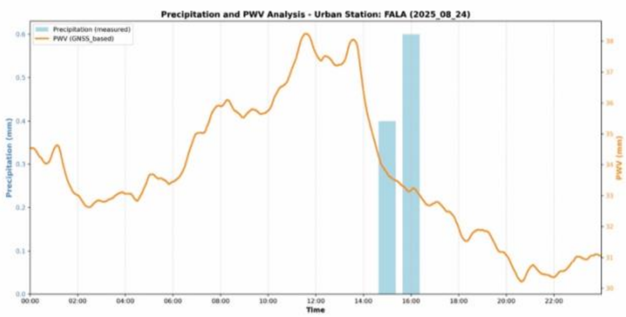
Precipitation and PWV Analysis - Urban Station: FALA (2025_08_24)
Precipitation (measured)
PWV (GNSS_based)
Precipitation (mm)
PWV (mm)
Time

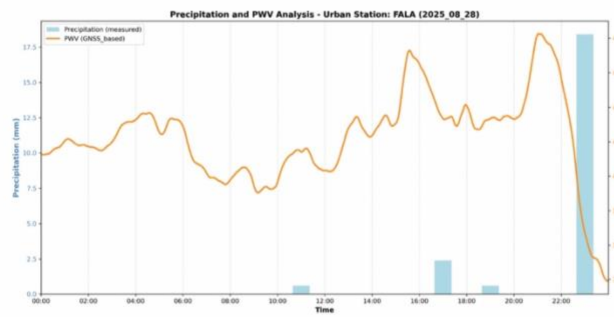
Precipitation and PWV Analysis - Urban Station: FALA (2025_08_28)
Precipitation (measured)
PWV (GNSS_based)
Precipitation (mm)
PWV (mm)
Time

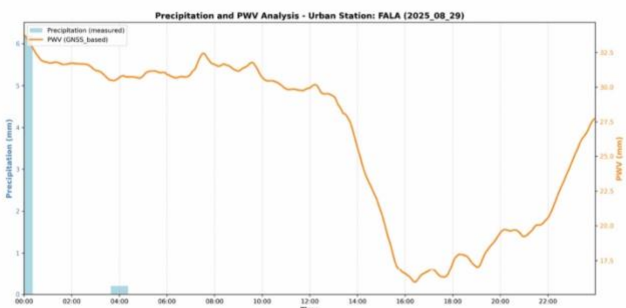
Precipitation and PWV Analysis - Urban Station: FALA (2025_08_29)
Precipitation (measured)
PWV (GNSS_based)
Precipitation (mm)
PWV (mm)
Time

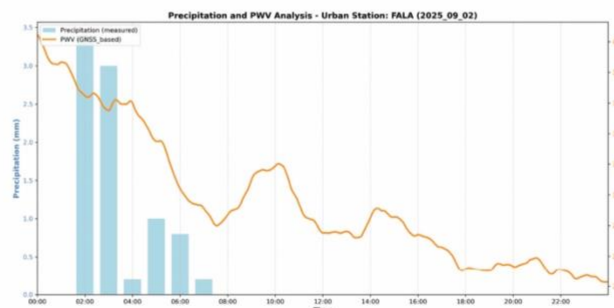
Precipitation and PWV Analysis - Urban Station: FALA (2025_09_02)
Precipitation (measured)
PWV (GNSS_based)
Precipitation (mm)
PWV (mm)
Time

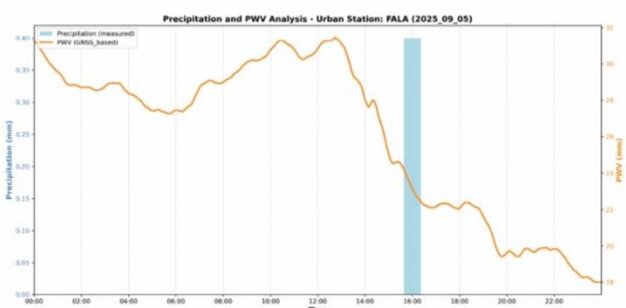
Precipitation and PWV Analysis - Urban Station: FALA (2025_09_05)
Precipitation (measured)
PWV (GNSS_based)
Precipitation (mm)
PWV (mm)
Time

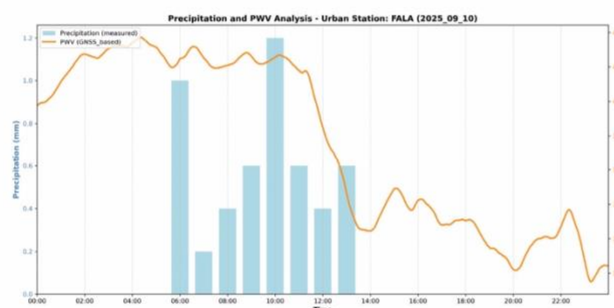
Precipitation and PWV Analysis - Urban Station: FALA (2025_09_10)
Precipitation (measured)
PWV (GNSS_based)
Precipitation (mm)
PWV (mm)
Time

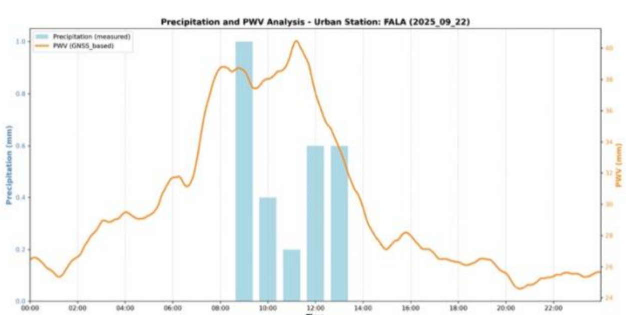
Precipitation and PWV Analysis - Urban Station: FALA (2025_09_22)
Precipitation (measured)
PWV (GNSS_based)
Precipitation (mm)
PWV (mm)
Time

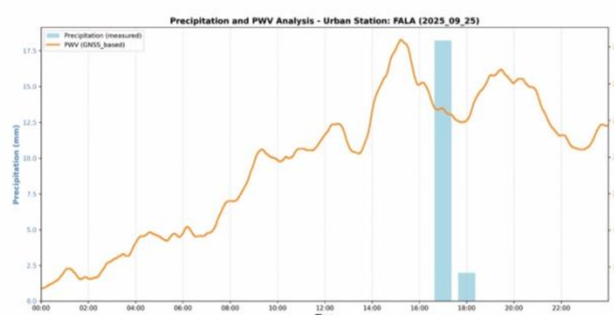
Precipitation and PWV Analysis - Urban Station: FALA (2025_09_25)
Precipitation (measured)
PWV (GNSS_based)
Precipitation (mm)
PWV (mm)
Time

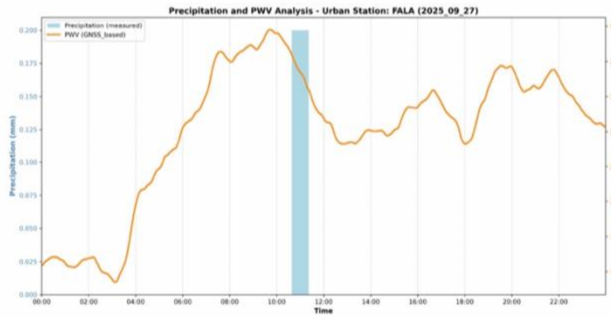
Precipitation and PWV Analysis - Urban Station: FALA (2025_09_27)
Precipitation (measured)
PWV (GNSS_based)
Precipitation (mm)
PWV (mm)
Time

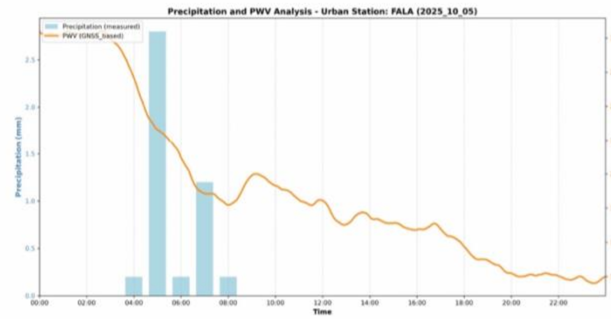
Precipitation and PWV Analysis - Urban Station: FALA (2025_10_05)
Precipitation (measured)
PWV (GNSS_based)
Precipitation (mm)
PWV (mm)
Time

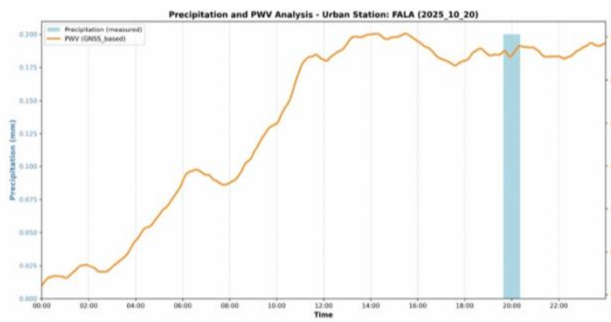
Precipitation and PWV Analysis - Urban Station: FALA (2025_10_20)
Precipitation (measured)
PWV (GNSS_based)
Precipitation (mm)
PWV (mm)
Time

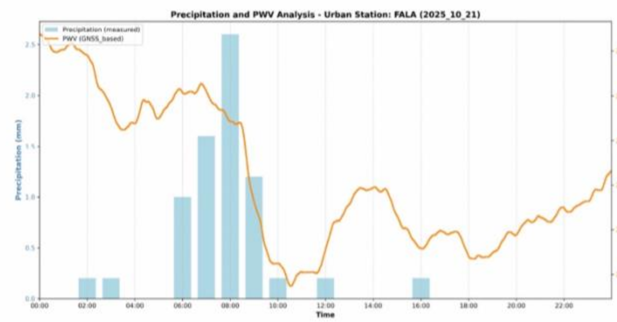
Precipitation and PWV Analysis - Urban Station: FALA (2025_10_21)
Precipitation (measured)
PWV (GNSS_based)
Precipitation (mm)
PWV (mm)
Time

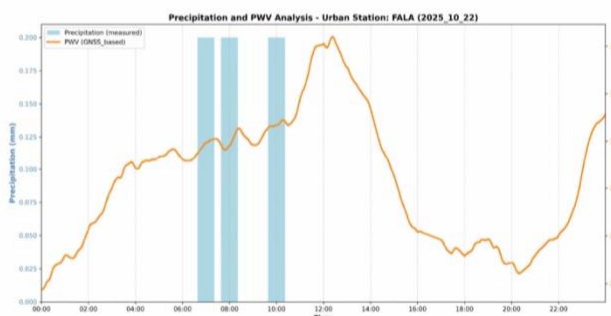
Precipitation and PWV Analysis - Urban Station: FALA (2025_10_22)
Precipitation (measured)
PWV (GNSS_based)
Precipitation (mm)
PWV (mm)
Time

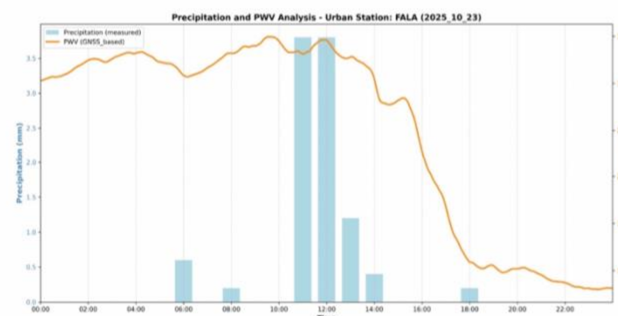
Precipitation and PWV Analysis - Urban Station: FALA (2025_10_23)
Precipitation (measured)
PWV (GNSS_based)
Precipitation (mm)
PWV (mm)
Time

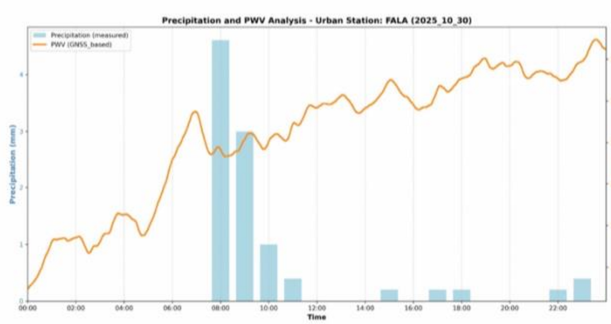
Precipitation and PWV Analysis - Urban Station: FALA (2025_10_30)
Precipitation (measured)
PWV (GNSS_based)
Precipitation (mm)
PWV (mm)
Time

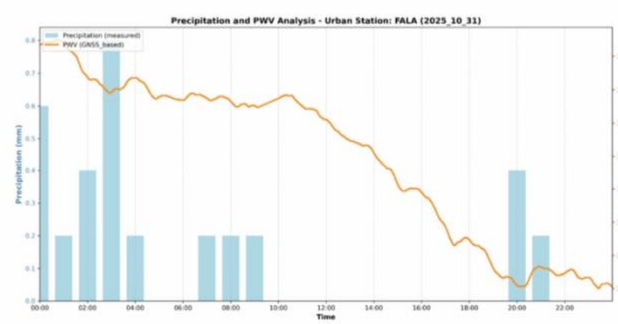
Precipitation and PWV Analysis - Urban Station: FALA (2025_10_31)
Precipitation (measured)
PWV (GNSS_based)
Precipitation (mm)
PWV (mm)
Time

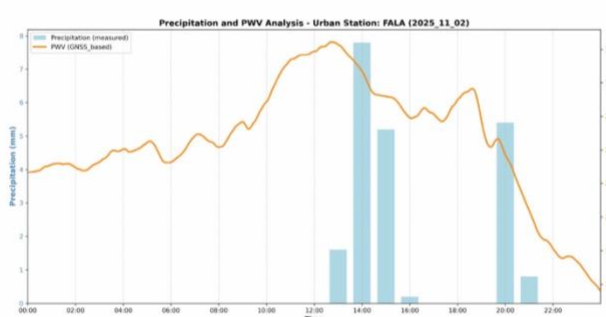
Precipitation and PWV Analysis - Urban Station: FALA (2025_11_02)
Precipitation (measured)
PWV (GNSS_based)
Precipitation (mm)
PWV (mm)
Time

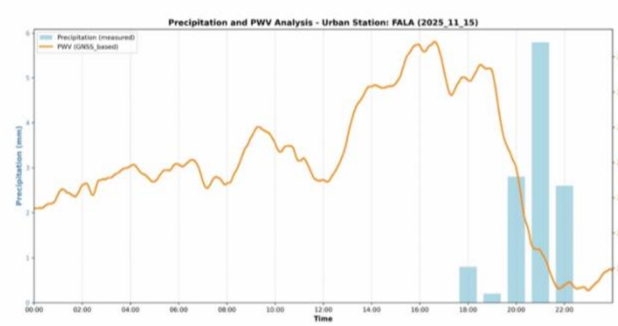
Precipitation and PWV Analysis - Urban Station: FALA (2025_11_15)
Precipitation (measured)
PWV (GNSS_based)
Precipitation (mm)
PWV (mm)
Time

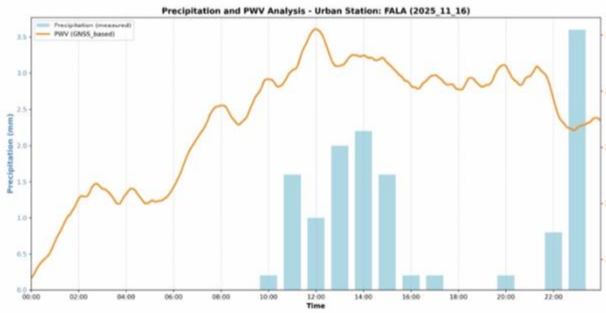
Precipitation and PWV Analysis - Urban Station: FALA (2025_11_16)
Precipitation (measured)
PWV (GNSS_based)
Precipitation (mm)
PWV (mm)
Time

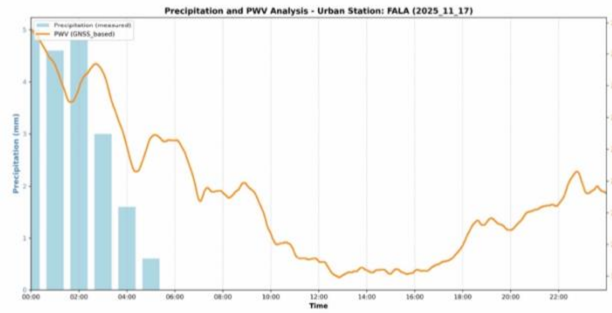
Precipitation and PWV Analysis - Urban Station: FALA (2025_11_17)
Precipitation (measured)
PWV (GNSS_based)
Precipitation (mm)
PWV (mm)
Time

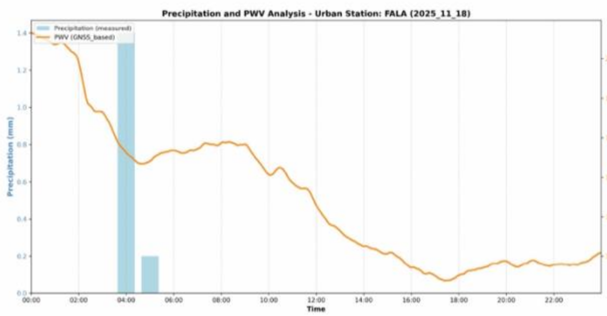
Precipitation and PWV Analysis - Urban Station: FALA (2025_11_18)
Precipitation (measured)
PWV (GNSS_based)
Precipitation (mm)
PWV (mm)
Time

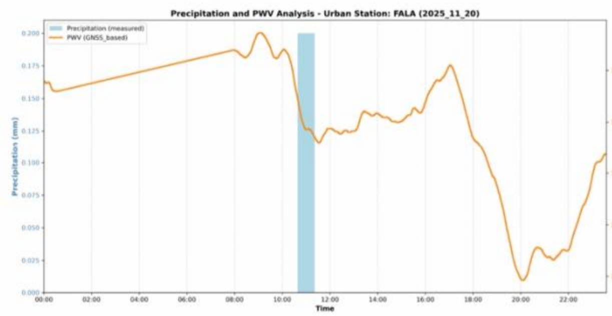
Precipitation and PWV Analysis - Urban Station: FALA (2025_11_20)
Precipitation (measured)
PWV (GNSS_based)
Precipitation (mm)
PWV (mm)
Time

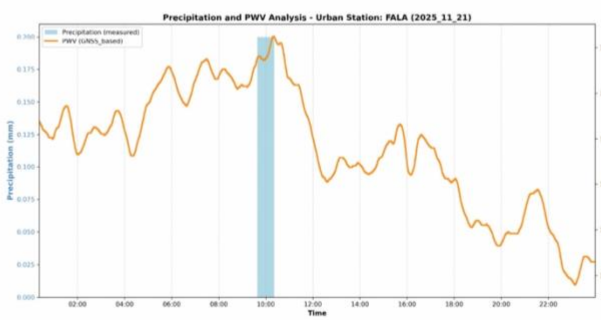
Precipitation and PWV Analysis - Urban Station: FALA (2025_11_21)
Precipitation (measured)
PWV (GNSS_based)
Precipitation (mm)
PWV (mm)
Time

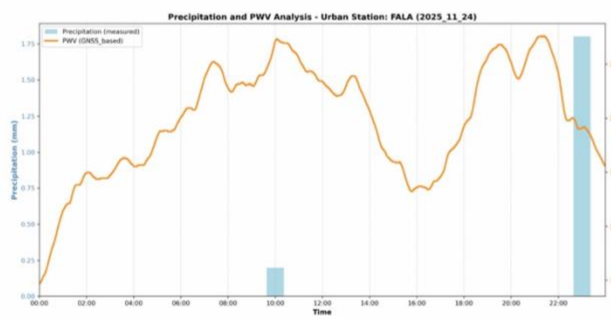
Precipitation and PWV Analysis - Urban Station: FALA (2025_11_24)
Precipitation (measured)
PWV (GNSS_based)
Precipitation (mm)
PWV (mm)
Time

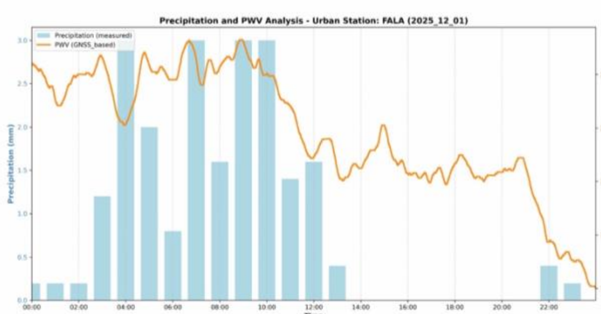
Precipitation and PWV Analysis - Urban Station: FALA (2025_12_01)
Precipitation (measured)
PWV (GNSS_based)
Precipitation (mm)
PWV (mm)
Time

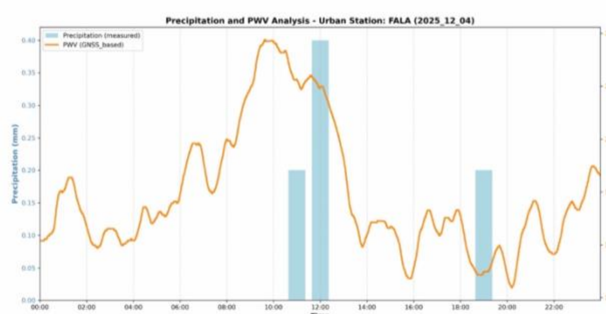
Precipitation and PWV Analysis - Urban Station: FALA (2025_12_04)
Precipitation (measured)
PWV (GNSS_based)
Precipitation (mm)
PWV (mm)
Time

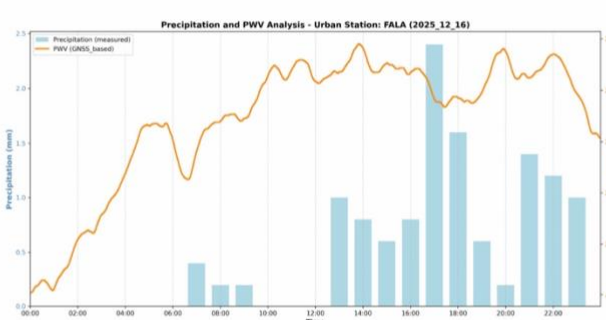
Precipitation and PWV Analysis - Urban Station: FALA (2025_12_16)
Precipitation (measured)
PWV (GNSS_based)
Precipitation (mm)
PWV (mm)
Time

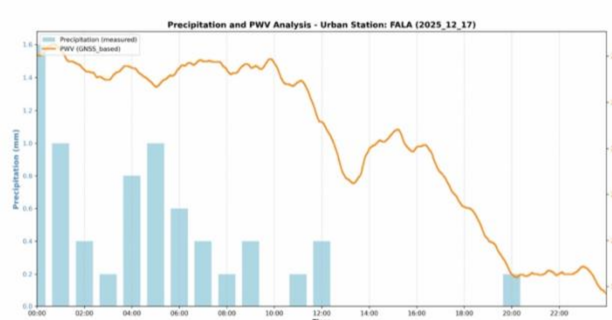
Precipitation and PWV Analysis - Urban Station: FALA (2025_12_17)
Precipitation (measured)
PWV (GNSS_based)
Precipitation (mm)
PWV (mm)
Time

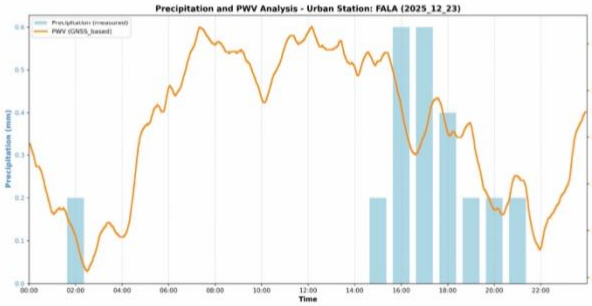

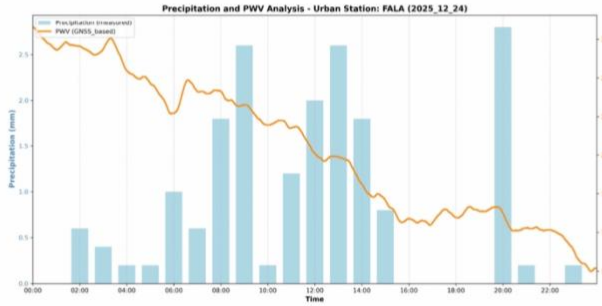

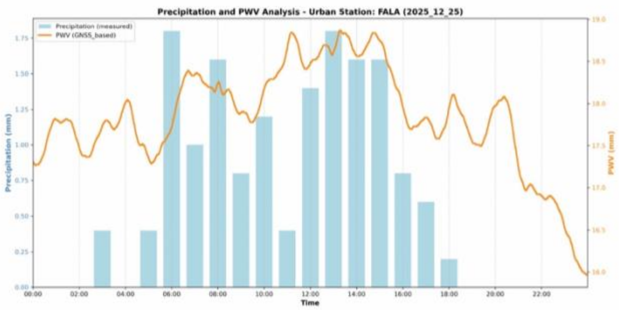

2. NICE

No.	Date	N	MBE (mm)	RMSE (mm)	R^2
1	2025-01-01	12	0.29	0.83	0.09
2	2025-01-02	10	-0.11	1.04	0.83
3	2025-01-03	12	-0.18	0.76	0.94
4	2025-01-04	14	1.30	1.54	0.98
5	2025-01-05	9	0.65	0.92	0.97
6	2025-01-06	12	1.92	2.38	0.10
7	2025-01-07	13	-0.70	1.31	0.99
8	2025-01-08	15	0.14	0.78	0.77
9	2025-01-09	14	-0.68	1.53	0.96
10	2025-01-10	7	0.23	1.07	0.94
11	2025-01-11	11	-0.67	0.88	0.67
12	2025-01-12	16	-0.61	1.32	0.15
13	2025-01-13	13	-1.47	1.66	0.00
14	2025-01-14	10	-1.14	1.46	0.69
15	2025-01-15	10	-1.73	2.02	0.06
16	2025-01-16	18	-0.64	0.89	0.51
17	2025-01-17	8	-0.12	0.44	0.43
18	2025-01-18	15	-0.18	1.27	0.97
19	2025-01-19	16	1.10	1.35	0.73
20	2025-01-20	19	1.14	1.24	0.47
21	2025-01-21	9	1.52	2.10	0.01
22	2025-01-23	13	-0.26	1.87	0.96
23	2025-01-24	12	-1.34	2.44	0.91
24	2025-01-25	12	0.70	1.39	0.21
25	2025-01-26	10	-0.28	2.20	0.96
26	2025-01-28	14	-0.89	1.47	0.97

27	2025-01-30	24	1.20	1.35	0.74
28	2025-01-31	21	1.65	1.94	0.57
29	2025-02-01	24	0.57	1.13	0.00
30	2025-02-02	24	-0.47	1.37	0.76
31	2025-02-03	22	-1.17	1.25	0.65
32	2025-02-04	24	-1.23	1.33	0.89
33	2025-02-05	24	-2.19	2.26	0.35
34	2025-02-06	24	-0.64	1.08	0.48
35	2025-02-07	24	-0.16	0.86	0.91
36	2025-02-08	24	0.86	1.13	0.19
37	2025-02-09	24	0.65	1.06	0.80
38	2025-02-10	24	-0.04	0.34	0.93
39	2025-02-11	24	1.07	1.69	0.16
40	2025-02-12	22	0.59	0.76	0.41
41	2025-02-13	24	0.42	0.62	0.94
42	2025-02-14	22	-1.54	2.24	0.57
43	2025-02-15	24	-1.58	1.76	0.13
44	2025-02-16	22	-0.68	1.02	0.89
45	2025-02-17	20	-1.58	1.62	0.81
46	2025-02-18	16	-0.01	0.38	0.84
47	2025-02-19	16	0.54	0.65	0.65
48	2025-02-20	16	0.27	0.74	0.49
49	2025-02-21	11	0.15	0.60	0.77
50	2025-02-22	11	1.04	1.28	0.85
51	2025-02-23	7	0.79	1.09	0.00
52	2025-02-24	9	0.26	1.05	0.50
53	2025-02-25	14	1.08	1.38	0.92
54	2025-02-26	16	-1.38	1.73	0.29
55	2025-02-27	10	-1.58	1.83	0.80
56	2025-02-28	14	-1.16	1.62	0.38
57	2025-03-01	16	-0.46	0.80	0.71
58	2025-03-02	14	-0.43	0.71	0.61
59	2025-03-03	10	-0.26	0.54	0.90
60	2025-03-04	7	-1.04	1.38	0.04
61	2025-03-18	3	0.15	0.33	0.03
62	2025-03-19	4	1.06	1.14	0.97
63	2025-03-20	5	0.59	0.81	0.98
64	2025-03-21	5	0.12	0.89	0.81
65	2025-03-23	3	1.27	1.96	0.44
66	2025-03-25	4	-1.21	1.52	0.21
67	2025-03-26	2	-0.69	0.72	1.00
68	2025-03-27	5	-0.61	1.13	0.95
69	2025-03-30	2	-3.78	3.79	1.00
70	2025-03-31	2	-2.44	2.58	1.00
71	2025-04-01	5	-1.10	1.21	0.90
72	2025-04-02	24	0.47	0.63	0.69
73	2025-04-03	19	0.27	0.53	0.32
74	2025-04-04	8	0.90	0.92	0.86

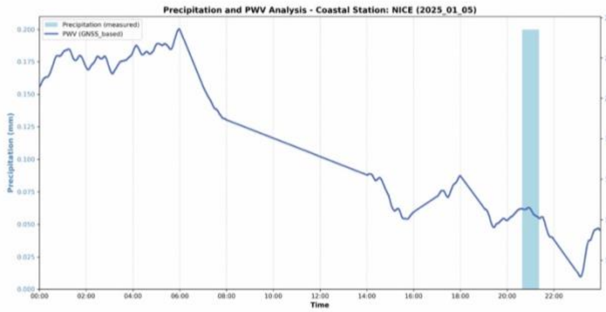
Precipitation and PWV Analysis - Coastal Station: NICE (2025_01_05)
Precipitation (measured)
PWV (GNSS_based)
Precipitation (mm)
PWV (mm)
Time

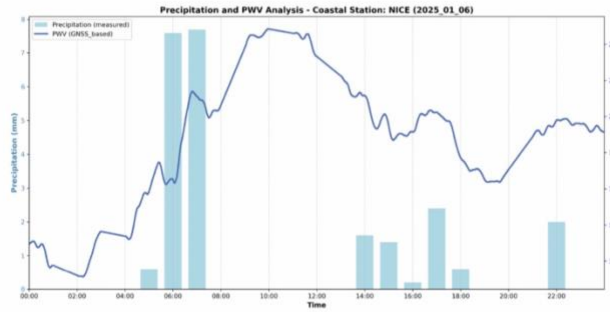
Precipitation and PWV Analysis - Coastal Station: NICE (2025_01_06)
Precipitation (measured)
PWV (GNSS_based)
Precipitation (mm)
PWV (mm)
Time

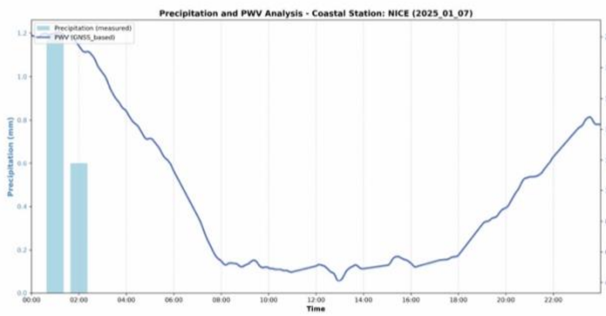
Precipitation and PWV Analysis - Coastal Station: NICE (2025_01_07)
Precipitation (measured)
PWV (GNSS_based)
Precipitation (mm)
PWV (mm)
Time

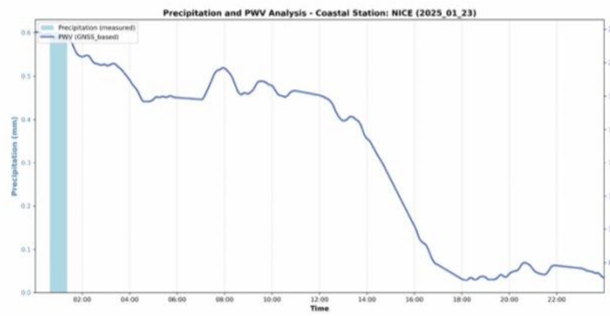
Precipitation and PWV Analysis - Coastal Station: NICE (2025_01_23)
Precipitation (measured)
PWV (GNSS_based)
Precipitation (mm)
PWV (mm)
Time

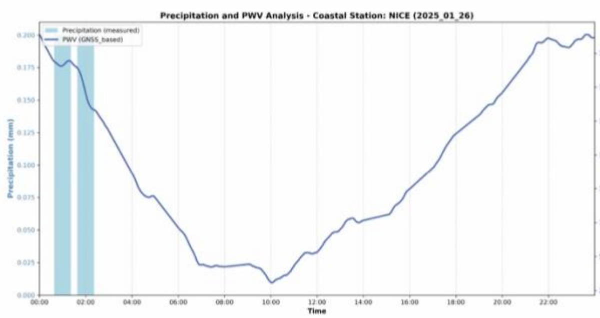
Precipitation and PWV Analysis - Coastal Station: NICE (2025_01_26)
Precipitation (measured)
PWV (GNSS_based)
Precipitation (mm)
PWV (mm)
Time

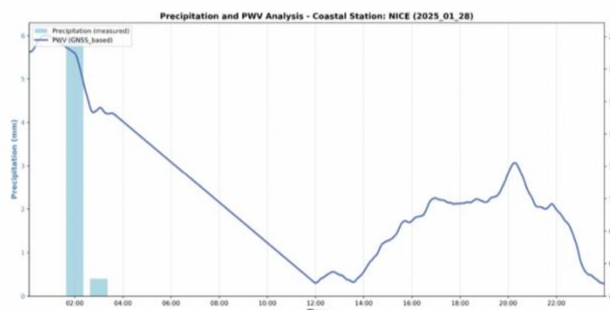
Precipitation and PWV Analysis - Coastal Station: NICE (2025_01_28)
Precipitation (measured)
PWV (GNSS_based)
Precipitation (mm)
PWV (mm)
Time

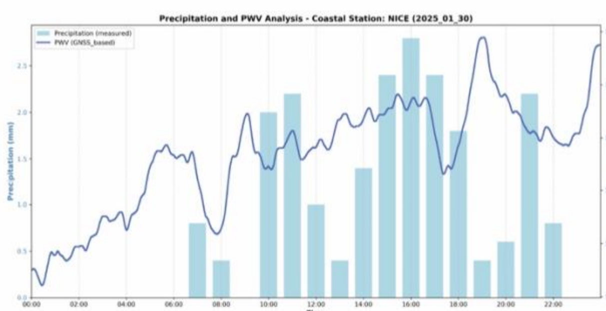
Precipitation and PWV Analysis - Coastal Station: NICE (2025_01_30)
Precipitation (measured)
PWV (GNSS_based)
Precipitation (mm)
PWV (mm)
Time

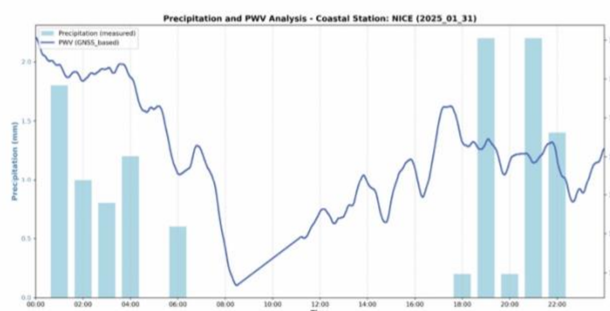
Precipitation and PWV Analysis - Coastal Station: NICE (2025_01_31)
Precipitation (measured)
PWV (GNSS_based)
Precipitation (mm)
PWV (mm)
Time

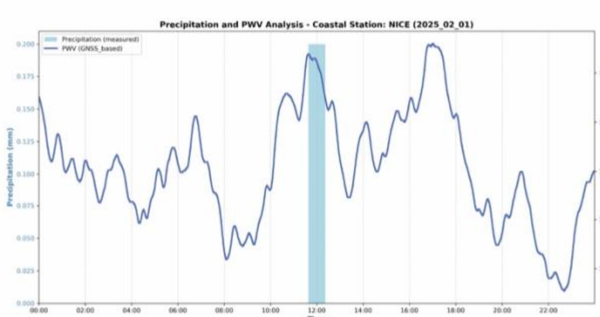
Precipitation and PWV Analysis - Coastal Station: NICE (2025_02_01)
Precipitation (measured)
PWV (GNSS_based)
Precipitation (mm)
PWV (mm)
Time

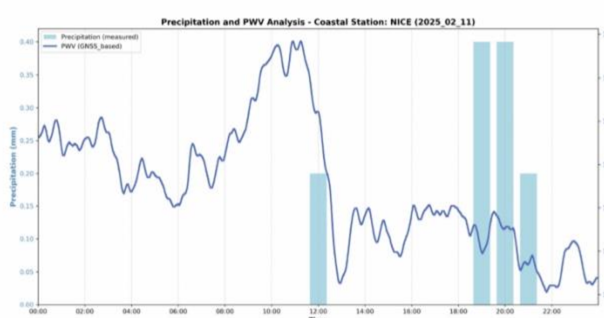
Precipitation and PWV Analysis - Coastal Station: NICE (2025_02_11)
Precipitation (measured)
PWV (GNSS_based)
Precipitation (mm)
PWV (mm)
Time

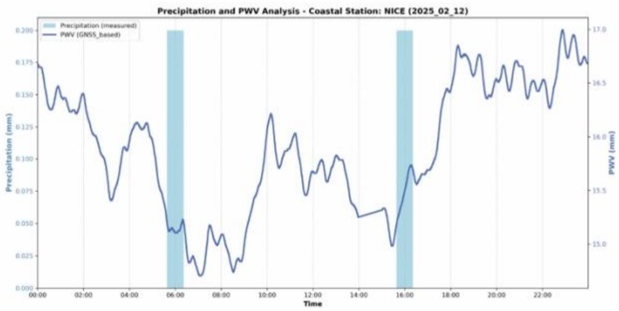

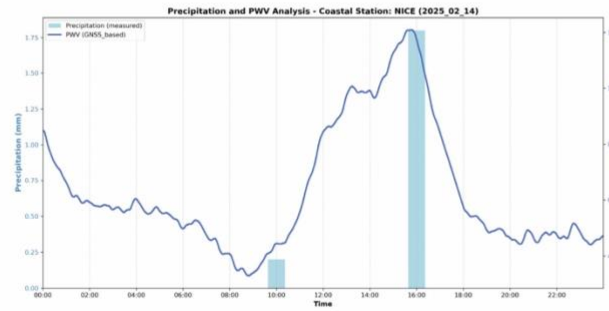

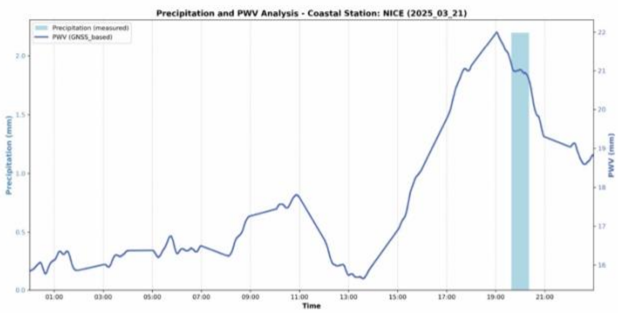

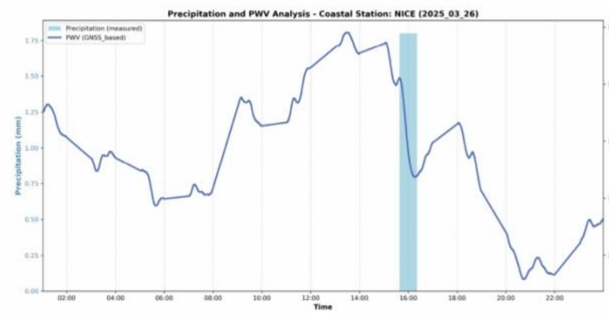

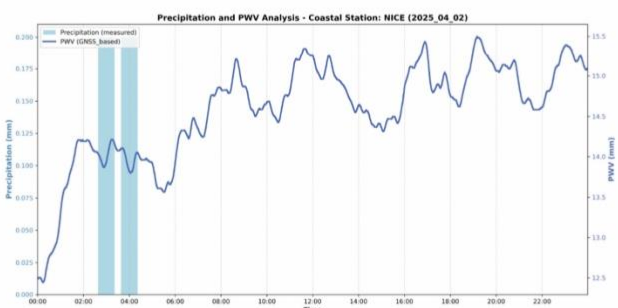

3. SAVE

No.	Date	N	MBE (mm)	RMSE (mm)	R^2
1	2025-05-19	14	-2.41	2.64	0.88
2	2025-05-20	24	-2.44	2.63	0.00
3	2025-05-21	24	-2.11	2.23	0.71
4	2025-05-22	24	-1.63	1.79	0.87
5	2025-05-23	24	-1.78	2.13	0.36
6	2025-05-24	22	-1.53	1.92	0.97
7	2025-05-25	24	-1.00	1.34	0.72
8	2025-05-26	24	-1.76	1.99	0.73
9	2025-05-27	24	-2.22	2.33	0.81
10	2025-05-28	24	-1.96	2.48	0.72
11	2025-05-29	24	-1.95	2.29	0.46
12	2025-05-30	24	-1.19	1.74	0.13
13	2025-05-31	24	-2.03	2.40	0.93
14	2025-06-01	24	-5.53	5.94	0.40

15	2025-06-02	24	-2.49	3.50	0.13
16	2025-06-03	24	-2.88	3.26	0.62
17	2025-06-04	23	-4.28	4.54	0.52
18	2025-06-05	24	-2.99	3.33	0.77
19	2025-06-06	24	-3.69	3.85	0.80
20	2025-06-07	24	-3.02	3.28	0.82
21	2025-06-08	24	-1.74	1.94	0.85
22	2025-06-09	24	-1.85	2.02	0.29
23	2025-06-10	24	-1.83	1.99	0.72
24	2025-06-11	24	-1.62	1.96	0.82
25	2025-06-12	24	-3.81	4.41	0.90
26	2025-06-13	24	-4.09	4.85	0.12
27	2025-06-14	24	-0.92	3.38	0.03
28	2025-06-15	24	-4.27	4.76	0.66
29	2025-06-16	24	-3.15	3.22	0.87
30	2025-06-17	24	-4.01	4.12	0.65
31	2025-06-18	24	-4.31	4.61	0.44
32	2025-06-19	22	-5.42	5.63	0.80
33	2025-06-20	24	-5.62	5.78	0.67
34	2025-06-21	24	-5.33	5.97	0.54
35	2025-06-22	24	-5.62	6.26	0.64
36	2025-06-23	24	-2.33	3.05	0.88
37	2025-06-24	24	-3.36	3.52	0.48
38	2025-06-25	24	-5.05	5.44	0.50
39	2025-06-26	24	-2.51	3.04	0.59
40	2025-06-27	24	-2.82	3.10	0.35
41	2025-06-28	24	-3.56	3.68	0.30
42	2025-06-29	24	-5.65	5.80	0.90
43	2025-06-30	20	-6.43	6.87	0.28
44	2025-07-01	19	-3.91	4.50	0.41
45	2025-07-02	24	-6.21	6.85	0.25
46	2025-07-03	24	-2.47	2.74	0.66
47	2025-07-04	24	-1.40	2.19	0.87
48	2025-07-05	24	-2.81	3.42	0.65
49	2025-07-07	24	-2.82	3.01	0.45
50	2025-07-08	24	-1.09	1.42	0.85
51	2025-07-09	21	-2.40	2.53	0.32
52	2025-07-10	24	-3.17	3.52	0.34
53	2025-07-11	24	-3.14	3.27	0.88
54	2025-07-12	24	-1.69	2.11	0.73
55	2025-07-13	24	-2.61	3.13	0.59
56	2025-07-14	24	-2.85	3.19	0.88
57	2025-07-15	24	-3.23	3.74	0.72
58	2025-07-16	24	-1.49	1.99	0.62
59	2025-07-17	24	-2.55	3.35	0.81
60	2025-07-18	24	-3.66	3.86	0.87
61	2025-07-19	23	-3.48	4.13	0.61
62	2025-07-20	24	-4.10	4.32	0.26
63	2025-07-21	24	-3.22	4.44	0.09
64	2025-07-22	24	-3.03	3.10	0.96
65	2025-07-23	24	-3.02	3.31	0.90

66	2025-07-24	24	-2.84	3.24	0.00
67	2025-07-25	24	-2.95	3.30	0.24
68	2025-07-27	24	-1.59	1.90	0.31
69	2025-07-28	24	-1.10	1.37	0.58
70	2025-07-29	24	-1.62	1.78	0.29
71	2025-07-30	24	-2.65	2.94	0.49
72	2025-07-31	24	-2.89	3.04	0.27
73	2025-08-01	24	-0.84	1.83	0.04
74	2025-08-02	24	-1.24	2.00	0.74
75	2025-08-03	24	-2.39	2.89	0.55
76	2025-08-04	24	-3.14	3.29	0.85
77	2025-08-05	24	-2.37	2.94	0.92
78	2025-08-06	24	-4.68	4.79	0.83
79	2025-08-07	24	-4.74	5.24	0.09
80	2025-08-08	24	-4.27	4.94	0.27
81	2025-08-09	24	-2.61	2.83	0.83
82	2025-08-10	24	-2.12	2.75	0.52
83	2025-08-11	24	-2.70	3.04	0.86
84	2025-08-12	24	-4.56	5.20	0.54
85	2025-08-13	24	-3.82	4.51	0.35
86	2025-08-14	24	-3.84	4.12	0.58
87	2025-08-15	24	-4.49	5.60	0.10
88	2025-08-16	24	-6.72	7.12	0.25
89	2025-08-17	24	-3.44	3.90	0.15
90	2025-08-18	24	-3.64	3.80	0.81
91	2025-08-19	24	-4.91	5.77	0.95
92	2025-08-20	24	-3.57	3.98	0.02
93	2025-08-21	24	-2.17	2.51	0.38
94	2025-08-22	24	-2.94	3.00	0.85
95	2025-08-23	24	-2.54	2.66	0.48
96	2025-08-24	24	-2.27	2.58	0.67
97	2025-08-25	24	-3.32	3.67	0.44
98	2025-08-26	24	-3.59	3.94	0.96
99	2025-08-27	24	-3.12	3.56	0.58
100	2025-08-28	24	-4.07	4.34	0.89
101	2025-08-29	24	-3.90	4.09	0.72
102	2025-08-30	24	-2.28	2.54	0.33
103	2025-09-01	24	-3.74	3.87	0.93
104	2025-09-02	24	-2.69	3.22	0.59
105	2025-09-03	24	-2.94	3.09	0.83
106	2025-09-04	24	-3.24	4.03	0.60
107	2025-09-05	24	-2.22	2.70	0.51
108	2025-09-06	24	-3.17	3.39	0.26
109	2025-09-07	24	-3.86	4.04	0.93
110	2025-09-08	24	-2.90	3.36	0.59
111	2025-09-09	24	-2.64	2.78	0.96
112	2025-09-10	24	-2.64	3.14	0.17
113	2025-09-11	20	-2.74	2.96	0.83
114	2025-09-12	18	-2.98	3.47	0.66
115	2025-09-13	7	-2.67	2.80	0.96
116	2025-09-15	2	-3.56	3.77	1.00

117	2025-09-17	2	-2.38	2.42	1.00
118	2025-09-18	13	-4.06	4.16	0.96
119	2025-09-19	24	-4.11	5.17	0.63
120	2025-09-20	24	-4.56	5.11	0.09
121	2025-09-21	24	-3.97	4.30	0.17
122	2025-09-22	24	-4.71	4.81	0.93
123	2025-09-23	24	-1.70	1.85	0.57
124	2025-09-24	23	-2.82	2.92	0.28
125	2025-09-25	24	-2.51	2.58	0.26
126	2025-09-26	24	-2.45	2.56	0.16
127	2025-09-27	24	-2.88	2.97	0.80
128	2025-09-28	24	-3.09	3.12	0.82
129	2025-09-30	24	-2.45	2.62	0.92
130	2025-10-01	24	-2.58	2.87	0.39
131	2025-10-02	24	-2.34	2.43	0.71
132	2025-10-03	24	-2.31	2.51	0.96
133	2025-10-04	24	-1.86	2.44	0.98
134	2025-10-05	24	-0.51	0.95	0.39
135	2025-10-06	24	-1.42	1.55	0.97
136	2025-10-07	24	-2.92	3.03	0.88
137	2025-10-08	24	-3.12	3.19	0.92
138	2025-10-09	24	-3.14	3.31	0.91
139	2025-10-10	24	-3.68	3.72	0.74
140	2025-10-11	24	-3.44	3.48	0.13
141	2025-10-12	24	-2.46	2.54	0.49
142	2025-10-13	24	-4.91	5.34	0.42
143	2025-10-15	24	-3.33	3.41	0.30
144	2025-10-16	23	-3.92	3.95	0.72
145	2025-10-17	24	-3.08	3.13	0.19
146	2025-10-18	24	-2.43	2.47	0.18
147	2025-10-19	24	-3.47	3.68	0.90
148	2025-10-20	24	-2.81	3.44	0.46
149	2025-10-21	24	-2.38	2.52	0.88
150	2025-10-22	24	-2.29	2.55	0.49
151	2025-10-23	24	-1.84	2.63	0.94
152	2025-10-25	24	-1.65	1.91	0.68
153	2025-10-28	24	-2.08	2.24	0.75
154	2025-10-30	24	-2.47	2.58	0.98
155	2025-10-31	24	-3.57	3.75	0.79
156	2025-11-01	24	-3.28	3.44	0.94
157	2025-11-02	24	-1.83	2.11	0.93
158	2025-11-03	24	-1.26	1.45	0.39
159	2025-11-04	24	-2.38	2.43	0.92
160	2025-11-05	24	-2.26	2.40	0.39
161	2025-11-06	24	-1.36	2.23	0.85
162	2025-11-07	24	-0.86	1.34	0.19
163	2025-11-08	24	-2.68	2.72	0.78
164	2025-11-09	24	-1.67	1.89	0.89
165	2025-11-10	24	-2.06	2.24	0.89
166	2025-11-11	24	-2.83	2.94	0.47
167	2025-11-12	22	-3.21	3.24	0.85

168	2025-11-13	24	-2.19	2.35	0.50
169	2025-11-14	23	-2.46	2.70	0.89
170	2025-11-15	24	-2.94	3.03	0.80
171	2025-11-16	24	-2.86	3.03	0.85
172	2025-11-17	24	-1.55	1.68	0.98
173	2025-11-18	24	-1.26	1.34	0.30
174	2025-11-20	24	-0.42	0.60	0.55
175	2025-11-21	24	-0.27	0.55	0.02
176	2025-11-22	24	-0.94	0.99	0.80
177	2025-11-23	24	-0.88	1.00	0.99
178	2025-11-24	24	-2.02	2.20	0.86
179	2025-11-25	24	-1.24	1.35	0.16
180	2025-11-26	24	-1.56	1.61	0.92
181	2025-11-27	24	-1.67	1.75	0.80
182	2025-11-28	24	-1.85	1.93	0.87
183	2025-11-29	24	-1.87	2.33	0.53
184	2025-11-30	23	-1.82	1.96	0.86
185	2025-12-01	24	-1.57	1.81	0.19
186	2025-12-02	24	-2.71	2.78	0.94
187	2025-12-03	24	-1.76	1.88	0.10
188	2025-12-04	24	-2.14	2.28	0.92
189	2025-12-05	24	-1.68	1.79	0.81
190	2025-12-06	24	-1.31	1.73	0.29
191	2025-12-07	24	-1.48	1.63	0.92
192	2025-12-08	24	-2.86	3.30	0.95
193	2025-12-09	24	-3.29	3.33	0.74
194	2025-12-10	24	-1.65	1.90	0.70
195	2025-12-11	24	-1.68	1.92	0.77
196	2025-12-12	24	-2.40	2.50	0.88
197	2025-12-13	24	-2.14	2.20	0.20
198	2025-12-14	24	-2.59	2.63	0.67
199	2025-12-15	23	-1.51	1.67	0.50
200	2025-12-16	24	-1.46	1.57	0.89
201	2025-12-17	24	-2.07	2.14	0.83
202	2025-12-20	24	-2.23	2.28	0.67
203	2025-12-21	24	-2.76	2.83	0.77
204	2025-12-22	24	-2.54	2.62	0.36
205	2025-12-23	24	-2.66	2.70	0.67
206	2025-12-24	24	-2.15	2.26	0.79
207	2025-12-25	24	-2.14	2.19	0.35
208	2025-12-26	24	-2.14	2.18	0.87
209	2025-12-27	24	-1.99	2.03	0.42
210	2025-12-28	24	-2.63	2.66	0.76
211	2025-12-29	24	-1.99	2.05	0.25
212	2025-12-30	24	-1.77	1.81	0.19
213	2025-12-31	24	-1.43	1.48	0.53

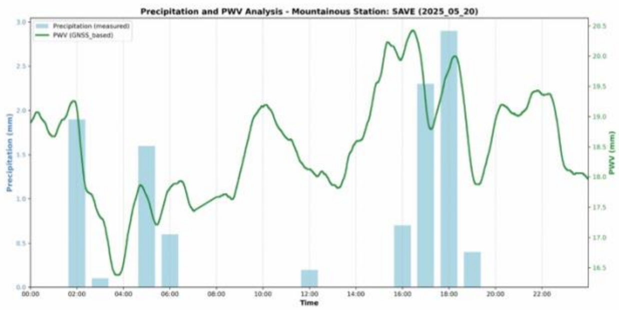
Precipitation and PWV Analysis - Mountainous Station: SAVE (2025_05_20)
Precipitation (measured)
PWV (GNSS_based)
Precipitation (mm)
PWV (mm)
Time

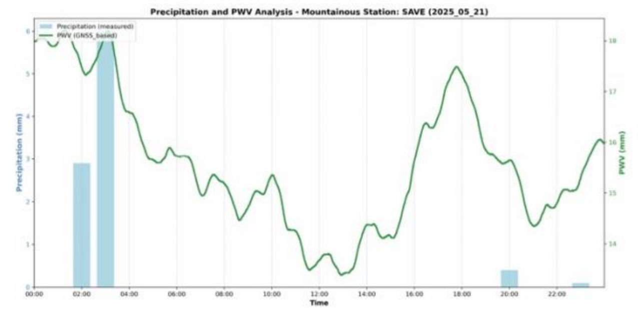
Precipitation and PWV Analysis - Mountainous Station: SAVE (2025_05_21)
Precipitation (measured)
PWV (GNSS_based)
Precipitation (mm)
PWV (mm)
Time

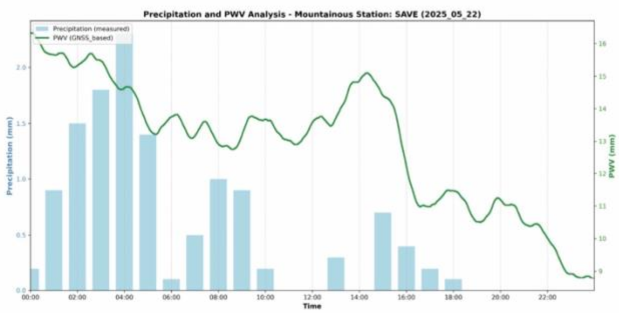
Precipitation and PWV Analysis - Mountainous Station: SAVE (2025_05_22)
Precipitation (measured)
PWV (GNSS_based)
Precipitation (mm)
PWV (mm)
Time

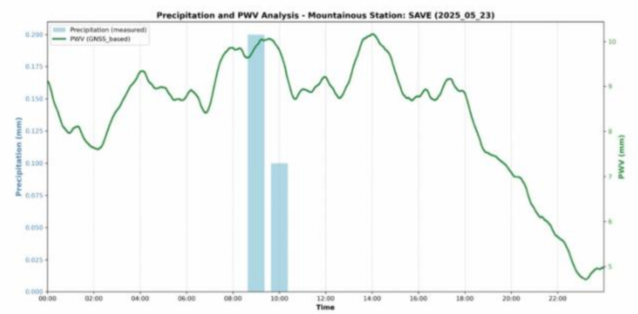
Precipitation and PWV Analysis - Mountainous Station: SAVE (2025_05_23)
Precipitation (measured)
PWV (GNSS_based)
Precipitation (mm)
PWV (mm)
Time

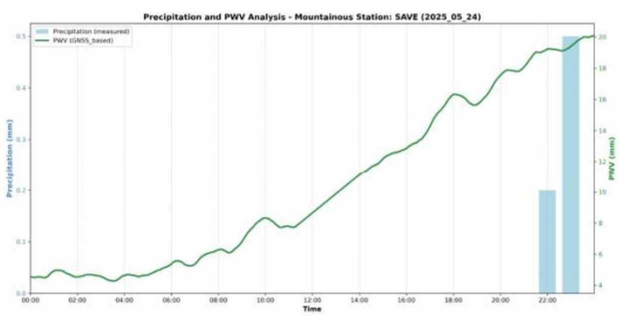
Precipitation and PWV Analysis - Mountainous Station: SAVE (2025_05_24)
Precipitation (measured)
PWV (GNSS_based)
Precipitation (mm)
PWV (mm)
Time

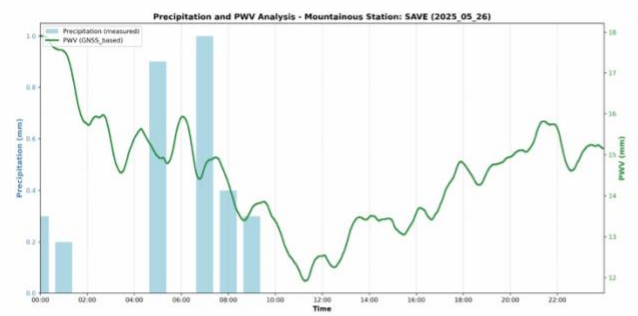
Precipitation and PWV Analysis - Mountainous Station: SAVE (2025_05_26)
Precipitation (measured)
PWV (GNSS_based)
Precipitation (mm)
PWV (mm)
Time

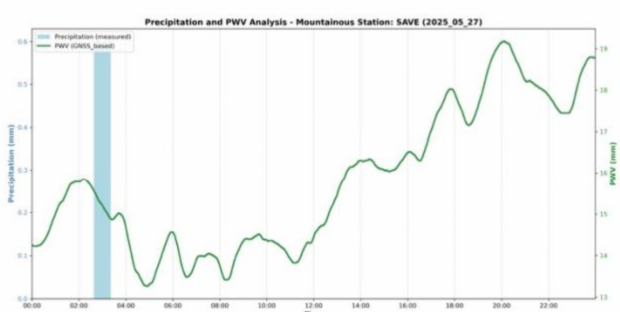
Precipitation and PWV Analysis - Mountainous Station: SAVE (2025_05_27)
Precipitation (measured)
PWV (GNSS_based)
Precipitation (mm)
PWV (mm)
Time

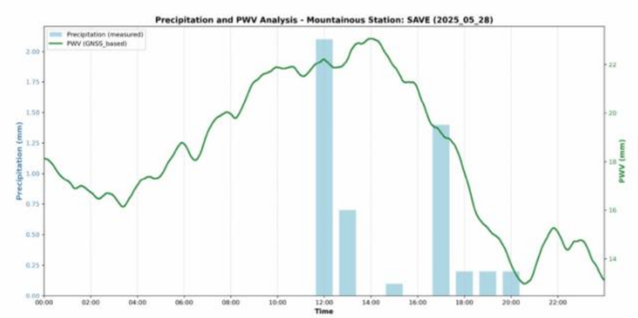
Precipitation and PWV Analysis - Mountainous Station: SAVE (2025_05_28)
Precipitation (measured)
PWV (GNSS_based)
Precipitation (mm)
PWV (mm)
Time

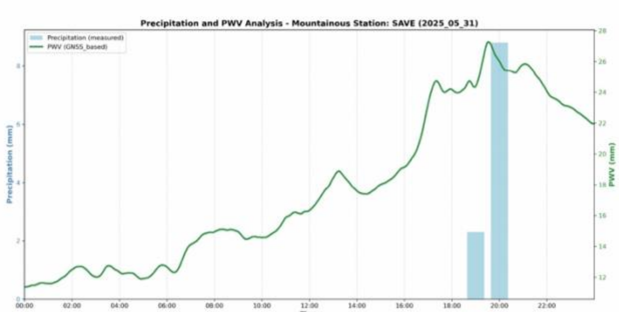
Precipitation and PWV Analysis - Mountainous Station: SAVE (2025_05_31)
Precipitation (measured)
PWV (GNSS_based)
Precipitation (mm)
PWV (mm)
Time

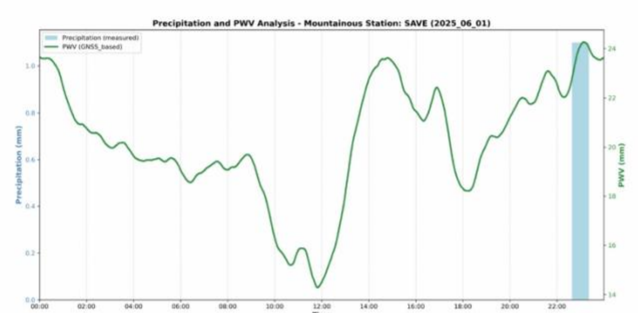
Precipitation and PWV Analysis - Mountainous Station: SAVE (2025_06_01)
Precipitation (measured)
PWV (GNSS_based)
Precipitation (mm)
PWV (mm)
Time

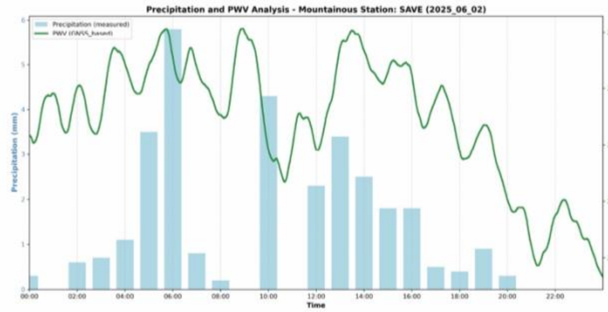
Precipitation and PWV Analysis - Mountainous Station: SAVE (2025_06_02)
Precipitation (measured)
PWV (GNSS_based)
Precipitation (mm)
PWV (mm)
Time

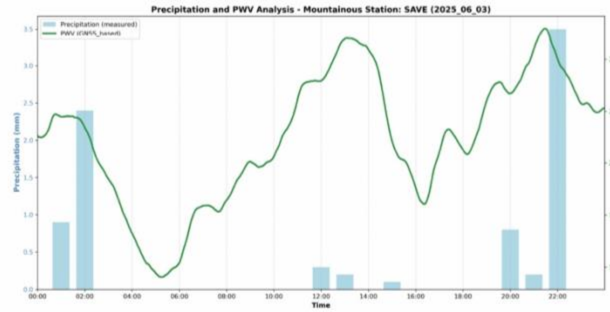
Precipitation and PWV Analysis - Mountainous Station: SAVE (2025_06_03)
Precipitation (measured)
PWV (GNSS_based)
Precipitation (mm)
PWV (mm)
Time

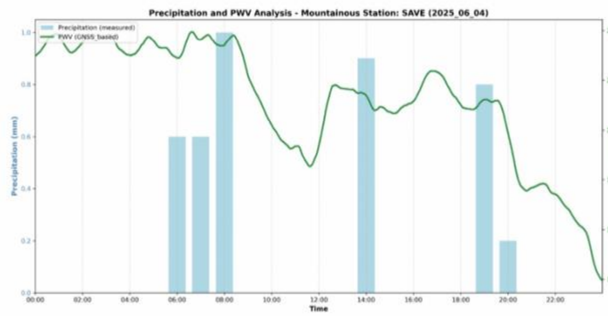
Precipitation and PWV Analysis - Mountainous Station: SAVE (2025_06_04)
Precipitation (measured)
PWV (GNSS_based)
Precipitation (mm)
PWV (mm)
Time

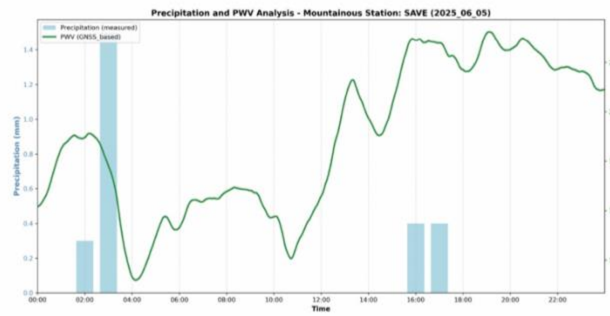
Precipitation and PWV Analysis - Mountainous Station: SAVE (2025_06_05)
Precipitation (measured)
PWV (GNSS_based)
Precipitation (mm)
PWV (mm)
Time

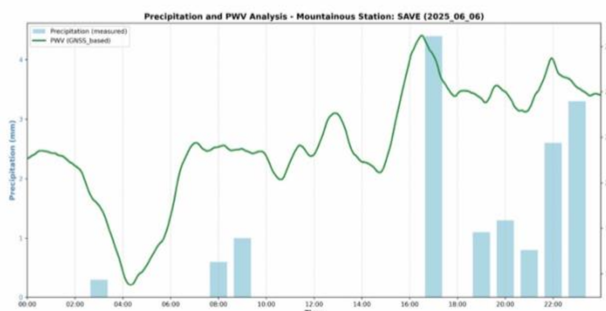
Precipitation and PWV Analysis - Mountainous Station: SAVE (2025_06_06)
Precipitation (measured)
PWV (GNSS_based)
Precipitation (mm)
PWV (mm)
Time

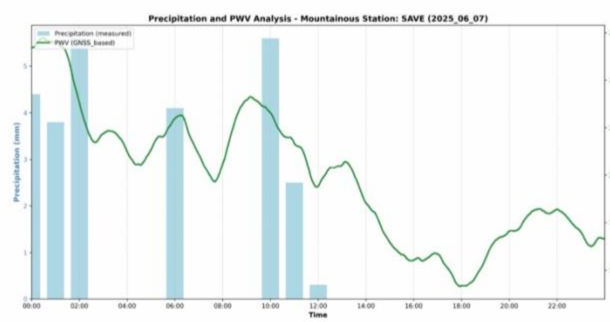
Precipitation and PWV Analysis - Mountainous Station: SAVE (2025_06_07)
Precipitation (measured)
PWV (GNSS_based)
Precipitation (mm)
PWV (mm)
Time

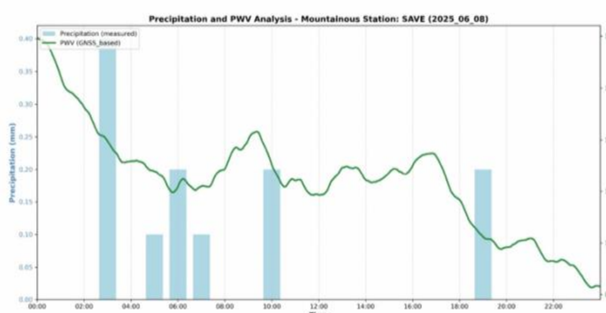
Precipitation and PWV Analysis - Mountainous Station: SAVE (2025_06_08)
Precipitation (measured)
PWV (GNSS_based)
Precipitation (mm)
PWV (mm)
Time

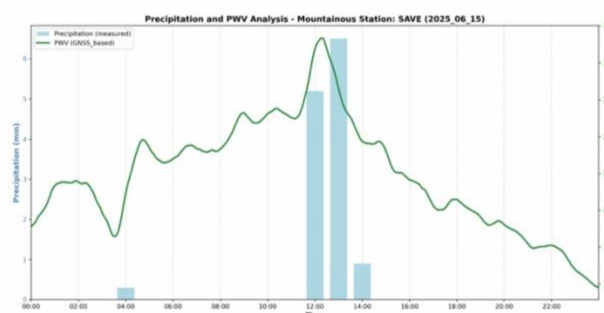
Precipitation and PWV Analysis - Mountainous Station: SAVE (2025_06_15)
Precipitation (measured)
PWV (GNSS_based)
Precipitation (mm)
PWV (mm)
Time

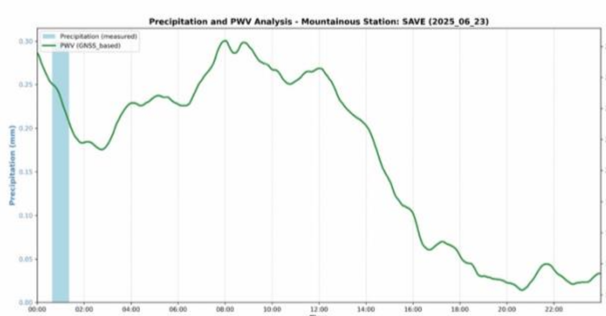
Precipitation and PWV Analysis - Mountainous Station: SAVE (2025_06_23)
Precipitation (measured)
PWV (GNSS_based)
Precipitation (mm)
PWV (mm)
Time

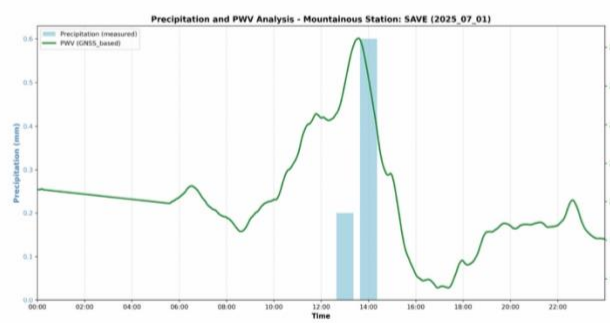
Precipitation and PWV Analysis - Mountainous Station: SAVE (2025_07_01)
Precipitation (measured)
PWV (GNSS_based)
Precipitation (mm)
PWV (mm)
Time

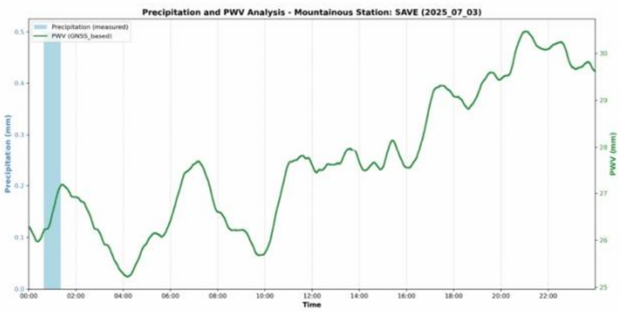
Precipitation and PWV Analysis - Mountainous Station: SAVE (2025_07_03)
Precipitation (measured)
PWV (GNSS_based)
Precipitation (mm)
PWV (mm)
Time

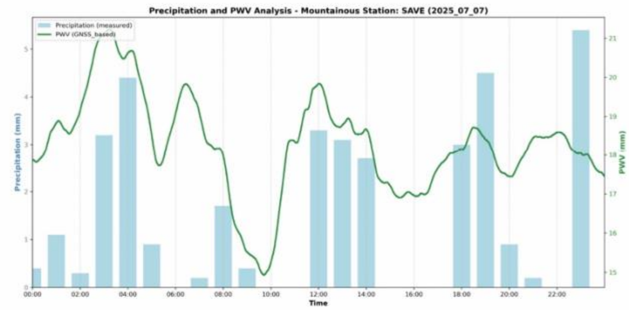
Precipitation and PWV Analysis - Mountainous Station: SAVE (2025_07_07)
Precipitation (measured)
PWV (GNSS_based)
Precipitation (mm)
PWV (mm)
Time

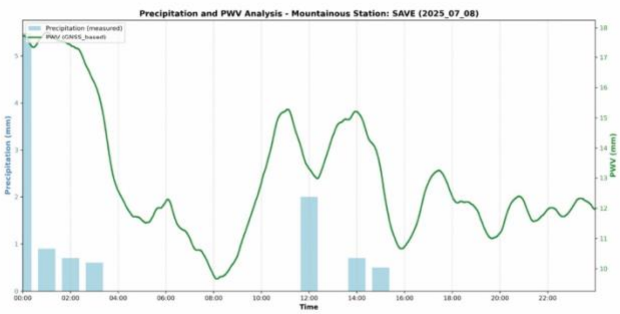
Precipitation and PWV Analysis - Mountainous Station: SAVE (2025_07_08)
Precipitation (measured)
PWV (GNSS_based)
Precipitation (mm)
PWV (mm)
Time

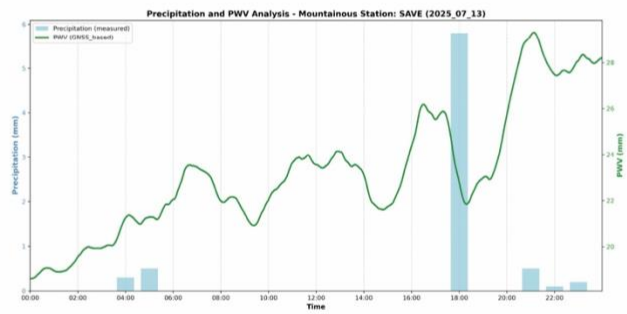
Precipitation and PWV Analysis - Mountainous Station: SAVE (2025_07_13)
Precipitation (measured)
PWV (GNSS_based)
Precipitation (mm)
PWV (mm)
Time

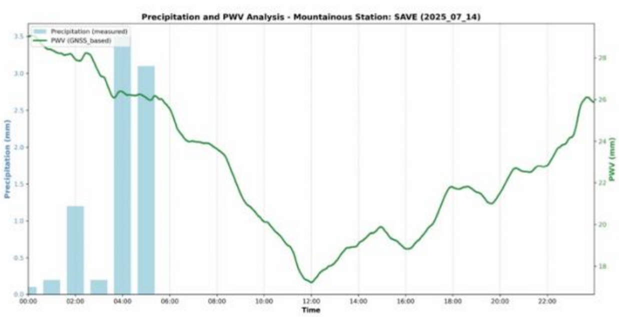
Precipitation and PWV Analysis - Mountainous Station: SAVE (2025_07_14)
Precipitation (measured)
PWV (GNSS_based)
Precipitation (mm)
PWV (mm)
Time

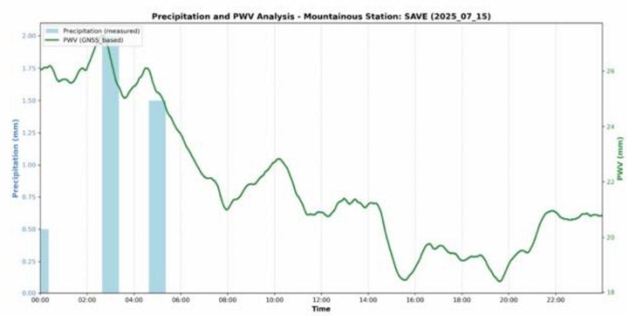
Precipitation and PWV Analysis - Mountainous Station: SAVE (2025_07_15)
Precipitation (measured)
PWV (GNSS_based)
Precipitation (mm)
PWV (mm)
Time

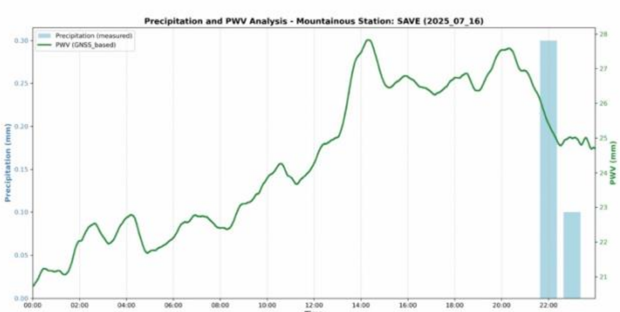
Precipitation and PWV Analysis - Mountainous Station: SAVE (2025_07_16)
Precipitation (measured)
PWV (GNSS_based)
Precipitation (mm)
PWV (mm)
Time

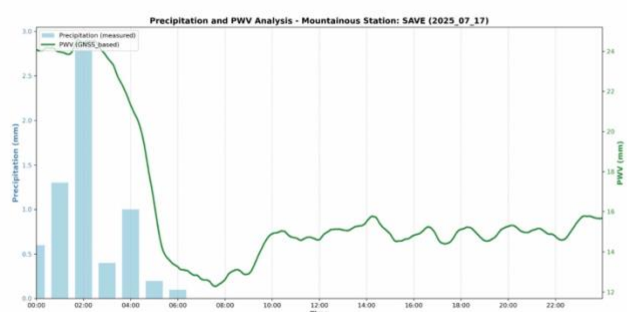
Precipitation and PWV Analysis - Mountainous Station: SAVE (2025_07_17)
Precipitation (measured)
PWV (GNSS_based)
Precipitation (mm)
PWV (mm)
Time

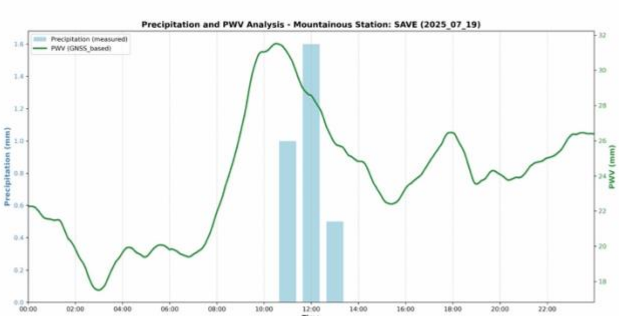
Precipitation and PWV Analysis - Mountainous Station: SAVE (2025_07_19)
Precipitation (measured)
PWV (GNSS_based)
Precipitation (mm)
PWV (mm)
Time

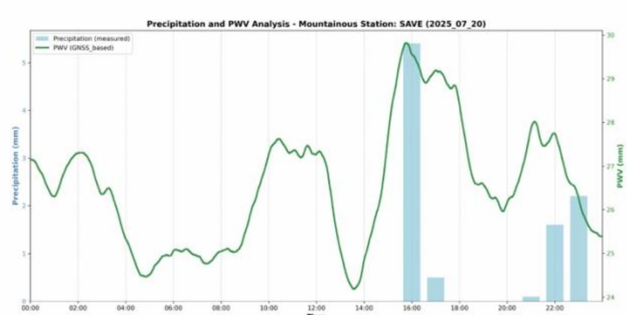
Precipitation and PWV Analysis - Mountainous Station: SAVE (2025_07_20)
Precipitation (measured)
PWV (GNSS_based)
Precipitation (mm)
PWV (mm)
Time

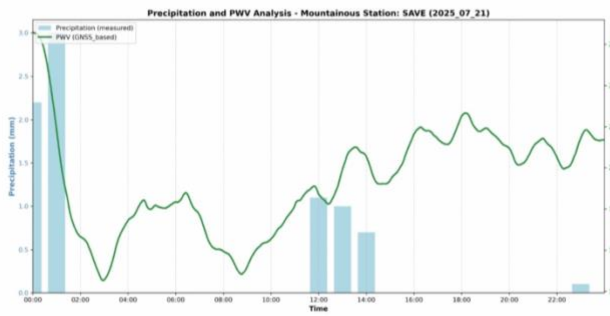
Precipitation and PWV Analysis - Mountainous Station: SAVE (2025_07_21)
Precipitation (measured)
PWV (GNSS_based)
Precipitation (mm)
PWV (mm)
Time

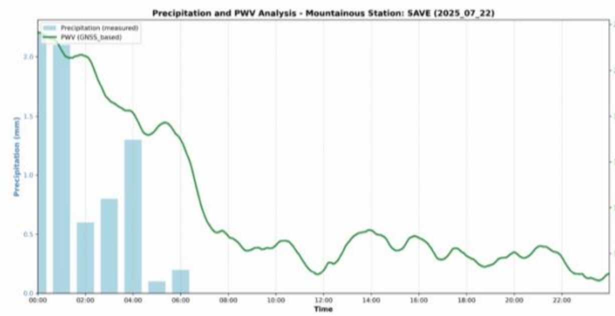
Precipitation and PWV Analysis - Mountainous Station: SAVE (2025_07_22)
Precipitation (measured)
PWV (GNSS_based)
Precipitation (mm)
PWV (mm)
Time

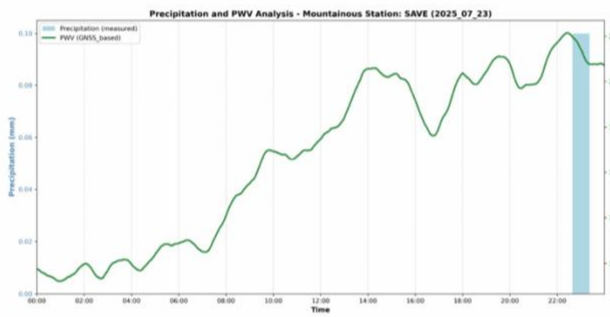
Precipitation and PWV Analysis - Mountainous Station: SAVE (2025_07_23)
Precipitation (measured)
PWV (GNSS_based)
Precipitation (mm)
PWV (mm)
Time

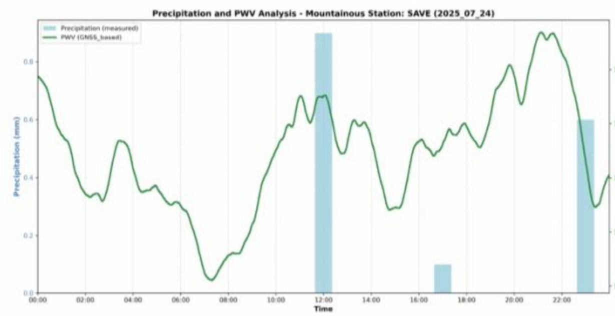
Precipitation and PWV Analysis - Mountainous Station: SAVE (2025_07_24)
Precipitation (measured)
PWV (GNSS_based)
Precipitation (mm)
PWV (mm)
Time

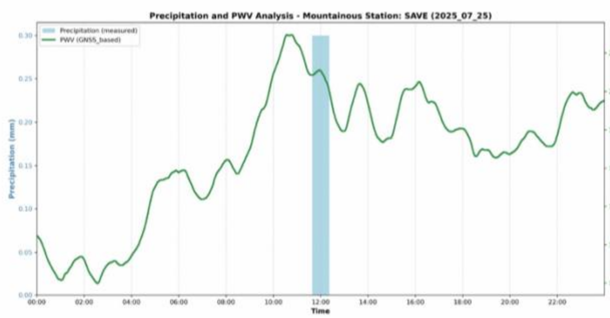
Precipitation and PWV Analysis - Mountainous Station: SAVE (2025_07_25)
Precipitation (measured)
PWV (GNSS_based)
Precipitation (mm)
PWV (mm)
Time

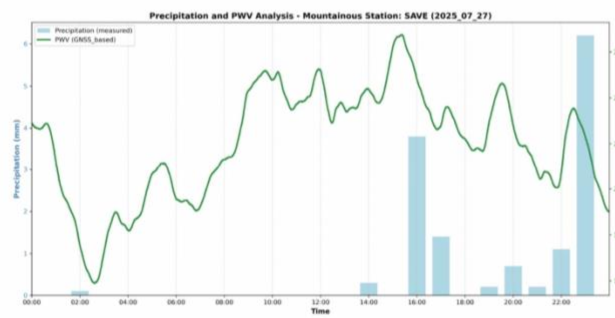
Precipitation and PWV Analysis - Mountainous Station: SAVE (2025_07_27)
Precipitation (measured)
PWV (GNSS_based)
Precipitation (mm)
PWV (mm)
Time

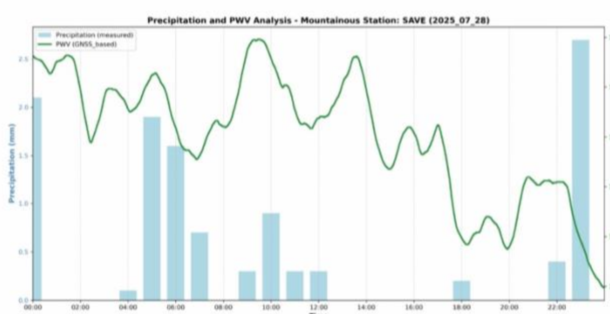
Precipitation and PWV Analysis - Mountainous Station: SAVE (2025_07_28)
Precipitation (measured)
PWV (GNSS_based)
Precipitation (mm)
PWV (mm)
Time

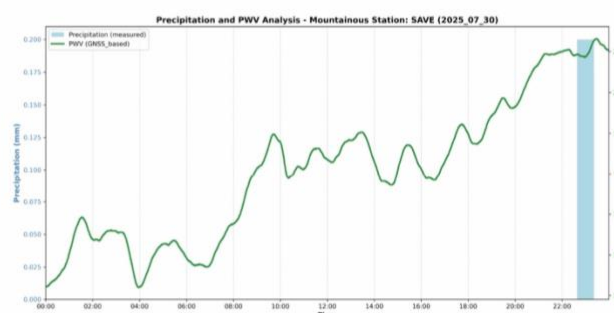
Precipitation and PWV Analysis - Mountainous Station: SAVE (2025_07_30)
Precipitation (measured)
PWV (GNSS_based)
Precipitation (mm)
PWV (mm)
Time

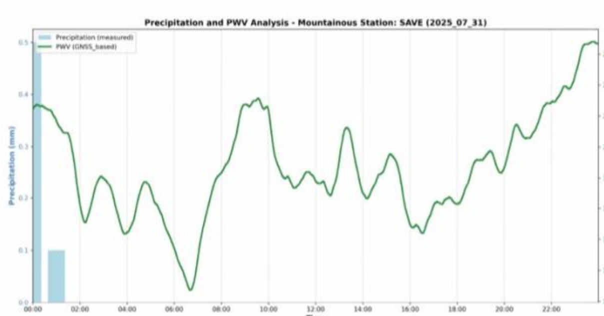
Precipitation and PWV Analysis - Mountainous Station: SAVE (2025_07_31)
Precipitation (measured)
PWV (GNSS_based)
Precipitation (mm)
PWV (mm)
Time

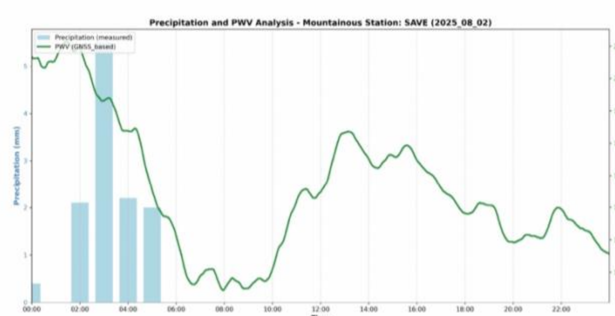
Precipitation and PWV Analysis - Mountainous Station: SAVE (2025_08_02)
Precipitation (measured)
PWV (GNSS_based)
Precipitation (mm)
PWV (mm)
Time

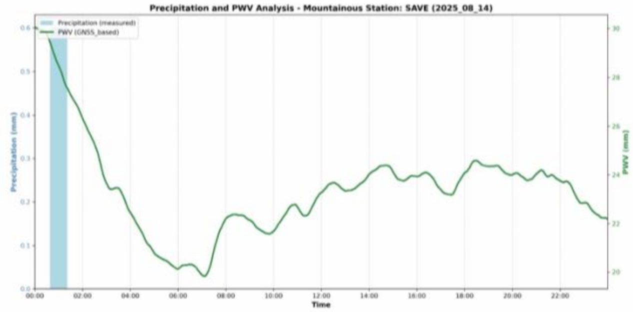
Precipitation and PWV Analysis - Mountainous Station: SAVE (2025_08_14)
Precipitation (measured)
PWV (GNSS_based)
Precipitation (mm)
PWV (mm)
Time

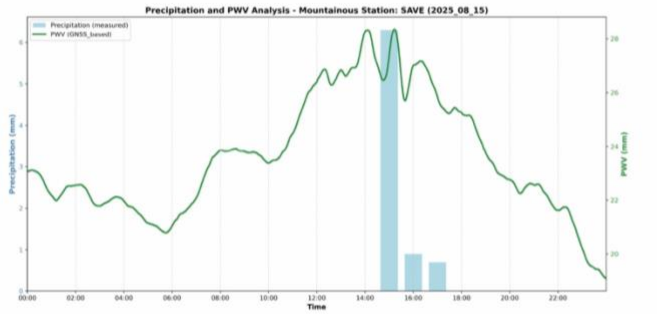
Precipitation and PWV Analysis - Mountainous Station: SAVE (2025_08_15)
Precipitation (measured)
PWV (GNSS_based)
Precipitation (mm)
PWV (mm)
Time

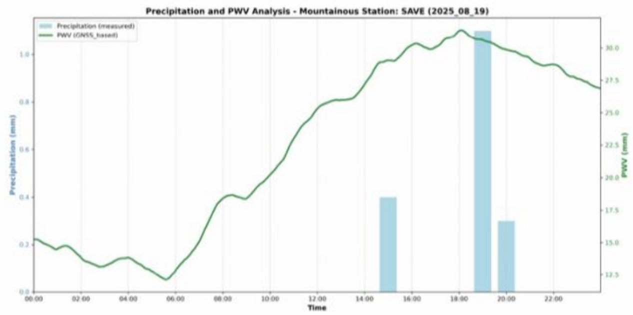
Precipitation and PWV Analysis - Mountainous Station: SAVE (2025_08_19)
Precipitation (measured)
PWV (GNSS_based)
Precipitation (mm)
PWV (mm)
Time

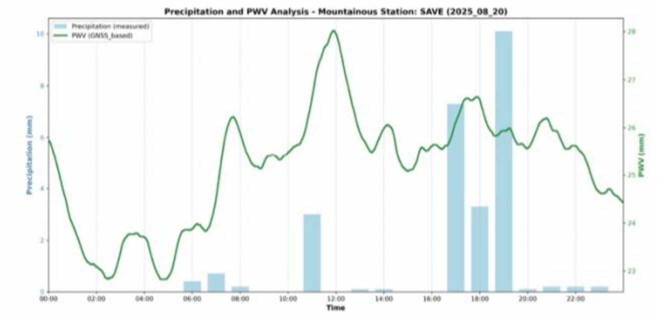
Precipitation and PWV Analysis - Mountainous Station: SAVE (2025_08_20)
Precipitation (measured)
PWV (GNSS_based)
Precipitation (mm)
PWV (mm)
Time

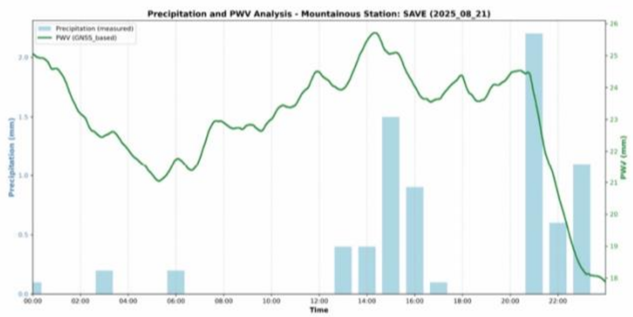
Precipitation and PWV Analysis - Mountainous Station: SAVE (2025_08_21)
Precipitation (measured)
PWV (GNSS_based)
Precipitation (mm)
PWV (mm)
Time

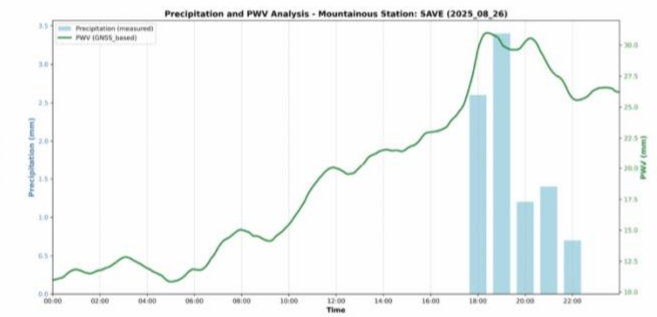
Precipitation and PWV Analysis - Mountainous Station: SAVE (2025_08_26)
Precipitation (measured)
PWV (GNSS_based)
Precipitation (mm)
PWV (mm)
Time

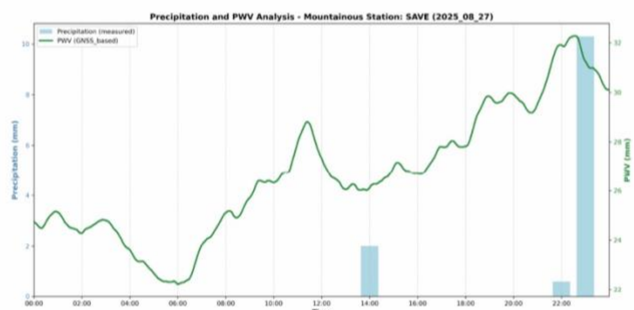
Precipitation and PWV Analysis - Mountainous Station: SAVE (2025_08_27)
Precipitation (measured)
PWV (GNSS_based)
Precipitation (mm)
PWV (mm)
Time

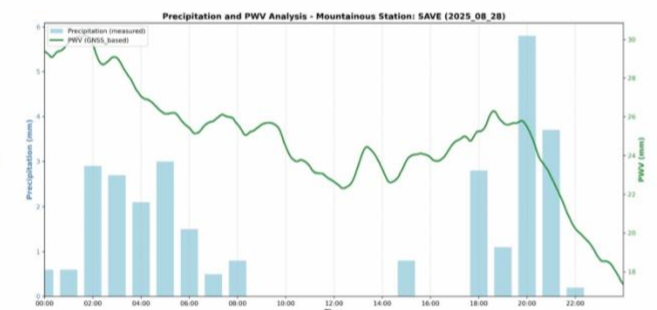
Precipitation and PWV Analysis - Mountainous Station: SAVE (2025_08_28)
Precipitation (measured)
PWV (GNSS_based)
Precipitation (mm)
PWV (mm)
Time

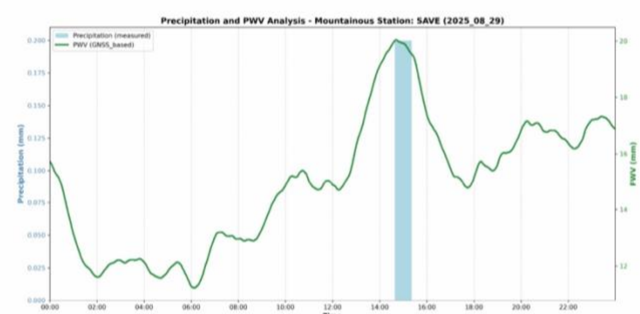
Precipitation and PWV Analysis - Mountainous Station: SAVE (2025_08_29)
Precipitation (measured)
PWV (GNSS_based)
Precipitation (mm)
PWV (mm)
Time

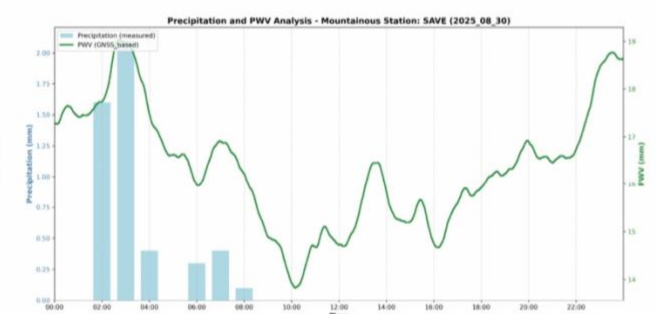
Precipitation and PWV Analysis - Mountainous Station: SAVE (2025_08_30)
Precipitation (measured)
PWV (GNSS_based)
Precipitation (mm)
PWV (mm)
Time

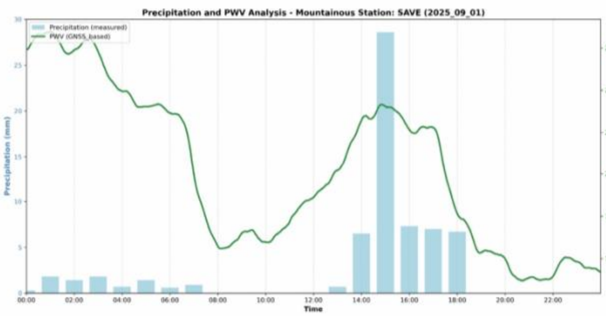
Precipitation and PWV Analysis - Mountainous Station: SAVE (2025_09_01)
Precipitation (measured)
PWV (GNSS_based)
Precipitation (mm)
PWV (mm)
Time

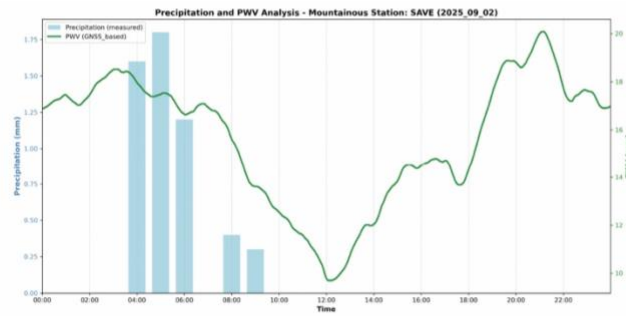
Precipitation and PWV Analysis - Mountainous Station: SAVE (2025_09_02)
Precipitation (measured)
PWV (GNSS_based)
Precipitation (mm)
PWV (mm)
Time

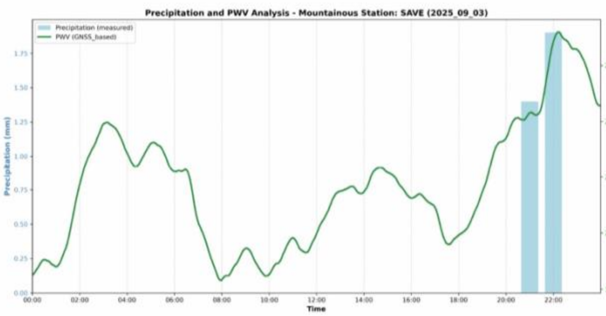
Precipitation and PWV Analysis - Mountainous Station: SAVE (2025_09_03)
Precipitation (measured)
PWV (GNSS_based)
Precipitation (mm)
PWV (mm)
Time

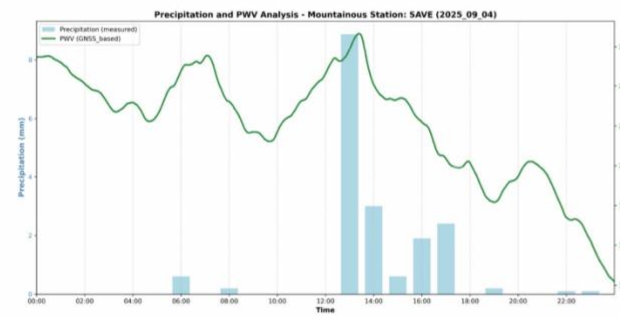
Precipitation and PWV Analysis - Mountainous Station: SAVE (2025_09_04)
Precipitation (measured)
PWV (GNSS_based)
Precipitation (mm)
PWV (mm)
Time

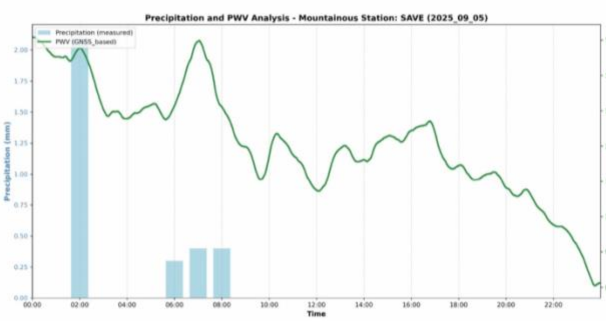
Precipitation and PWV Analysis - Mountainous Station: SAVE (2025_09_05)
Precipitation (measured)
PWV (GNSS_based)
Precipitation (mm)
PWV (mm)
Time

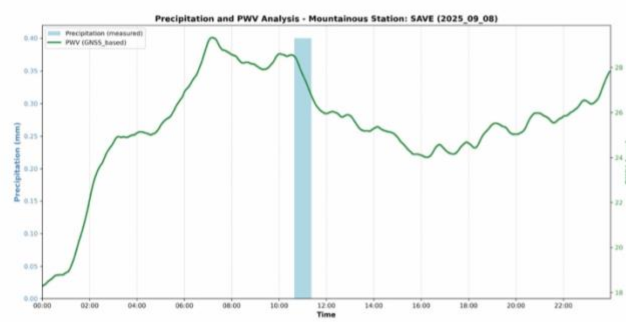
Precipitation and PWV Analysis - Mountainous Station: SAVE (2025_09_08)
Precipitation (measured)
PWV (GNSS_based)
Precipitation (mm)
PWV (mm)
Time

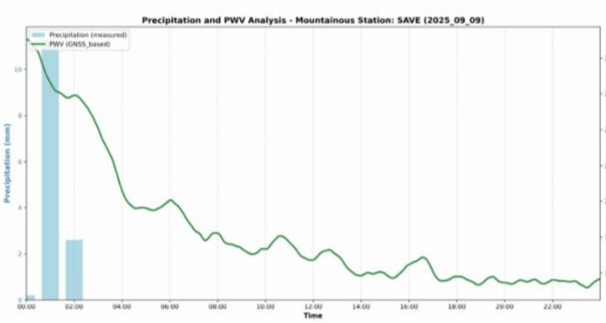
Precipitation and PWV Analysis - Mountainous Station: SAVE (2025_09_09)
Precipitation (measured)
PWV (GNSS_based)
Precipitation (mm)
PWV (mm)
Time

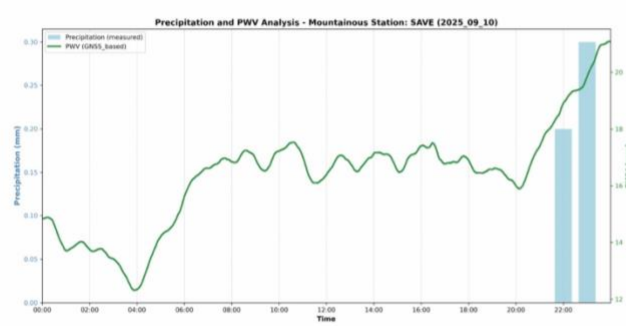
Precipitation and PWV Analysis - Mountainous Station: SAVE (2025_09_10)
Precipitation (measured)
PWV (GNSS_based)
Precipitation (mm)
PWV (mm)
Time

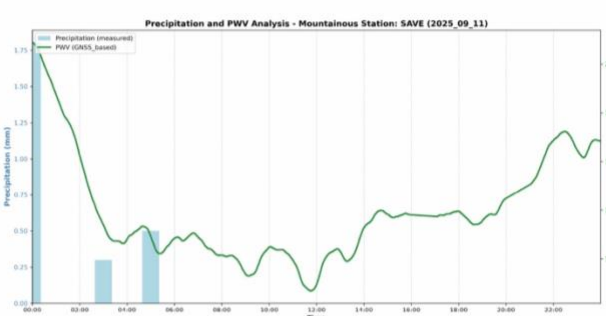
Precipitation and PWV Analysis - Mountainous Station: SAVE (2025_09_11)
Precipitation (measured)
PWV (GNSS_based)
Precipitation (mm)
PWV (mm)
Time

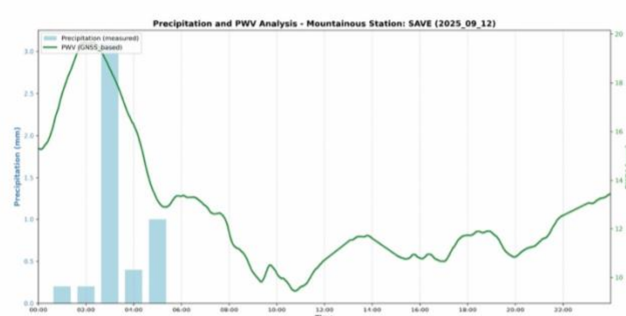
Precipitation and PWV Analysis - Mountainous Station: SAVE (2025_09_12)
Precipitation (measured)
PWV (GNSS_based)
Precipitation (mm)
PWV (mm)
Time

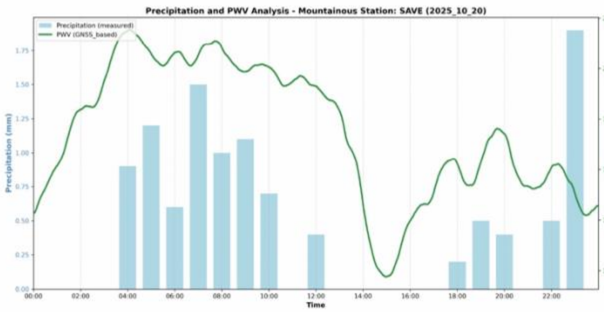
Precipitation and PWV Analysis - Mountainous Station: SAVE (2025_10_20)
Precipitation (measured)
PWV (GNSS_based)
Precipitation (mm)
PWV (mm)
Time

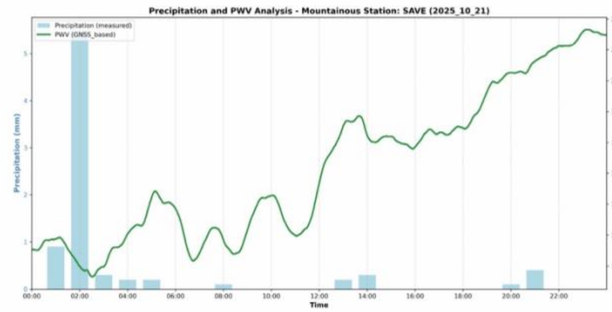
Precipitation and PWV Analysis - Mountainous Station: SAVE (2025_10_21)
Precipitation (measured)
PWV (GNSS_based)
Precipitation (mm)
PWV (mm)
Time

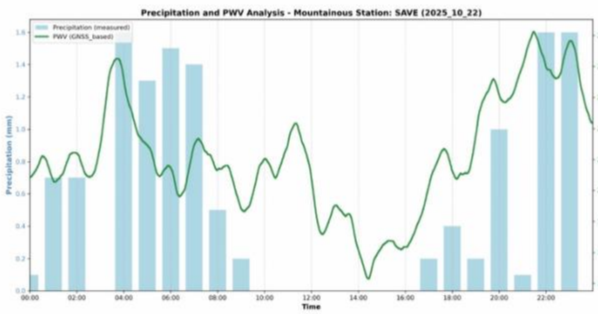
Precipitation and PWV Analysis - Mountainous Station: SAVE (2025_10_22)
Precipitation (measured)
PWV (GNSS_based)
Precipitation (mm)
PWV (mm)
Time

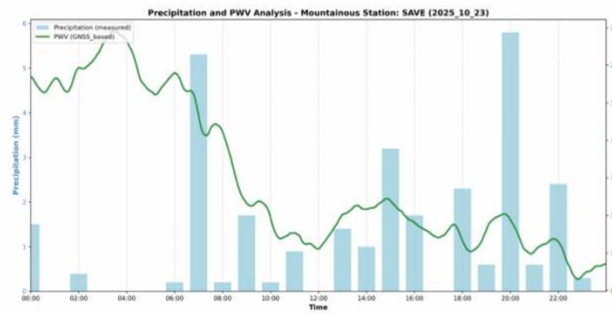
Precipitation and PWV Analysis - Mountainous Station: SAVE (2025_10_23)
Precipitation (measured)
PWV (GNSS_based)
Precipitation (mm)
PWV (mm)
Time

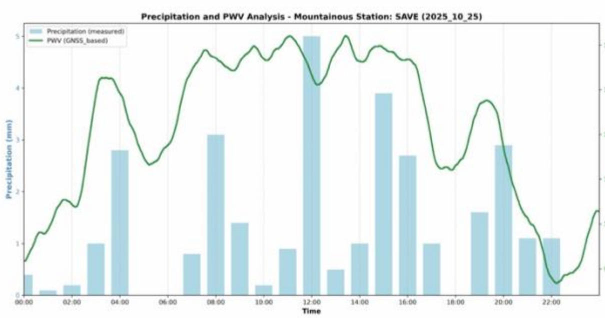
Precipitation and PWV Analysis - Mountainous Station: SAVE (2025_10_25)
Precipitation (measured)
PWV (GNSS_based)
Precipitation (mm)
PWV (mm)
Time

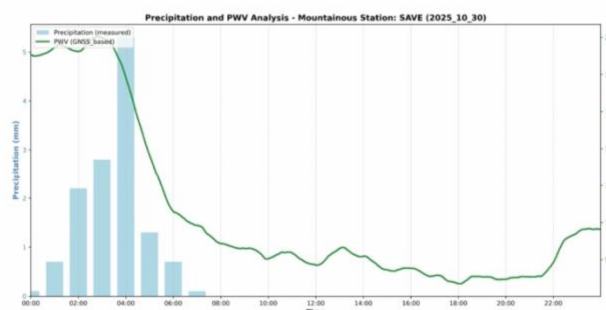
Precipitation and PWV Analysis - Mountainous Station: SAVE (2025_10_30)
Precipitation (measured)
PWV (GNSS_based)
Precipitation (mm)
PWV (mm)
Time

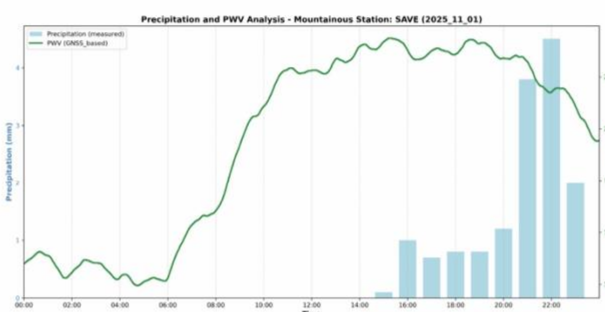
Precipitation and PWV Analysis - Mountainous Station: SAVE (2025_11_01)
Precipitation (measured)
PWV (GNSS_based)
Precipitation (mm)
PWV (mm)
Time

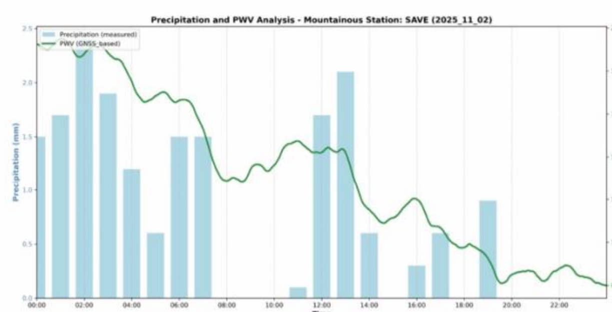
Precipitation and PWV Analysis - Mountainous Station: SAVE (2025_11_02)
Precipitation (measured)
PWV (GNSS_based)
Precipitation (mm)
PWV (mm)
Time

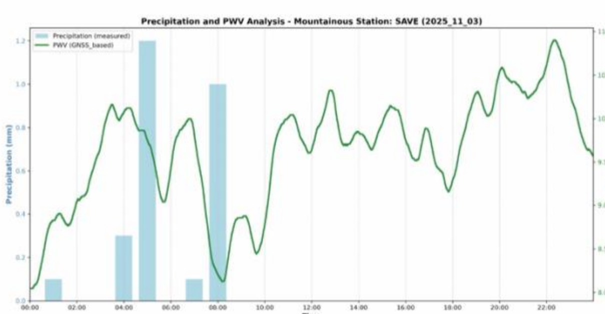
Precipitation and PWV Analysis - Mountainous Station: SAVE (2025_11_03)
Precipitation (measured)
PWV (GNSS_based)
Precipitation (mm)
PWV (mm)
Time

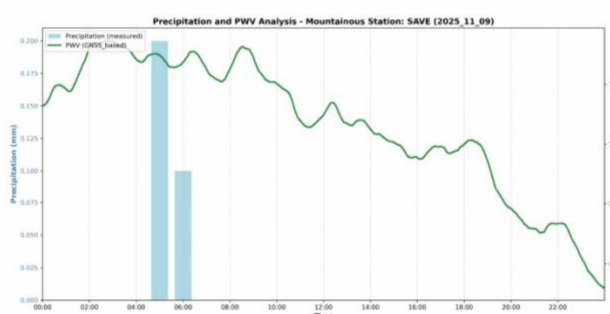
Precipitation and PWV Analysis - Mountainous Station: SAVE (2025_11_09)
Precipitation (measured)
PWV (GNSS_based)
Precipitation (mm)
PWV (mm)
Time

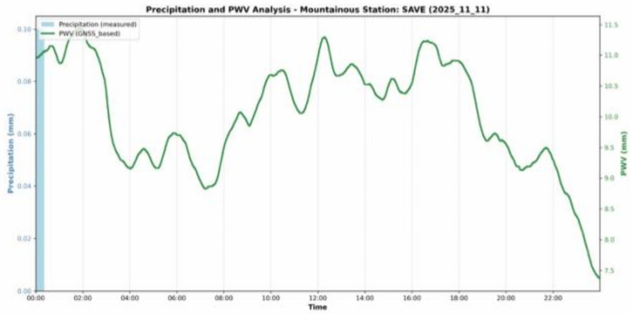
Precipitation and PWV Analysis - Mountainous Station: SAVE (2025_11_11)
Precipitation (measured)
PWV (GNSS_based)
Precipitation (mm)
PWV (mm)
Time

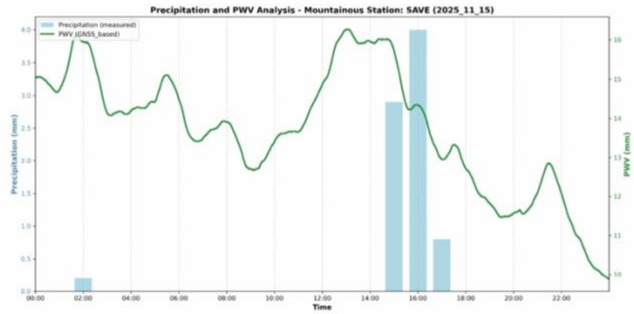
Precipitation and PWV Analysis - Mountainous Station: SAVE (2025_11_15)
Precipitation (measured)
PWV (GNSS_based)
Precipitation (mm)
PWV (mm)
Time

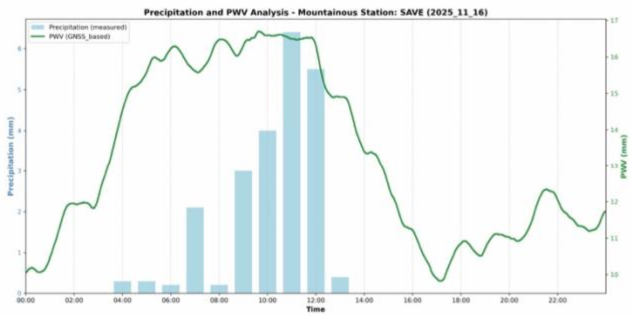
Precipitation and PWV Analysis - Mountainous Station: SAVE (2025_11_16)
Precipitation (measured)
PWV (GNSS_based)
Precipitation (mm)
PWV (mm)
Time

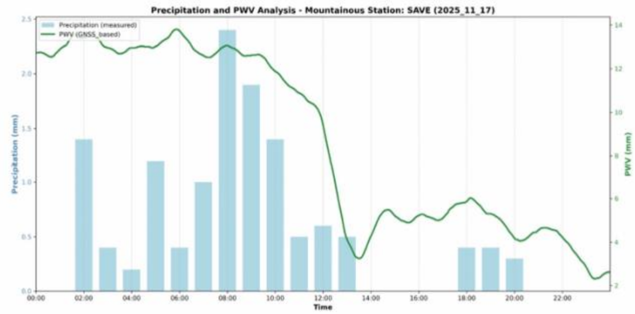
Precipitation and PWV Analysis - Mountainous Station: SAVE (2025_11_17)
Precipitation (measured)
PWV (GNSS_based)
Precipitation (mm)
PWV (mm)
Time

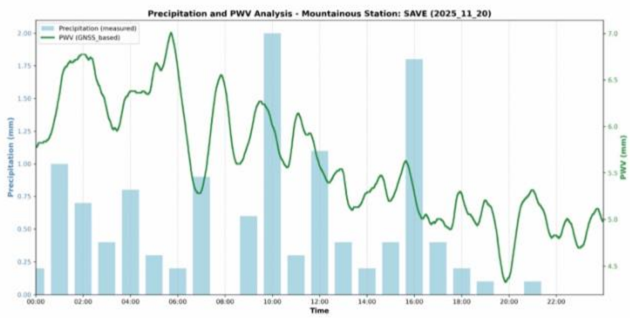
Precipitation and PWV Analysis - Mountainous Station: SAVE (2025_11_20)
Precipitation (measured)
PWV (GNSS_based)
Precipitation (mm)
PWV (mm)
Time

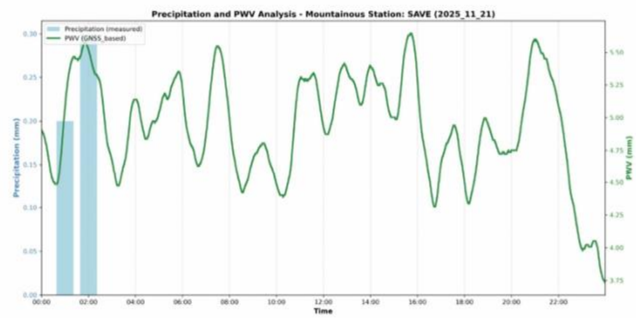
Precipitation and PWV Analysis - Mountainous Station: SAVE (2025_11_21)
Precipitation (measured)
PWV (GNSS_based)
Precipitation (mm)
PWV (mm)
Time

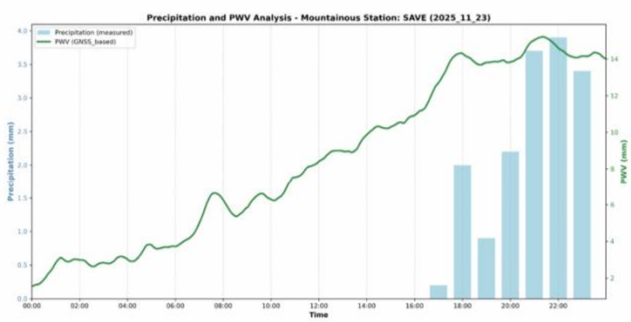
Precipitation and PWV Analysis - Mountainous Station: SAVE (2025_11_23)
Precipitation (measured)
PWV (GNSS_based)
Precipitation (mm)
PWV (mm)
Time

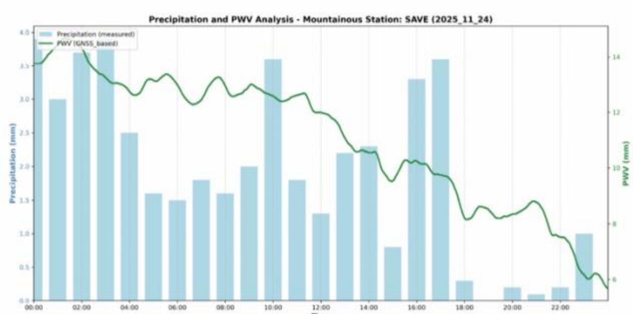
Precipitation and PWV Analysis - Mountainous Station: SAVE (2025_11_24)
Precipitation (measured)
PWV (GNSS_based)
Precipitation (mm)
PWV (mm)
Time

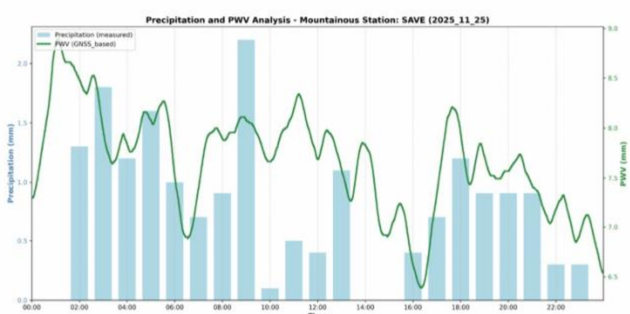
Precipitation and PWV Analysis - Mountainous Station: SAVE (2025_11_25)
Precipitation (measured)
PWV (GNSS_based)
Precipitation (mm)
PWV (mm)
Time

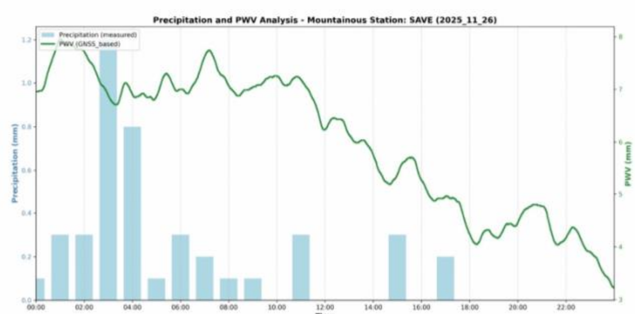
Precipitation and PWV Analysis - Mountainous Station: SAVE (2025_11_26)
Precipitation (measured)
PWV (GNSS_based)
Precipitation (mm)
PWV (mm)
Time

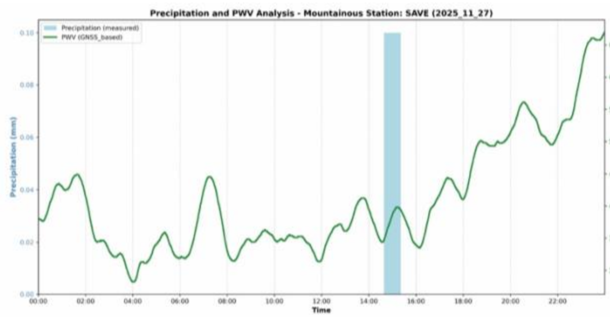
Precipitation and PWV Analysis - Mountainous Station: SAVE (2025_11_27)
Precipitation (measured)
PWV (GNSS_based)
Precipitation (mm)
PWV (mm)
Time

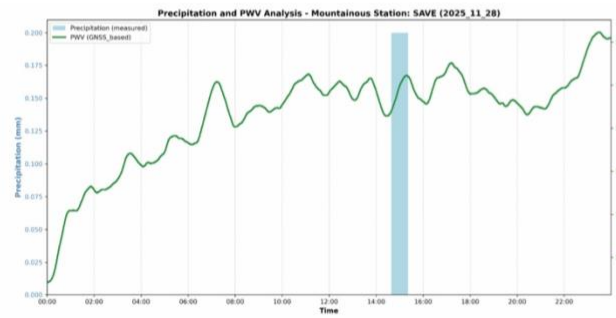
Precipitation and PWV Analysis - Mountainous Station: SAVE (2025_11_28)
Precipitation (measured)
PWV (GNSS_based)
Precipitation (mm)
PWV (mm)
Time

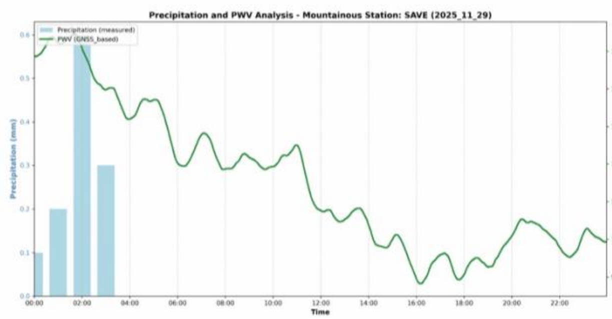
Precipitation and PWV Analysis - Mountainous Station: SAVE (2025_11_29)
Precipitation (measured)
PWV (GNSS_based)
Precipitation (mm)
PWV (mm)
Time

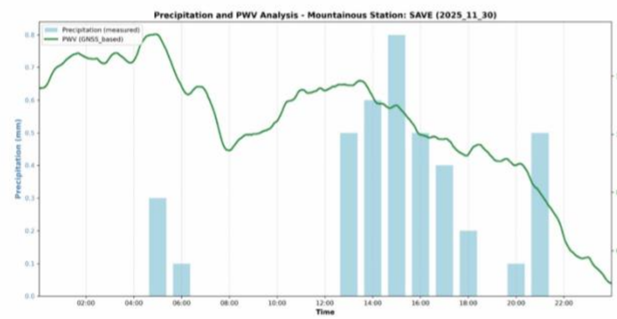
Precipitation and PWV Analysis - Mountainous Station: SAVE (2025_11_30)
Precipitation (measured)
PWV (GNSS_based)
Precipitation (mm)
PWV (mm)
Time

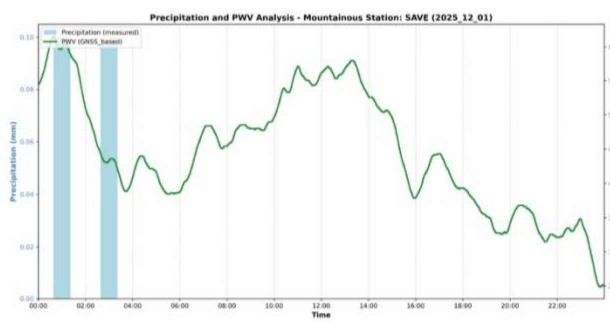
Precipitation and PWV Analysis - Mountainous Station: SAVE (2025_12_01)
Precipitation (measured)
PWV (GNSS_based)
Precipitation (mm)
PWV (mm)
Time

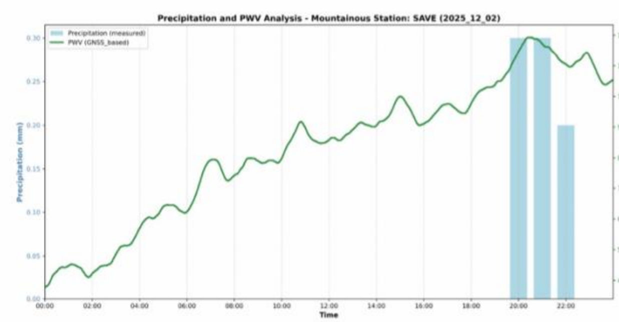
Precipitation and PWV Analysis - Mountainous Station: SAVE (2025_12_02)
Precipitation (measured)
PWV (GNSS_based)
Precipitation (mm)
PWV (mm)
Time

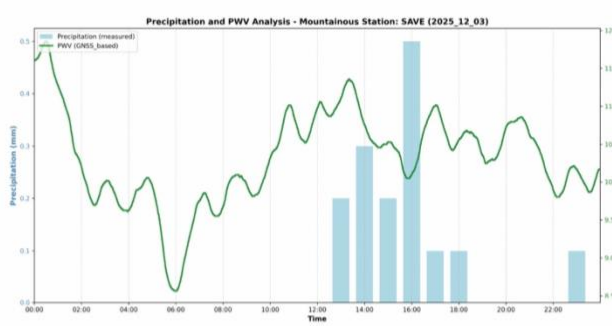
Precipitation and PWV Analysis - Mountainous Station: SAVE (2025_12_03)
Precipitation (measured)
PWV (GNSS_based)
Precipitation (mm)
PWV (mm)
Time

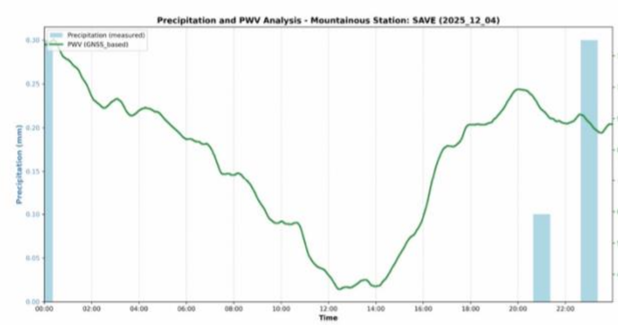
Precipitation and PWV Analysis - Mountainous Station: SAVE (2025_12_04)
Precipitation (measured)
PWV (GNSS_based)
Precipitation (mm)
PWV (mm)
Time

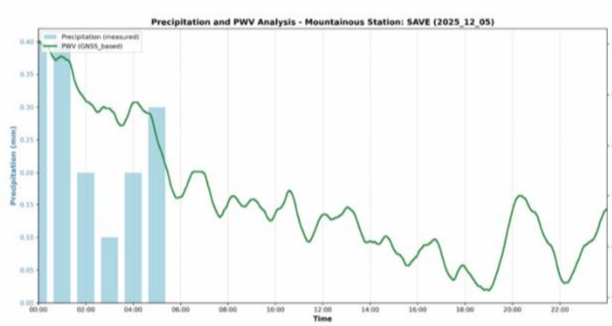
Precipitation and PWV Analysis - Mountainous Station: SAVE (2025_12_05)
Precipitation (measured)
PWV (GNSS_based)
Precipitation (mm)
PWV (mm)
Time

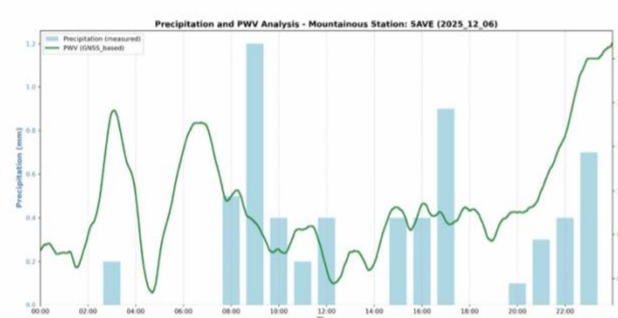
Precipitation and PWV Analysis - Mountainous Station: SAVE (2025_12_06)
Precipitation (measured)
PWV (GNSS_based)
Precipitation (mm)
PWV (mm)
Time

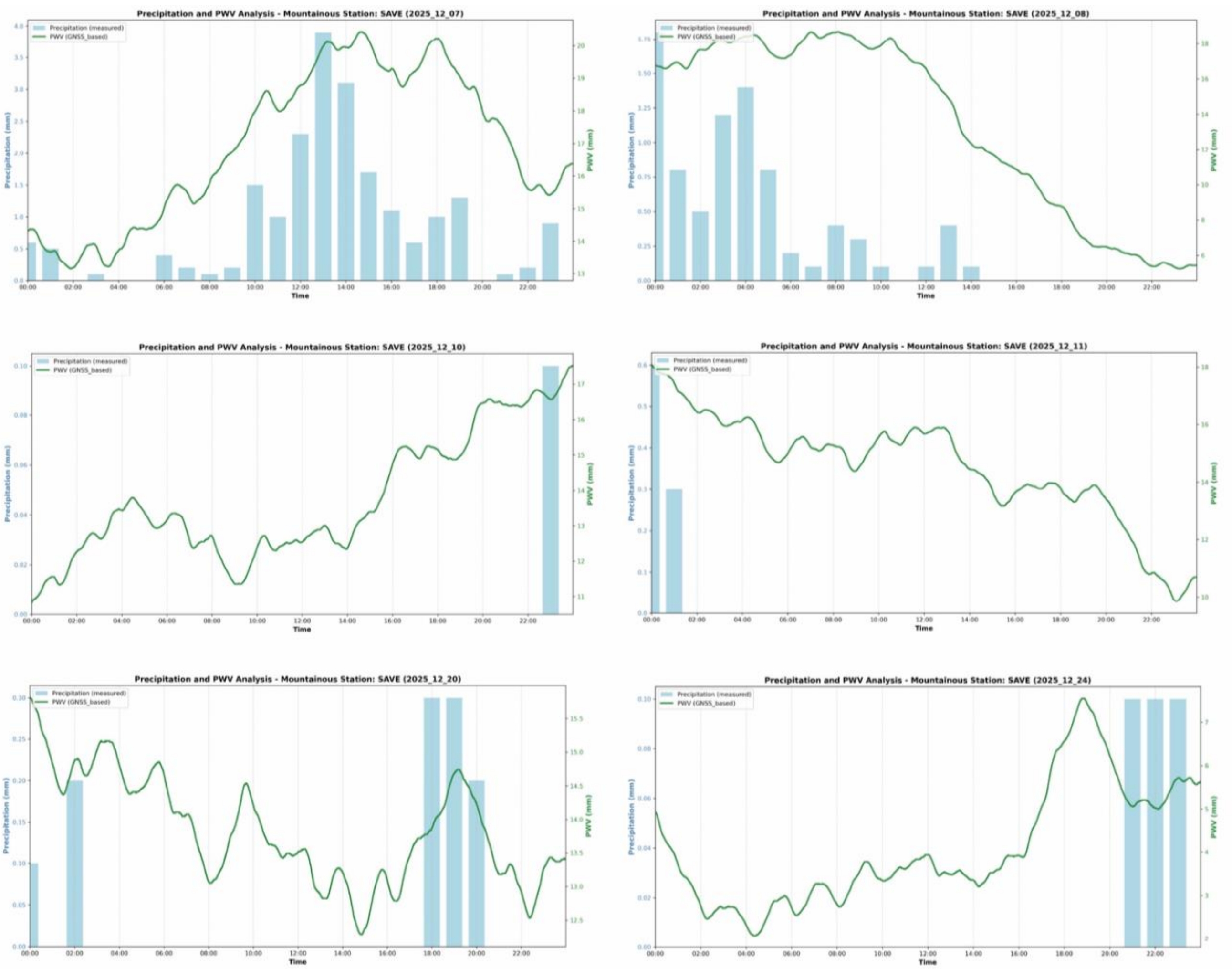

Precipitation and PWV Analysis - Mountainous Station: SAVE (2025_12_07)
Precipitation and PWV Analysis - Mountainous Station: SAVE (2025_12_08)
Precipitation and PWV Analysis - Mountainous Station: SAVE (2025_12_10)
Precipitation and PWV Analysis - Mountainous Station: SAVE (2025_12_11)
Precipitation and PWV Analysis - Mountainous Station: SAVE (2025_12_20)
Precipitation and PWV Analysis - Mountainous Station: SAVE (2025_12_24)
Precipitation (measured)
PWV (GNSS_based)
Precipitation (mm)
PWV (mm)
Time